

4-2017

Wave Energy Assessment in Southern Central Java Island and Control Method for Maximizing the Captured Power in Wave Energy Converters

Fatima Sultan Ghdayer Ali Alaryani

Follow this and additional works at: https://scholarworks.uaeu.ac.ae/all_theses

Part of the [Engineering Commons](#)

Recommended Citation

Ali Alaryani, Fatima Sultan Ghdayer, "Wave Energy Assessment in Southern Central Java Island and Control Method for Maximizing the Captured Power in Wave Energy Converters" (2017). *Theses*. 622.
https://scholarworks.uaeu.ac.ae/all_theses/622

This Thesis is brought to you for free and open access by the Electronic Theses and Dissertations at Scholarworks@UAEU. It has been accepted for inclusion in Theses by an authorized administrator of Scholarworks@UAEU. For more information, please contact fadl.musa@uaeu.ac.ae.



جامعة الإمارات العربية المتحدة
United Arab Emirates University

United Arab Emirates University

College of Engineering

Department of Electrical Engineering

WAVE ENERGY ASSESSMENT IN SOUTHERN CENTRAL JAVA
ISLAND AND CONTROL METHOD FOR MAXIMISING THE
CAPTURED POWER IN WAVE ENERGY CONVERTERS

Fatima Sultan Ghdayer Ali Alaryani

This thesis is submitted in partial fulfilment of the requirements for the degree of
Master of Science in Electrical Engineering

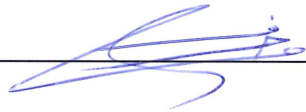
Under the Supervision of Dr. Addy Wahyudie

April 2017

Declaration of Original Work

I, Fatima Sultan Ghdayer Ali Alaryani, the undersigned, a graduate student at the United Arab Emirates University (UAEU), and the author of this thesis entitled “*Wave Energy Assessment in Southern Central Java Island and Control Method for Maximizing the Captured Power in Wave Energy Converters*”, hereby, solemnly declare that this thesis is my own original research work that has been done and prepared by me under the supervision of Dr. Addy Wahyudie, in the College of Engineering at UAEU. This work has not previously been presented or published, or formed the basis for the award of any academic degree, diploma or a similar title at this or any other university. Any materials borrowed from other sources (whether published or unpublished) and relied upon or included in my thesis have been properly cited and acknowledged in accordance with appropriate academic conventions. I further declare that there is no potential conflict of interest with respect to the research, data collection, authorship, presentation and/or publication of this thesis.

Student's Signature: _____



Date: _____

18/5/2017

Copyright © 2017 Fatima Sultan Ghdayer Ali Alaryani
All Rights Reserved

Approval of the Master Thesis


This Master Thesis is approved by the following Examining Committee Members:

- 1) Advisor (Committee Chair): Dr. Addy Wahyudie

Title: Assistant Professor

Department of Electrical Engineering

College of Engineering

Signature 


Date 11-5-2017

- 2) Member: Dr. Hussain Shareef

Title: Associate Professor

Department of Electrical Engineering

College of Engineering

Signature 

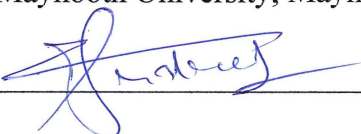
Date 11/5/2017

- 3) Member (External Examiner): Dr. John Ringwood

Title: Professor

Department of Electronic Engineering

Institution: Maynooth University, Maynooth, Ireland.


Signature 

Date 11-05-2017

Dr. M.S. LAGHARI on behalf of Prof. John Ringwood
EE Graduate
Program coordinator.

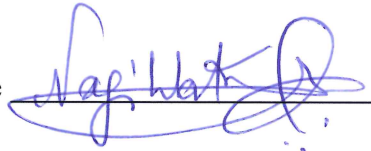
This Master Thesis is accepted by:

Dean of the College of Engineering Professor Sabah Alkass

Signature 

Date 18/05/2017

Dean of the College of Graduate Studies: Professor Nagi T. Wakim

Signature 

Date 18/5/2017

Abstract

This thesis discusses the wave energy potential of the Indian Ocean on the south coast of Central Java Island, where no previous known similar study has been conducted. A control technique that involves a dynamic electrical model was established. The following objectives were achieved. The first was to determine the ideal location to implement wave energy conversion (WEC), and the second objective was to simulate the significant wave height by using the novel control method.

To achieve these goals, the following steps and procedures were implemented. Wave energy assessment was conducted for the Indian Ocean on the south coast of Central Java Island, Indonesia. Results are analyzed with MIKE 21 Spectral Wave by adopting a 10-year hindcast spectral wave model. The model was developed by incorporating wind data from the European Centre for Medium-Range Weather Forecasts with a 0.125° spatial interval and an hourly time resolution. The model was validated with buoy observation data provided by *Badan Pengkajian dan Penerapan Teknologi* or Agency for the Assessment and Application of Technology, Indonesia. The buoy is located at a longitude of 110.547° and a latitude of -8.1364° and provides monthly data on significant wave height and wave period at an hourly data interval (June 2014). Validation showed that the model result matches the data, and the average error is approximately 0.042%. Time domain monthly analysis revealed that the minimum mean wave power appeared in December, January, and February, whereas the maximum mean wave power occurred in July, August, and September with a value of more than 10 kW/m during the dry season in Indonesia. The dominant significant wave height was between 1 and 2 m. The spatial analysis provided six coordinate points in Penyu Bay and Yogyakarta Coast as candidates for WEC location; the 10-year mean wave power was approximately 13–16 kW/m, and the distance from the coast was less than 350 m.

Furthermore, modeling and a control strategy for WECs were discussed. The heaving point absorber from Uppsala University was adopted. The control objective of the proposed method was to maximize the captured mechanical power under the constraint of the maximum control force. The proposed method comprised high-level

and low-level controllers. The high-level controller produced the optimum reference in terms of reference velocity to satisfy the control objective. The low-level controller tracked the reference and provided robustness against model uncertainties. The low-level controller was designed before the high-level controller. The main controller in the low-level controller is a proportional–integral–derivative controller. This controller was designed with H_∞ theory, and the genetic algorithm was utilized to solve the infinity norm of the robustness problem. The high-level controller was designed by using the obtained dynamic of the feedback control system in the low-level controller with the mechanical model of WECs. Simulation studies were also conducted. Results of nominal and perturbation cases and those of monochromatic and polychromatic sea states were compared.

Keywords: Renewable energy, Wave energy converter, Wave energy assessment, Hindcast, Java Island, Indonesia, MIKE 21 Spectral Wave

Title and Abstract (in Arabic)

تقييم طاقة الامواج جنوب جزيرة جاوا و تحديد طريقة التحكم لتحقيق اقصى حصد من الطاقة في محولات الطاقة

المخلص

تهدف هذه الأطروحة الي دراسة تقييم طاقة الامواج في المحيط الهندي على وسط ساحل جاوا في اندونيسيا. باستخدام التحليل الطيفي (MIKE 21 Spectral Wave) يتم توليد وتحليل هذه الامواج اعتمادا على (Hindcast spectral wave model) لفترة زمنية تمتد 10 سنوات. وهذا النموذج تم إيجاده عن طريق ادراج بيانات الرياح من البيانات المتاحة من المركز الأوروبي للتنبؤات الجوية المتوسطة (ECMWF) المسجلة على 0.125 درجة المكانية، مع الفترة الزمنية المسجلة بالساعة. تم التحقق من هذا النموذج مع البيانات التي تم رصدها عن طريق العوامة. قدمت هذه البيانات من وكالة لتقييم وتطبيق التكنولوجيا (BPPT) في اندونيسيا. تقع العوامة على خط طول 8.1364- ودائرة عرض 110.547. وفرت هذه الجهة بيانات شهر يونيو سنة 2014 لكل من (ارتفاع الموجة والفترة الزمنية للموجة لكل ساعة). اظهر التحقق من ان النموذج يتناسب مع البيانات المسجلة في الواقع، ويبلغ متوسط الخطأ تقريبا 0.042%. ووفقا للتحليل الشهري، اظهر ان ادنى قيمة لمتوسط طاقة الامواج كان في ديسمبر، يناير و فبراير بينما اقصى قيمة لمتوسط الطاقة كان في يوليو، اغسطس و سبتمبر بقيمة اكثر من 10 كيلو وات/م وذلك تقريبا في موسم الجفاف في اندونيسيا. يتم ذلك على ارتفاع موجي يتراوح ما بين (1 - 2) م.

في الجزء الثاني من الاطروحة تم مناقشة استراتيجيات نموذج (تحويل طاقة الامواج). طريقة (the heaving point absorber) متخذة من جامعة اوبسالا في السويد. هدف التحكم من الطريقة المقترحة هي تحقيق اقصى حصد من الطاقة الميكانيكا الكامنة مع الحرص على عدم تجاوز القيمة المحددة لضبط القوة. الطريقة المقترحة تتألف من جزئين: وحدة تحكم عالي المستوى ووحدة تحكم منخفض المستوى. وحدة تحكم عالي المستوى تنتج أفضل اشارة مرجعية فيما يتعلق بالسرعة المرجعية لتلبية هدف المراقبة. وحدة التحكم في المستوى المنخفض يتبع مسار الاشارة المرجعية ويوفر القوة المقاومة لإعادة المسار للنموذج عند مواجهة عدم اتزان في النموذج. في هذه الدراسة، التحكم في المستوى المنخفض صمم قبل التحكم في عالي المستوى.

وحدة التحكم الرئيسية في انخفاض مستوى التحكم هي (PID). هذا المراقب صمم باستخدام نظرية (H_∞) و (genetic algorithm) استخدمت لحل مشكلة (infinity norm). صممت وحدة تحكم عالي المستوى باستخدام التغذية المرتدة التي تم الحصول عليها من خلال نظام التحكم الديناميكي في وحدة تحكم منخفضة المستوى. واجريت دراسات المحاكاة. مقارنة النتائج بين حالات بسيطة، وحالات بها تشويش، وكذلك في حالات البحر (monochromatic) و (polychromatic).

مفاهيم البحث الرئيسية: الطاقة المتجددة، تحويل طاقة الامواج، تقييم طاقة الامواج، جزيرة جاوا، اندونيسيا.

Acknowledgements

My thanks go to Dr. Addy Wahyudie who supports me during the preparation of my thesis, providing unlimited assistance, and encouraged me when I faced any difficulties, As well as being patience in front of my mistakes. I'm grateful for being my advisor.

I would like to thank our best teamwork (wave energy group) for their support, their help in collection the data and working together as one family. Especially, Eng. Omsalama Mubark, Eng. Tri Bagus Susilo, Eng. Abdulrahman Daher and Eng. Bisni Fahad.

I would like to thank the chair and all members of the Department of Electrical Engineering at the United Arab Emirates University for assisting me all over my studies and research. My special thanks are extended to my duty manager Eng. Mohammed Al Mazroui in AlAin Distribution Company (AADC) and my colleagues for providing me the support.

Last but not least of course, my sincere gratitude goes to my dear family. Thanks go to my lovely mother, for her endless support throughout all aspects of my life including this stage. My father, sisters and brother whose helped me along the way. In addition, special thanks are extended to Alaryani and Alyahyae families for their assistance and friendship. Thank you.

Dedication

To my beloved parents and family

Table of Contents

Title	i
Declaration of Original Work	ii
Copyright	iii
Approval of the Master Thesis	iv
Abstract	vi
Title and Abstract (in Arabic)	viii
Acknowledgements	x
Dedication	xi
Table of Contents	xii
List of Tables.....	xiv
List of Figures	xv
List of Abbreviations.....	xvii
Chapter 1: Introduction	1
1.1 Capability of Wave Energy	1
1.2 Source of Wave Energy	2
1.3 Wave Energy Conversion	4
1.4 Research Problem Statement	7
1.5 Wave Energy Assessment Literature Review	8
1.5.1 Studies Conducted Based on Geographical Location	8
1.5.2 Wave Resource Assessment Programs	12
1.5.3 Review of Control Techniques.....	20
1.6 Thesis Structure.....	22
Chapter 2: WEC Assessment Methodology.....	23
2.1 MIKE 21 SW program	23
2.2 Study Domain (Indonesia)	25
2.2.1 Simulation Domain	26
2.3 Model Setup	32
2.3.1 Data Collection.....	33
2.3.2 Boundary Conditions.....	43
2.3.3 Mesh Generation	44
2.3.4 Bathymetry Interpolation	45
2.4 Model Validation.....	46
Chapter 3: Mechanical and Electrical Modeling.....	50
3.1 The Mechanical Model	51

3.2 The Electrical Model.....	54
Chapter 4: Proposed Control Strategy.....	56
4.1 Servo Feedback Control System	57
4.2 Reference Generation.....	63
Chapter 5: WEC Assessment Simulation Results and Discussion.....	67
5.1 Time Domain Analysis	67
5.1.1 10-Year Mean Analysis.....	67
5.1.2 Monthly Analysis	73
5.2 Spatial Analysis.....	86
5.2.1 DIY Coastline.....	89
Chapter 6: Control Simulation Results and Discussion	92
6.1 Simulation Setup and Controller Design.....	92
6.2 Simulation Strategy	97
6.3 Results and Analysis	99
Chapter 7: Conclusion.....	107
7.1 Main Research Outcomes	107
7.2 Future Work	109
References	111

List of Tables

Table 1: Coastline Digital Data Resources	26
Table 2: Five Resolution Types of GSHHG Coastline Data	27
Table 3: Point Candidates for WEC Location in Penyu Bay	89
Table 4: Point Candidates for WEC Location in DIY Coastline	91
Table 5: Electrical and Mechanical Parameters of the WEC	92
Table 6: Look-up Table for $R \times 10^6$ [Ns/m] for Various Values of H_S [m], ω_p [rad/s] and γ	94
Table 7: Different Perturbation Scenarios in fs and fl using PT-RB Method	104
Table 8: Different Perturbation Scenarios in fs and fl using RL Method	104

List of Figures

Figure 1: Worldwide Annual Average Wave Power Level in kW/m Created by the ECMWF (European Center for Medium-Range Weather Forecasts) using WAM Model	3
Figure 2: Graphical Drawing of the Uppsala University Point Absorber Organized in a Farm of WECs	6
Figure 3: Pacitan River in East Java Indonesia.....	24
Figure 4: Map of Indonesia.....	25
Figure 5: Indian Ocean of Central Java and DIY, Java Island, Indonesia	26
Figure 6: World Coastline Data from GSHHG.....	28
Figure 7: Selected Coastline Data above Real World Map.....	28
Figure 8: GEODAS-NG Software	29
Figure 9: SHAPE File of Selected Area Shown in Coastline Extractor	30
Figure 10: Sample of XYZ File Extracted from GEODAS-NG Software.....	30
Figure 11: Mesh Generator Feature under MIKE Zero Package	31
Figure 12: Final Simulation Region for Central Java and DIY Regions	31
Figure 13: Hindcast block diagram	33
Figure 14: Date, Time and Step Selection Menu from ECMWF Website.....	34
Figure 15: Parameter Selection Menu from ECMWF Website	34
Figure 16: Wind Speed, Wind Direction and Wind Velocity u and v Components ..	35
Figure 17: Wind Velocity u Profile in June 1 st 2014 at 12:00 AM.....	36
Figure 18: Wind Velocity u Profile in June 1 st 2014 at 03:00 AM.....	36
Figure 19: Wind Velocity v Profile in June 1 st 2014 at 12:00 AM	37
Figure 20: Wind Velocity v Profile in June 1 st 2014 at 03:00 AM	37
Figure 21: Significant Wave Height Profile in June 1 st 2014 at 12:00 AM.....	38
Figure 22: Significant Wave Height Profile in June 1 st 2014 at 03:00 AM.....	39
Figure 23: Wave Direction Regulation	39
Figure 24: Mean Wave Direction Profile in June 1 st 2014 at 12:00 AM.....	40
Figure 25: Mean Wave Direction Profile in June 1 st 2014 at 03:00 AM.....	40
Figure 26: Wave Types Based on Wave Period.....	41
Figure 27: Wave Period Profile in June 1 st 2014 at 12:00 AM.....	42
Figure 28: Wave Period Profile in June 1 st 2014 (a) at 03:00 AM	42
Figure 29: Scattered Bathymetry Data.....	43
Figure 30: Boundary Condition Codes	44
Figure 31: Triangular Meshes with Nodes and Elements	44
Figure 32: Generated Mesh.....	45
Figure 33: Interpolated Bathymetry Profile	45
Figure 34: Observed and Simulated Significant Wave Height for Baron Observation Station.....	48
Figure 35: Error Percentage Significant Wave Height for Baron Observation Station	49

Figure 36: Configuration of the Proposed Control System for WEC Systems.....	50
Figure 37: Corresponding circuit of the PMLG.....	55
Figure 38: Proposed control system configuration for WEC Systems	58
Figure 39: Flow Chart for Complex Polynomial Stabilization	62
Figure 40: Distribution of 10-year Mean Wave Period	68
Figure 41: Histogram of 10-year mean Wave Period	69
Figure 42: Distribution of 10-year Mean Significant Wave Height	70
Figure 43: Histogram of 10-year Mean Significant Wave Height.....	71
Figure 44: Distribution of 10-year Mean Wave Power.....	72
Figure 45: Histogram of 10-year Mean Wave Power	73
Figure 46: Distribution of 10-year Mean Wave Power of January	74
Figure 47: Distribution of 10-year Mean Wave Power of February	75
Figure 48: Distribution of 10-year Mean Wave Power of March.....	76
Figure 49: Distribution of 10-year Mean Wave Power of April.....	77
Figure 50: Distribution of 10-year Mean Wave Power of May.....	78
Figure 51: Distribution of 10-year Mean Wave Power of June.....	79
Figure 52: Distribution of 10-year Mean Wave Power of July.....	80
Figure 53: Distribution of 10-year Mean Wave Power of August.....	81
Figure 54: Distribution of 10-year Mean Wave Power of September	82
Figure 55: Distribution of 10-year Mean Wave Power of October	83
Figure 56: Distribution of 10-year Mean Wave Power of November	84
Figure 57: Distribution of 10-year Mean Wave Power of December.....	85
Figure 58: Monthly Mean Wave Power Potential Based on 10-year Assessment Data	86
Figure 59: Penyu Bay Area.....	87
Figure 60: Distribution of 10-year Mean Wave Power in Penyu Bay Area and Pin Points of WEC Location Candidates.....	88
Figure 61: Histogram of 10-year Mean Wave Power in Penyu Bay.....	88
Figure 62: Beaches along DIY Coastline.....	90
Figure 63: Distribution of 10-year Mean Wave Power along DIY Coastline and Pin Points of WEC Location Candidates.....	90
Figure 64: Simulation Results Obtained by the RL, P1-RB, PT-RB, and SPT-RB Methods for Regular (Monochromatic) Waves with $H_s = 1m$	99
Figure 65: Simulation Results Obtained by the RL, P1-RB, PT-RB, and SPT-RB Methods for Regular (Monochromatic) Waves with $H_s = 2m$	101
Figure 66: Simulation Results in Terms of Mechanical Quantities Obtained using the PT-RB Methods for Irregular (Polychromatic) Waves with $H_s = 2m$ and $\omega_p = 0.7rad/s$	102
Figure 67: Simulation Results in Terms of Electrical Quantities Obtained using the PT-RB Methods for Irregular (Polychromatic) Waves with $H_s = 2m$ and $\omega_p = 0.7rad/s$	103

List of Abbreviations

BPPT	Badan Pengkajian dan Penerapan Teknologi
CO ₂	Carbon dioxide
CPU	Central Processing Unit
DDP	Directionally Decoupled Parametric
DHI	Danish Hydraulic Institute
DIA	Direct Interaction Approximation
ECMWF	European Centre for Medium-Range Weather Forecasts
EIA	Energy Information Administration
EU	European Union
FEM	Finite Element Method
FS	Fully Spectral
GEBCO	General Bathymetry Chart of the Ocean
GEODAS-NG	Geophysical Data System - Next Generation
GIS	Geographic Information System
GSHHG	Global Self-consistent, Hierarchical, and High-resolution Geography
HIRLAM	High Resolution Limited Area Model
HPA	Heaving Point Absorber
LTA	Linear Transition Approximation
MPC	Model Predictive Control
MPPT	Maximum Power Point Tracking
MSE	Mean Square Error
NCEI	National Centers for Environmental Information
NOAA	National Oceanic and Atmospheric Administration

OS	Ordnance Survey
P1-RB	Proposed Method with $\gamma = 1$
PID	Proportional-Integral-Derivative
PMLG	Permanent Magnet Linear Generator
PT-RB	Proposed Method with $\gamma =$ tuned value
PTO	Power Take-Off
QGIS	Quantum-GIS
RAM	Random-Access Memory
RL	Resistive Loading
RMAE	Relative Mean Absolute Error
SPT-RB	Simplified Version of PT-RB where $\gamma =$ fixed value
SWAN	Simulating WAVes Nearshore
TOMAWAC	TELEMAC-based Operational Model Addressing Wave Action Computation
WAM	Wave Model
WEC	Wave Energy Converters
WGS84	World Geodetic System

Chapter 1: Introduction

1.1 Capability of Wave Energy

Sustainable advancement has become a fundamental topic in many countries. Challenges, such as global warming and energy shortage, have motivated the governments of these countries to implement serious actions to increase further the renewable energy allocated to their local energy markets. According to the Energy Information Administration, the worldwide renewable energy utilization in the power business sector would develop at an average yearly rate of 2.6% from 2007 to 2035. Therefore, the relative growth of renewable energy utilization in the power business sector would increase at an average yearly rate of 5%, thereby prompting a utilization rate of 23% by 2035 [1]. Further dependence on fossil fuel sources, which account for the largest portion of the current global energy utilization, is inevitable because naturally extracted oil is expected to increase by 2030. Notably, 74% of the total CO_2 emissions are produced from fossil fuel sources [2].

The most encouraging renewable energy resource is marine energy because of the lack of current exploitation and the size of resources with a large power potential. The worldwide marine energy potential is predicted to be around 32 TW. The European Union (EU) is planning to increase the marine energy split in the EU to more than 3% by 2020 [3]. The existing marine energy market is a combination of wave energy, tidal energy, and energy produced from ocean salinity and temperature differences [4].

Wave energy has an expected worldwide potential of 2 TW, which is almost comparable to the world's power consumption. With the challenges encountered in

exploiting this asset, only 25% of the accessible potential can be exploited (i.e., 0.5 TW) [5].

1.2 Source of Wave Energy

Wave energy can be regarded as a dense shape of solar energy. Wind is generated due to distinctions in atmospheric pressure and solar energy distribution. As a consequence, wind is created and blown over the surface of vast ocean waves. The average power flow intensity of ocean waves is roughly $2\text{--}3 \text{ kW}/\text{m}^2$ compared with only $0.5 \text{ kW}/\text{m}^2$ for wind, which has significantly less intensity than solar energy (i.e., $0.1\text{--}0.3 \text{ kW}/\text{m}^2$) [6]. The high average power intensity is mostly due to the higher density of water compared with air.

Normally, the wave potential in a specific area is assessed with wave energy transport J measured in kW/m , which is characterized as the wave power per meter width of the wave front. The global wave energy is concentrated in the center to high-latitude zones on both sides of the equator, especially from 40° to 60° latitude [5]. Figure 1 presents the worldwide average yearly wave energy transport. As shown in the map, regions near the center have a humble wave energy potential (i.e., $\leq 20 \text{ kW}/\text{m}$). The southern side of the equator has the most energetic areas because less seasonal wave diversity is present in this part of the world than in the northern half.

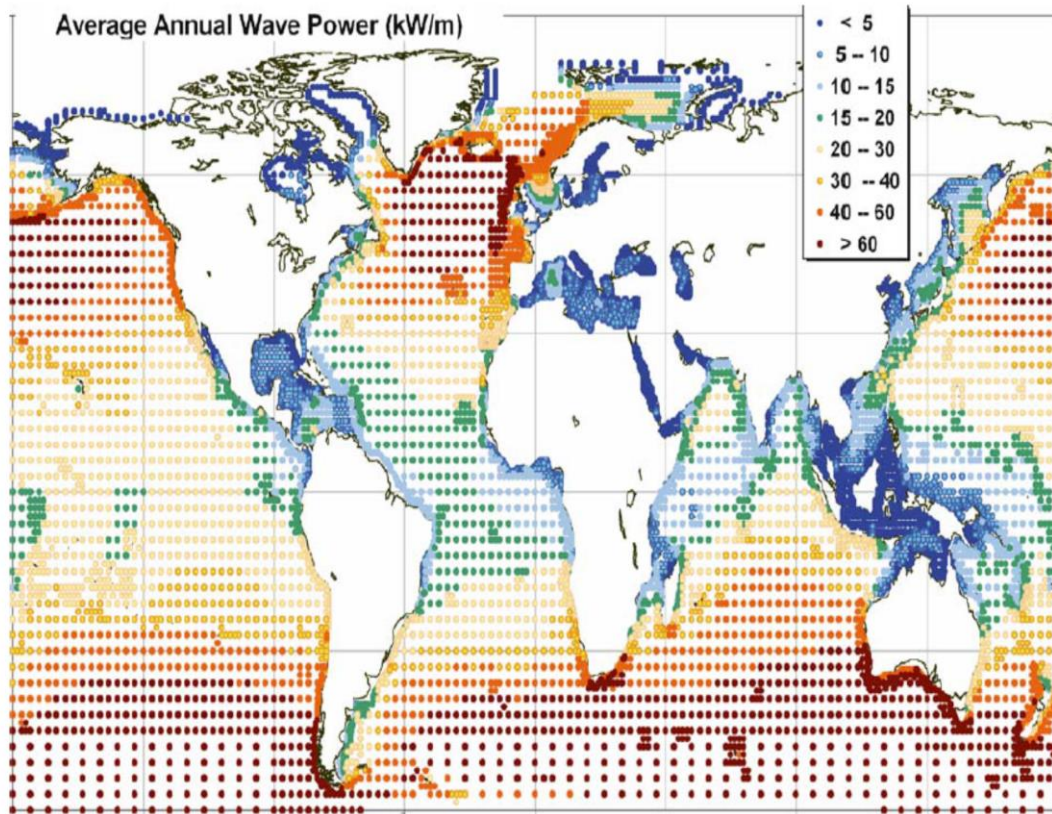


Figure 1: Worldwide Annual Average Wave Power Level in kW/m Created by the ECMWF (European Center for Medium-Range Weather Forecasts) using WAM Model [5]

In sea building, ocean waves are typically characterized by an arrangement of measurable measurements using records of wave heights and wave periods. With regard to wave height, the most widely recognized metric is significant wave height H_s or, from another perspective, one-third wave height $H_{1/3}$, which is characterized as the average height of 33% of the collective number of waves that are mostly seen in the wave spectral distribution [7]. By utilizing spectral moments, critical wave height H_s can be computed as

$$H_s = 4\sqrt{m_0}, \quad (1)$$

where m_0 is the zeroth moment and is known as

$$m_0 = \int S(\omega) d\omega, \quad (2)$$

where $S(\omega)$ is the wave spectral density. The greatest wave period T_m or peak frequency ω_p is used to express how quickly or slowly the waves propagate [8].

For a monochromatic ocean state in deep waters, wave energy transport J in W/m can be computed as

$$J = \frac{\rho g^2}{32\pi} TH, \quad (3)$$

where ρ is the water density in kg/m^3 , g is gravitational acceleration in m/s^2 , T is the wave period in s , and H is the wave height in m [9]. J is calculated in W/m . Thus, the episode wave power can be predicted by multiplying J with the meter width of the body capturing the wave. For polychromatic waves that exist in actuality, wave power transport J can be computed as [10]

$$J = \frac{\rho g^2}{2} \int_0^\infty \frac{S(\omega)}{\omega} d\omega. \quad (4)$$

Numerous wave spectral models have been developed in marine engineering literature. Examples include Pierson–Moskowitz spectra and JONSWAP spectra [7]. These spectra are utilized to produce unpredictable wave profiles that can be promptly utilized in processor simulations to energize wave energy converters.

1.3 Wave Energy Conversion

The mechanical energy transmitted by water waves is captured with devices known as wave energy converters (WECs). Various WEC topologies have been recommended, but almost none has been used for the business sector. WECs depend on the level of flexibility for movement, such as heave and surge. For example, a force take-off instrument regulates drive, hydraulic, and mechanical power, and its purpose is to determine responses, such as those of the seabed and submerged body;

the device is placed near the shore or offshore [5].

Initial efforts to create WECs date back to the late 1940s and were headed by the Japanese maritime authority Yoshio Masuda, who imagined a wave energy-powered route [11]. Subsequent efforts were exerted by Stephen Salter (UK), Johannes Falnes (Norway), Kjell Budal (Norway), and McCormick (USA) in the 1970s [6].

Research and development of WECs have advanced significantly in terms of the illustration of the aftereffect of serious governmental diversions in engineering. Pelamis stands out among WECs. The majority of fruitful WECs contain cylindrical joints that move comparatively to one another when the devices are stimulated by waves. The movement of the joints is resistant to water-powered rams that pump oil on water-powered motors, which drive rotating generators. Pelamis is the first popularized grid-connected WEC in the world [12].

Another example is Uppsala University's single-body purpose absorber introduced in the Lysekil Project (capacity of 40 kW) located off the western coastlines from Sweden. The Uppsala University point absorber oscillates in heaves and uses an immediate drive rule to excite a linear generator located on the seabed (Figure 1.2) [11, 13]. Presently, the sea-based industry is conducting 10 MW proofing wave energy development off the coastline of Stones, Sweden.

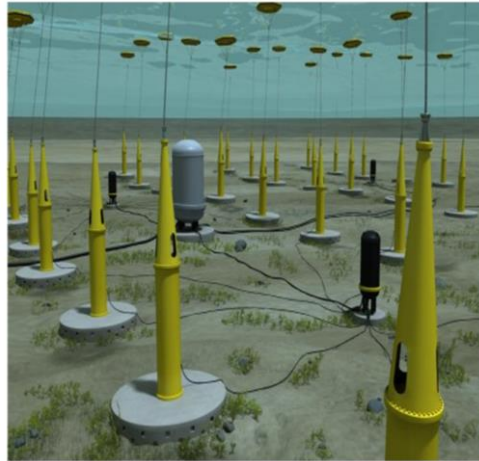


Figure 2: Graphical Drawing of the Uppsala University Point Absorber Organized in a Farm of WECs [14]

After completion, this project will become the world's largest grid-connected wave energy farm [14]. Other remarkable examples of point absorbers include the L-10 WEC created by Oregon State University (USA) [11] and the Archimedes Wave Swing established by Atlantic Wind Connection Ocean Energy (UK) [5]. Heaving WEC, as a suitable wave absorber, is also a suitable wave generator. It can produce waves that destructively overlap with future approaching waves [9]. This phenomenon can be captured by applying control in the WEC. Hence, a well-controlled WEC boosts the captured power, which is characterized as $P_{int} = P_{ex} - P_r$, where P_{ex} is the wave excitation power and P_r is the wave radiation power. The intercepted power, P_{cap} , is then captured through the power take-off device. Useful electrical power, P_{conv} , is produced from the converted captured mechanical power [15]. Wave energy conversion mainly involves two types of control strategies: passive and active. Passive control strategies include electric circuits adjusted at the maximum possible wave significant height and peak frequency of the location through an analytical study. The models use resistive loading and resonance circuits [16]. Passive control strategies are easy to implement and cost effective. However, passive

control strategies do not offer sufficient flexibility to react in the case of continuously fluctuating sea climate, thus causing a narrow absorption bandwidth. On the contrary, active control strategies are online control management techniques that can adjust the WEC dynamics quickly. Despite the effectiveness of active control strategies, these methods are more complicated and expensive than passive methods. Furthermore, to implement rapid control (wave-to-wave control), precise prediction algorithms are required [17].

1.4 Research Problem Statement

To improve the study on WECs, wave energy assessment was carefully selected as the topic of this research. Various studies have focused on marine energy in general and wave energy in particular. However, only a few studies have been implemented in reality. Each research differs in terms of objectives, methodology, strategic control methods used, and final results. The geographic territory of the project is a significant factor in WEC studies. Therefore, wave energy assessment is a highly important topic in marine research.

The purpose of this study is to determine the best location to implement WEC in terms of seabed geography, wind power, and remoteness of the area from the beach to generate the largest amount of electricity.

The location and landscape of the place help define the principal parameters in the study on WECs (wave height and wave period). Depending on these parameters, the following can be selected.

- The most appropriate control method
- Critical devices related to the system specifications

Southern Java Island was selected as the location for this research because no previous study has been conducted in this area. Considering that real data (wave parameters H_s and T) can be obtained, the simulation result was validated against actual data in the final stage, and the designed simulation system was tuned appropriately.

1.5 Wave Energy Assessment Literature Review

This chapter includes a brief previous research work regarding WEC assessments, which contains two sections. The first section is a list of studies done based on the geographical location. The second section shows a different type of program used for WEC simulation.

1.5.1 Studies Conducted Based on Geographical Location

Menorca (Spain) Case

This study was performed to analyze the wave energy resources in Menorca Island by using forecast series data of 17 years. The spatial conveyance of wave power was examined by utilizing information from 12 points around the island. The obtained resources (average wave power of about 8.9 kW/m and average annual wave energy of around 78 MWh/m) were generally modest but were the largest among the Mediterranean Sea region. The most productive areas were the northeast and east locations of the island. Extensive occasional inconstancy was observed, with winters being harsh and summers being mellow. The power matrices of three WECs were considered to evaluate the average power yield at all points. Four spots were identified as the ideal candidates for WEC deployment.

Two accessible datasets for Menorca were used. The first was a hindcast

wave climate database (1996–2013) for 17 years. This wave statistics set was obtained by utilizing the WAM model under the constraint of the wind production of the HIRLAM territorial atmospheric model. The second information source was a wave buoy placed near the island at a depth of 300 *m*. The recorded data were used to validate the numerical wave data. Calculations were performed for significant wave characteristics by using the relative mean absolute error [18].

Portuguese Case

This assessment was performed along the Portuguese coast to analyze the near-shore wave energy resource. The assessment focused on identifying applicable locations for the analysis and development of WEC for commercial application. The study covered the complete west seaside by dividing the region into seven areas parallel to the coast at 50 *m* depths. The accessible wave energy in each area was calculated from near-shore wave parameters by utilizing 15-year ocean wind–wave model simulation data.

This work shows that autonomous wave energy of the measured criteria can be utilized, and the investigation indicates that the part from Peniche to Nazaré with an annual wave energy of approximately 200 *MWh/m* is a reasonable area for near-shore wave energy exploitation, followed by the neighboring area from Nazaré to Figueira da Foz.

The main differences between offshore and near-shore wave energy resources are as follows: the energy resource decreases to under 7% from offshore to near the shore. On the off chance, the exploitable idea can be regarded as a resource measure. The energy resource could surpass 14% if the standard non-constrained basis of assessing accessible energy is utilized.

Two primary conclusions were obtained from this work.

- Establishing a near-shore energy assessment construct with respect to offshore wave conditions only is insufficient and incorrect. A major reduction in wave power is predictable when the coastline does not confront the mean wave path, thus turning a promising offshore district into an uninteresting near-shore range for energy conversion.
- Exposed near-shore areas confronting the leading offshore wave path with a small wave height in the background diminish by refraction. As a result, an unimportant wave control reduction is likely to occur as waves move shoreward. Several near-shore territories can possess a comparable wave energy potential as the corresponding offshore areas [19].

Australia Case

Another study was performed along the Australian shelf (<300 *m*) waters. The AusWAM model for wave direction hindcast from 1997 to 2008 was used. In addition to the available significant wave height and period, wave energy and power were considered.

The important results are summarized as follows:

- Wave power is the most noteworthy on the 3000 *km* long southern Australian rack (southern Western Australia, South Australia, and Tasmania/Victoria), where it produces a time-average value of 25–35 *kW/m* and conveys an average of 800–1100 *GJ/m* of energy in a year.
- New South Wales and southern Queensland racks, with direct time-average wave power of 10–20 *kW/m*, are potential locales for power because they

have a comparative unwavering quality in resource conveyance toward the southern edge.

- The time-average wave power for the large part of the northern Australian rack is $<10 \text{ kW/m}$ [20].

Korean Peninsula Case

In this study, wave assessment was performed for the territory around the Korean peninsula. Offshore wave power was acquired from significant peak periods, wave heights, and wave directions hindcasted for the period of 24 years (1979–2003).

The maximum monthly averaged wave power, which was around 25 kW/m , was detected on the southwestern side of the peninsula in winter. To acquire the wave power value around Hongdo, numerical simulations were executed by observing the averaged monthly waves. The relationship between the significant wave height and energy period was measured to adjust the near-shore wave power acquired from the simulation. Then, wave buoy data were compared with the simulated data validated through the adjustment procedure.

Basically, this work obtained offshore and near-shore wave energies by using different methodology approaches. In offshore wave energy, the hindcast data were used and wind data were re-analyzed as guided by the European Centre for Medium-Range Weather Forecasts (ECMWF); the data were then introduced to the grid-focused points and time steps of the wave simulation model. In the near-shore wave energy, the Simulating WAVes Nearshore (SWAN) coastal wave model was utilized in the assessment. SWAN determines the evolution of wave action density by

utilizing the action balance equation. Two motivations were used to investigate the near-shore wave energy around Hongdo. First, a definite database was used to determine the capacity of the wave energy converter, and second, the methodology was verified to evaluate near-shore wave energy resources involving the correction factor [21].

Mediterranean Case

A high-resolution assessment of the wave energy resources in the Mediterranean was performed. The energy resources were assessed through a numerical simulation using a third-generation ocean wave model for the period 2001–2010.

The model outcomes were in line with a large portion of the accessible wave buoy and satellite altimeter data. Starting with the model outcomes, a point-by-point investigation of wave energy availability in the Mediterranean Sea was completed. The western Sardinia coast and the Sicilian Channel are considered to be among the most profitable territories in the entire Mediterranean. The simulation outcomes revealed the presence of major spatial variations in wave power availability even on small spatial measures along these coastlines. For various selected areas in these two ranges, an in-depth investigation of the dispersion of wave energy, including wave heights, periods, and directions, was presented. Moreover, the regular and inter-annual variations in wave energy potential were analyzed and discussed [22].

1.5.2 Wave Resource Assessment Programs

This section shows different wave simulation commercial programs that are commonly used in wave energy study for modeling and simulation purposes. A

number of programs are available on the market, and these programs vary with regard to the way they work, data type, type of waves, the depth at which the study is applied, and accuracy of the results. Several of them are available for free, and others must be purchased.

SWAN program

SWAN is a third-generation wave model that computes random, short-crested, wind-generated waves in coastal regions and inland waters [23]. The model is used to obtain realistic estimations of wave parameters in coastal areas, lakes, and estuaries from given wind, bottom, and current situations.

SWAN can also be used on any scale identified with wind-created surface gravity waves. The model depends on the wave activity-adjusted condition with sources and sinks [24].

SWAN was developed at Delft University of Technology and is available for free at <http://www.swan.tudelft.nl>. SWAN is used by many government authorities, research institutes, and consultants worldwide [25].

Grids are of two types: structured and unstructured. Structured grids can be rectilinear and uniform or wavy. They generally comprise quadrilaterals in which the number of framework cells that meet one another in an inside lattice point is 4. In unstructured grids, this number can be self-imposed (often between 4 and 10). Thus, the level of adaptability regarding the framework point dissemination of unstructured matrices is much more ideal than that of structured grids.

Unstructured grids can have triangles or a combination of triangles and quadrilaterals (hybrid grids). In the updated SWAN version, only triangular meshes

can be employed.

SWAN has several limitations. The DIA approximation for quadruplet wave–wave interactions relies on the width of the directional appropriation of the wave spectrum. SWAN works reasonably in many cases but demonstrates poor approximation for long-crested waves (narrow directional distribution).

Additionally, SWAN depends on frequency resolution. It works reasonably in many cases but demonstrates poor approximation for frequency resolutions with proportions far different from 10%. This is an essential issue in SWAN compared with other third-generation wave models, such as WAM and Wave Watch III.

LTA approximation for triad wave–wave associations relies on the width of the directional circulation of the wave spectrum. The present tuning in SWAN (for default settings, see command triad) works sensibly as a rule but has been acquired from perceptions in a narrow wave flume (long-crested waves).

As an alternative SWAN process wave-induced setup, in 1D cases, the calculations depend on exact equations. In 2D cases, the calculations depend on approximate equations. This estimation in SWAN can only be applied to open coasts (boundless supply of water from outside the domain, such as near-shore coasts and estuaries) and cannot be applied to closed basins, such as lakes. The effects of wave-induced currents are constantly ignored. SWAN does not compute wave-induced currents. Such currents must be provided as an input to SWAN.

Diffraction must be utilized in regions where variations in wave height are large within a horizontal scale of a couple of wavelengths. The calculation of diffraction in arbitrary geophysical conditions is complicated and requires significant

processing. To avoid this inconvenience, a phase-decoupled approach is utilized in SWAN so that the same subjective conduct of spatial redistribution and changes in wave direction are obtained. However, this approach cannot effectively handle diffraction in harbors or before reflecting obstacles. SWAN is particularly intended for coastal applications that do not require such flexibility in scale [24].

TOMAWAC program

TOMAWAC is a logical and scientific program that models progressions in time and spatial domains of the power range of wind-driven waves and wave tumult for applications in the oceanic field and intercontinental seas in addition to coastal areas. The model uses limited components of formalism in discretizing an ocean area and is built “based on the computational subroutines of the TELEMAC system as developed by the EDF R&D’s Laboratoire National d’Hydraulique et Environnement.” The acronym TOMAWAC used to name the program was acquired from the corresponding English translation “TELEMAC-based Operational Model Addressing Wave Action Computation.”

TOMAWAC is one of the models that make up the TELEMAC system; it addresses different issues that are identified with free surface sea type and river, underground flows, and the associated physical processes of water quality and bed-load transport [26].

TOMAWAC can consider any of the following physical phenomena.

- Refraction by currents
- Dissipation through bathymetric wave breaking
- Dissipation through counter-current wave breaking

- Wind-generated waves
- Refraction on the bottom

In each purpose of the computational mesh, TOMAWAC obtains the following information.

- Significant wave height
- Mean wave direction
- Wave-induced currents
- Mean wave frequency
- Peak wave frequency
- Radiation stresses [27]

TOMAWAC has various applications but possesses several limitations. TOMAWAC is intended to be applied from the ocean field up to the coastal territory. The limits of the application scope can be controlled by the estimation of relative profundity d/L , where d represents the water height (in meters) and L represents the wave length (in meters) corresponding to the peak spectral frequency for unpredictable waves.

The TOMAWAC application domain involves the following:

- **Oceanic field** described by vast water depths (above 0.5 m). The predominant physical processes are non-linear quadruplet interactions, wind driven waves, and white-capping dissipation.
- **Continental seas and medium depths** described by a relative water depth ranging between 0.05 and 0.5 m . Bottom friction, shoaling (wave development because of a base ascent), and impacts of refraction caused by

the bathymetry and/or currents are also considered.

- **Coastal domain**, including shoals or near-shore regions (water depth lower than 0.05 *m*). For these shallow water zones, such physical processes as bottom friction, bathymetric breaking, and non-linear triad interactions among waves should be considered. In addition, considering the impacts of unsteady sea level and currents could be valuable because of the tide and weather-dependent surges. Through a limited component spatial discretization, one computational grid may incorporate mesh cells, among which the proportion of the largest sizes to the smallest ones may reach or even exceed 100.

These reasons make TOMAWAC applicable to an ocean domain that has highly variable relative water depths. Specifically, coastal zones can be finely represented.

The application space of TOMAWAC excludes harbor regions and, in general, every case in which the impacts of reflection on structures and diffraction may not be ignored.

The initial version of a diffraction model is accessible in TOMAWAC and can represent several diffraction effects. However, the model still presents limitations. The use of phase-resolving models is highly recommended when a detailed simulation of diffraction effects is required [26].

MIKE 21 Spectral Wave

MIKE 21 Spectral Wave (SW) is a state-of-the-art third-generation spectral wind-wave model established by the Danish Hydraulic Institute (DHI). This model

can simulate the growth, decay, and wind-generated wave transformation and swells in offshore and coastal zones.

MIKE 21 SW has two different formulations.

- Fully spectral formulation
- Directional decoupled parametric formulation

The first formulation (fully spectral formulation) is constructed based on the wave action conservation equation. The second formulation (directional decoupled parametric formulation) is constructed based on a parameterization of the wave action conservation equation. Parameterization is achieved in the frequency domain by presenting the zeroth and first moments of the wave action spectrum. Fundamental conservation equations are formulated in either Cartesian coordinate small-scale applications or polar circular coordinates for extensive applications.

The following physical phenomena are included in the fully spectral model.

- Wave growth by the action of wind
- Dissipation due to bottom friction
- Dissipation due to depth-induced wave breaking
- Dissipation due to white capping
- Non-linear wave–wave interaction
- Effect of ice coverage on the wave field
- Effect of time-varying water depth
- Refraction and shoaling due to depth variations

- Wave–current interaction

An unstructured mesh procedure is utilized in the geographical domain. A fractional step approach is used for time integration, and a multi-sequence explicit technique is applied for the propagation of wave action.

MIKE 21 SW has several features, which are presented below.

- The two decoupled parametric formulations are available (fully spectral and directional)
- Source capacities based on state-of-the-art third-generation formulations
- Stationary and semi-stationary solutions
- Optimal level of flexibility in defining bathymetry and ambient flow conditions
- Coupling with hydrodynamic flow for the modeling of wave current interaction and time-varying water depth
- Flooding and drying regarding time-varying water depths
- Cell-centered finite volume method
- Extensive model output parameters

MIKE 21 SW has various application areas and limitations. MIKE 21 SW is utilized for the assessment of wave environments in offshore and coastal territories in hindcast and forecast modes. A main application zone is the design of offshore, coastal, and port structures in which exact assessment of wave loads is of extreme significance to the safe and cost-effective design of these structures.

Measured data are often unavailable from periods that are sufficiently long to consider the establishment of sufficiently precise estimates of extreme sea states. For this situation, the measured data can be complemented with hindcast data through the

simulation of wave conditions through historical storms by using MIKE 21 SW.

MIKE 21 SW is particularly appropriate for simultaneous wave forecast and analysis on regional and local scales. Coarse spatial and transient determinations are utilized for the regional part of the mesh with a high-resolution boundary, and the shallow water environment at the coastline is defined by a depth-adaptive mesh.

MIKE 21 SW can be utilized to analyze wave conditions and the related radiation stresses. Long-shore currents and sediment transport are then computed by utilizing the flow. Sediment transport models are accessible in the MIKE 21 package. For particular uses, the directional decoupled parametric formulation of MIKE 21 SW is an excellent combination of computational effort and accuracy [28]. Further explanations on MIKE 21 SW and its functions are presented in Section 2.1.

1.5.3 Review of Control Techniques

Many reviews have been conducted on the utilization of control techniques to enhance the execution of heaving point absorbers (HPAs). Basically, the movement of an HPA buoy is controlled in such a manner that a reverberation state is reached between the buoy and incoming waves [9]. This state is commonly realized by controlling the force applied on the buoy by utilizing a power take-off (PTO) device, such as linear generators and related power converters. The proposed control techniques for HPAs can generally be classified into two: reference-based and non-reference-based control techniques.

In the reference-based control strategy, an ideal or imperfect velocity reference for the buoy is created. Then, the buoy's actual velocity is adjusted to follow the velocity reference by utilizing a servo feedback control system regardless

of the presence of modelling uncertainties. A case of this type of control procedure can be found in [41]. In this strategy, the created reference velocity and servo feedback control system use radiation impedance and model predictive control (MPC).

However, the proposed clarification has several disadvantages, such as the way the reference is tuned at a single-peak wave frequency, the standard MPC is computationally costly, and the robustness of the MPC is not adopted. An additional reference-based approach for irregular sea states was proposed in [42, 10], in which a look-up table was built based on the radiation resistance and features of irregular sea states with a maximum control force constraint.

The servo feedback control system is executed by utilizing an internal model control. A sliding model control was used for the controller in the servo feedback control system in [43, 44]. A comparative approach was proposed in [45], in which the reference was produced by utilizing a linear quadratic problem constrained by the buoy's excursion, and the servo feedback control system used a model-free controller.

In the non-reference-based control strategy, the least difficult type of these controllers uses passive control strategies. Examples include the resistive and reactive loading techniques mentioned in [46]. Intelligent control is likewise conceivable and applied using either fuzzy controllers or a combination of a fuzzy controller and online optimization algorithms, such as what was considered in [47, 48]. A maximum power point tracking (MPPT) method has been recommended and was tried numerically and experimentally in [49]. The MPPT method did not generate an optimum reference, and conventional "observe and perturb" was

executed by using power electronic components. A constrained linear MPC strategy was used in [38]. Although MPPT is easy to formulate, this procedure suffers from model uncertainties. A nonlinear MPC procedure was proposed in [39], in which improved robustness abilities were achieved at the expense of an expanded computational burden.

1.6 Thesis Structure

This thesis is organized into seven chapters. Chapter 1 presents the introduction and literature review. Chapter 2 contains the methodology of the wave energy converter assessment. Chapter 3 presents the mechanical and electrical modeling. Chapter 4 explains the servo feedback control system and presents the reference generation method. The proposed control technique is also compared with various existing reference-based and non-reference-based WEC control techniques. Chapter 5 presents the most important assessment results. Chapter 6 displays the control result. Chapter 7 summarizes the primary discoveries and conclusions obtained from this study and describes future research work that will be completed by UAE University's wave energy research team.

Chapter 2: WEC Assessment Methodology

2.1 MIKE 21 SW program

The model in this study was developed with a powerful program called MIKE 21 SW from DHI. MIKE 21 SW is one of the packages in the MIKE Zero program. DHI, previously known as DHI Institute for Water and Environment, is an international company that develops programs and engineering solutions with specialization in hydrological modeling. DHI has dedicated more than 50 years to researching and developing solutions for real-life challenges in water environments, including rivers, coastlines, oceans, and urban water systems. Furthermore, DHI has implemented solutions to actual problems in more than 140 countries.

The MIKE Zero program powered by DHI contains various packages (shown below).

- **MIKE Hydro**

MIKE Hydro includes Basin Module and River Module. MIKE Hydro Basin Module is a versatile and highly flexible model framework for various applications concerning management and planning aspects of water resources within a river basin. MIKE Hydro River Module is the modeling framework used for defining and executing 1D river models for various river-related project applications. Figure 3 shows a picture of Pacitan River in East Java Indonesia.



Figure 3: Pacitan River in East Java Indonesia

- **MIKE 11**

MIKE 11 is mostly used for river modeling. It can handle various projects, such as river navigation, flooding, water quality, forecasting, sediment transport, and a combination of these projects.

- **MIKE 21**

MIKE 21 is mostly used for modeling coasts and seas. It can handle physical, chemical, and biological processes in coastal or marine areas.

- **MIKE 3**

MIKE 3 handles the simulation for 3D modeling free surface flows and water quality processes. It is mostly used as a standard program for environmental and ecological studies.

- **MIKE FLOOD**

MIKE FLOOD is a package for modeling flooding phenomena. It is a comprehensive module for understanding the flooding process and for the analysis and even testing of mitigation measures. It integrates flood plains, rivers, streets, weather, and buildings into one package.

- MIKE SHE

MIKE SHE is a unique program for coupled and integrated surface water and groundwater modeling. It can handle process models for unsaturated and overland flows, vegetation-based evapotranspiration, groundwater flow, and water quality.

2.2 Study Domain (Indonesia)

Indonesia is the world's largest archipelagic country. It is located mainly in Southeast Asia. Figure 4 shows the map of Indonesia and its more than 15000 islands, including the five largest islands, namely, Sumatera, Kalimantan (Borneo), Sulawesi, Irian Jaya, and Java. Indonesia lies between the Indian Ocean and Pacific Ocean. This condition makes Indonesia the most strategic route in oceanic trading. Furthermore, Indonesia might have the largest amount of potential wave energy resources.



Figure 4: Map of Indonesia

The domain in this work is in the Indian Ocean on the Java Island coastline because the demand for electricity in Java Island is tremendously high. In fact, Java Island is the most populated island in Indonesia; its population accounts for around 58% of the total population of Indonesia (>237 million) [40]. Additionally, Java

Island is the center of the economic process in Indonesia and houses major industries. Furthermore, the domain is squished to be the central part of Java Island, Central Java Province, and Daerah Istimewa Yogyakarta (DIY)/Special Region of Yogyakarta Province. Figure 5 shows the area of study and observation buoy position, which is close to the office of *Badan Pengkajian dan Penerapan Teknologi* (BPPT) or Agency for the Assessment and Application of Technology located in Baron Beach. The buoy is located precisely at a longitude of 110.547° and a latitude of -8.1364° .

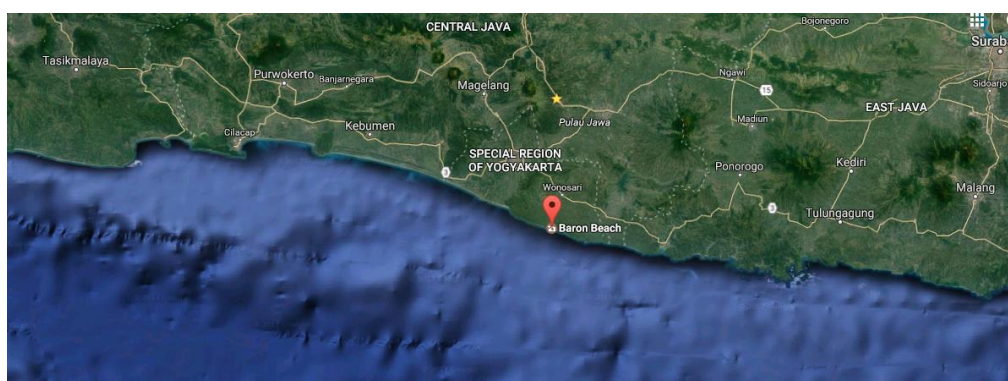


Figure 5: Indian Ocean of Central Java and DIY, Java Island, Indonesia

2.2.1 Simulation Domain

To determine the domain, coastline digital data were extracted. Table 1 shows the resources used to download or digitalize coastline data.

Table 1: Coastline Digital Data Resources

Source	Details
National Oceanic and Atmospheric Administration (NOAA), U.S. Department of Commerce	World Geodetic System (WGS84) datum
Digitization from Map/Chart	Program dependent
Sea zone	Coarse data (unfree)
Ordnance Survey (OS) Master map	British National Grid datum

Owing to its resolution, data details, and free access, National Oceanic and Atmospheric Administration (NOAA) is known as the finest source and was used in this work. The details of the process are listed below.

Download the Coastline Data from NOAA

The download link is <https://www.ngdc.noaa.gov/mgg/shorelines/gshhs.html>. The site shows the database of global self-consistent, hierarchical, and high-resolution geography (GSHHG) data. The five available resolutions acquired from the website are shown in Table 2.

Table 2: Five Resolution Types of GSHHG Coastline Data

Resolution Type	Symbol	Resolution Details
Full Resolution	f	Original resolution
High Resolution	h	~80% reduction from f in quality and size
Intermediate Resolution	i	~80% reduction from h
Low Resolution	l	~80% reduction from i
Crude Resolution	c	~80% reduction from l

Full resolution was utilized to achieve a good result. However, the format of GSHHG data is SHAPE data type, which does not match the MIKE program. The MIKE program can process XYZ files, which can be converted from the SHAPE format. Prior to this conversion, the file provided by GSHHG is fully world coastline data, which make up a huge file and cost much in terms of processing and editing time. To reduce the cost, a calculation domain of interest was selected.

Area Selection

In this step, geographic information system (GIS) software is required to select a particular area. The QGIS software, which was previously known as the Quantum-GIS (QGIS) software, was used to extract the area around Java Island. Figure 6 shows the world coastline data shown in QGIS software, and Figure 7 shows the area after selection (dark blue region).

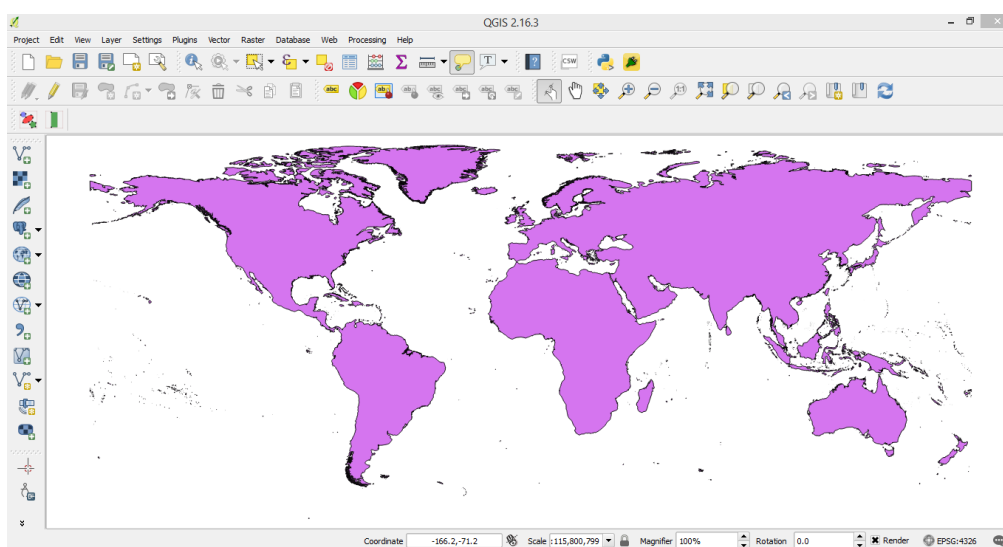


Figure 6: World Coastline Data from GSHHG

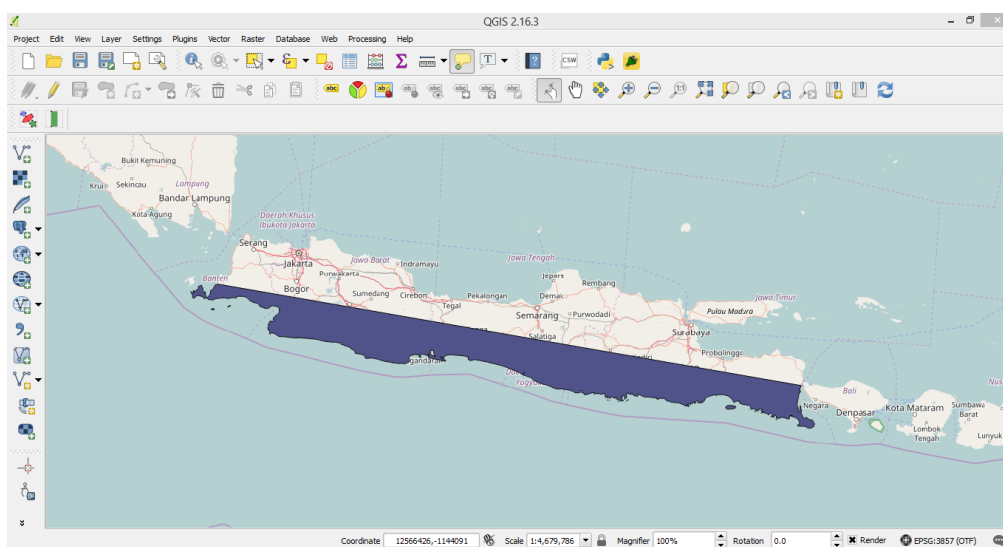


Figure 7: Selected Coastline Data above Real World Map

Convert Shape to XYZ Data Type

To convert a SHAPE file to the XYZ format, the Geophysical Data System–Next Generation (GEODAS-NG) software in Coastline Extractor provided by the National Centers for Environmental Information and NOAA was utilized. The software is free and can be downloaded from the website <https://www.ngdc.noaa.gov/mgg/geodas/>.

Figures 8 and 9 show the GEODAS-NG software and SHAPE file of the selected area, respectively.

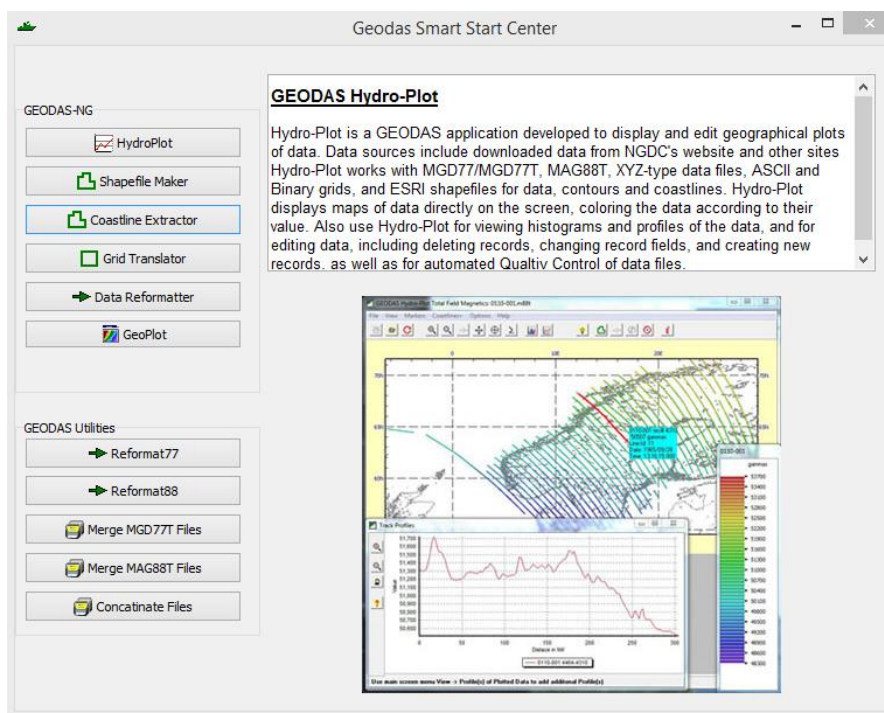


Figure 8: GEODAS-NG Software

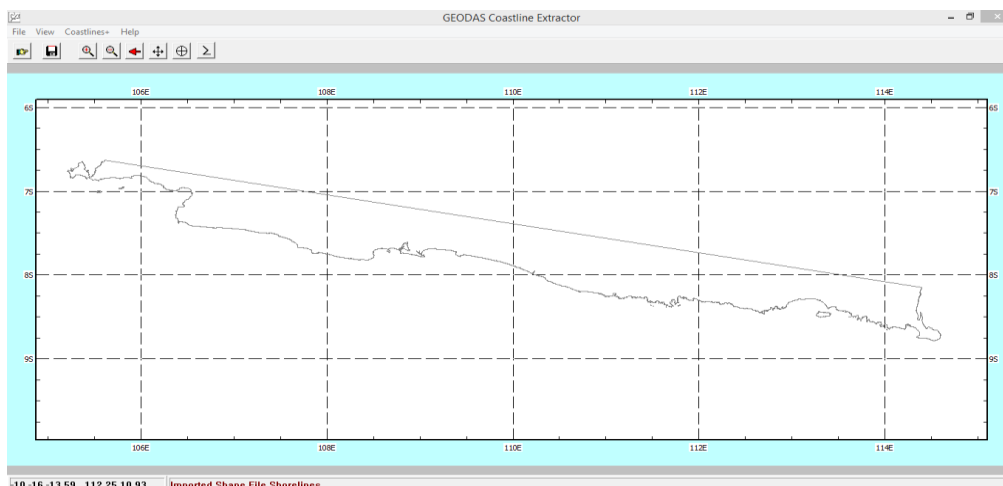


Figure 9: SHAPE File of Selected Area Shown in Coastline Extractor

The XYZ file from GEODAS-NG software is a three-column text file that consists of longitude, latitude, and zero values, as shown in Figure 10. This file was edited in the MIKE program for the final simulation geometry.

```

108.882917 -7.752500 0.00
108.883306 -7.752111 0.00
108.884139 -7.752111 0.00
108.884972 -7.752111 0.00
108.885417 -7.752528 0.00
108.884972 -7.752917 0.00
108.884139 -7.752917 0.00
108.883306 -7.752917 0.00
108.882917 -7.752500 0.00
114.023750 -8.606694 0.00
114.024361 -8.606069 0.00

```

Figure 10: Sample of XYZ File Extracted from GEODAS-NG Software

Finalizing Simulation Domain

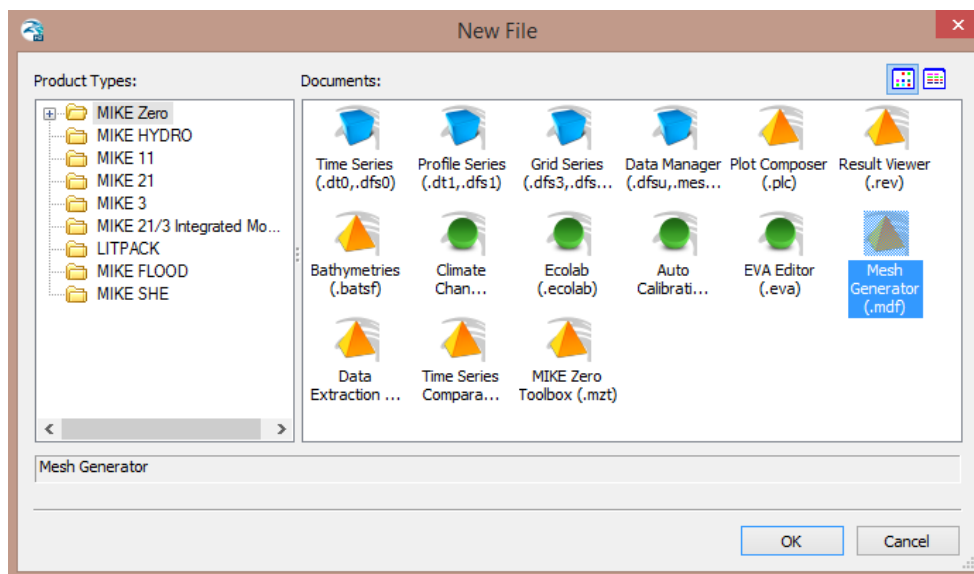


Figure 11: Mesh Generator Feature under MIKE Zero Package

Determining the simulation domain is important because it is related to the number of meshes and nodes, which affects the simulation time. The domain from the generated XYZ file was edited with the mesh generator feature in the MIKE Zero program, as shown in Figure 11.

The final simulation domain of the Central Java and DIY region was set to a minimum 5 km ocean region, as depicted in Figure 12.

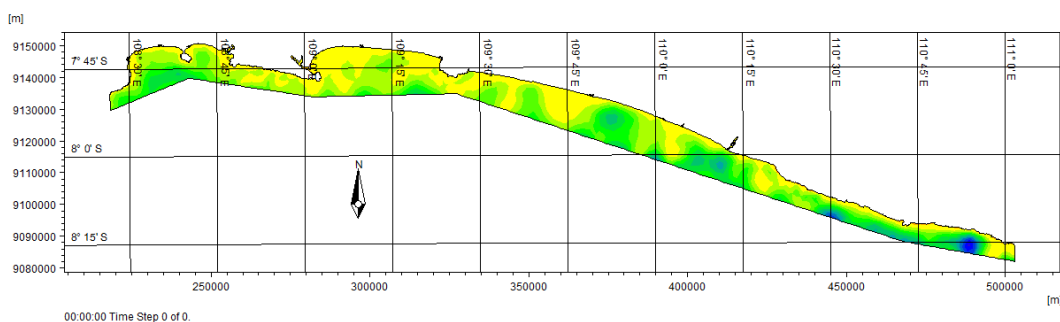


Figure 12: Final Simulation Region for Central Java and DIY Regions

2.3 Model Setup

MIKE 21 SW can hindcast or forecast the assessment of wave climates in coastal and offshore areas. Hindcasting or backtesting, also known as historical re-forecasting, is a method that utilizes known or closely estimated past data to test the quality of a mathematical model in comparison with current observed information. Figure 13 shows a time block diagram of the hindcast method.

Furthermore, MIKE 21 SW covers several physical phenomena, such as the following:

- Wave growth by wind
- Nonlinear wave-to-wave interaction
- White capping dissipation
- Bottom friction dissipation
- Depth-induced wave breaking dissipation
- Refraction and shoaling due to depth variations
- Current and wave interaction
- Effect of time-varying water depth, flooding, and drying

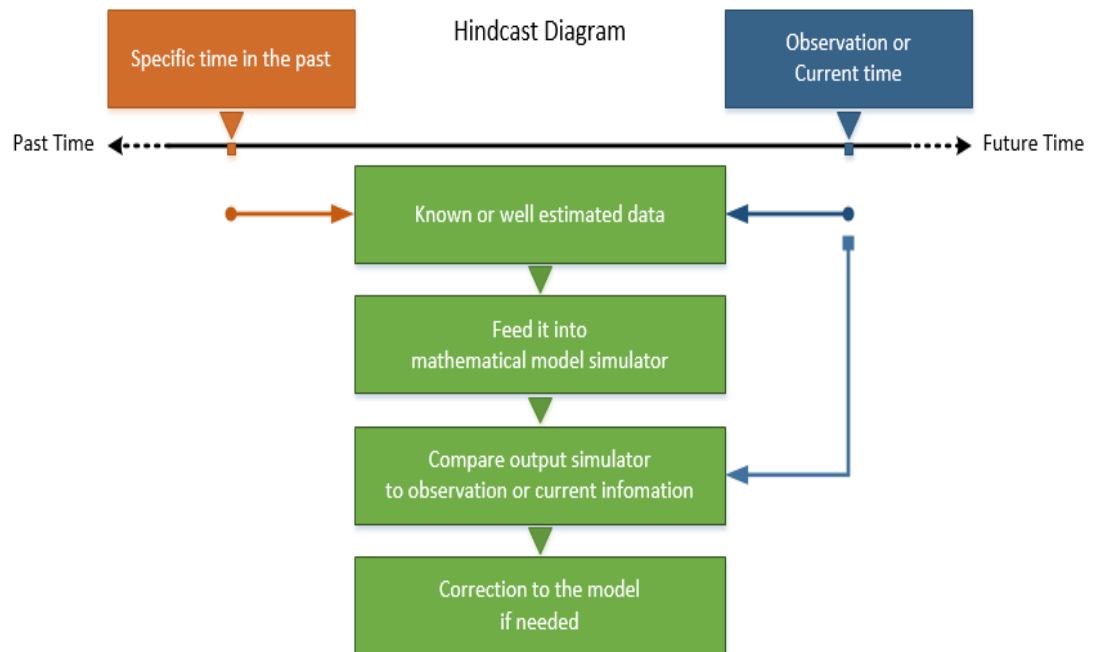


Figure 13: Hindcast block diagram

2.3.1 Data Collection

Several types of data, such as wind velocities, wave periods, significant wave height, mean wave direction, and bathymetry, are required to complete the model. The first four types of data are available in the ECMWF official website, namely, <http://apps.ecmwf.int/datasets/data/interim-full-daily/levtype=sfc/>. Figures 14 and 15 show the appearance of the user-friendly menu from the website, where the date, time step, and parameters can be selected.

Select date

Select a date in the interval 1979-01-01 to 2016-12-31

Start date: End date:

Select a list of months

	Jan	Feb	Mar	Apr	May	Jun	Jul	Aug	Sep	Oct	Nov	Dec	Jan	Feb	Mar	Apr	May	Jun	Jul	Aug	Sep	Oct	Nov	Dec
1979	<input type="checkbox"/>	<input type="checkbox"/>	<input type="checkbox"/>	<input type="checkbox"/>	<input type="checkbox"/>	<input type="checkbox"/>	<input type="checkbox"/>	<input type="checkbox"/>	<input type="checkbox"/>	<input type="checkbox"/>	<input type="checkbox"/>	<input type="checkbox"/>	1980	<input type="checkbox"/>	<input type="checkbox"/>	<input type="checkbox"/>	<input type="checkbox"/>	<input type="checkbox"/>	<input type="checkbox"/>	<input type="checkbox"/>	<input type="checkbox"/>	<input type="checkbox"/>	<input type="checkbox"/>	<input type="checkbox"/>
1981	<input type="checkbox"/>	<input type="checkbox"/>	<input type="checkbox"/>	<input type="checkbox"/>	<input type="checkbox"/>	<input type="checkbox"/>	<input type="checkbox"/>	<input type="checkbox"/>	<input type="checkbox"/>	<input type="checkbox"/>	<input type="checkbox"/>	<input type="checkbox"/>	1982	<input type="checkbox"/>	<input type="checkbox"/>	<input type="checkbox"/>	<input type="checkbox"/>	<input type="checkbox"/>	<input type="checkbox"/>	<input type="checkbox"/>	<input type="checkbox"/>	<input type="checkbox"/>	<input type="checkbox"/>	<input type="checkbox"/>
1983	<input type="checkbox"/>	<input type="checkbox"/>	<input type="checkbox"/>	<input type="checkbox"/>	<input type="checkbox"/>	<input type="checkbox"/>	<input type="checkbox"/>	<input type="checkbox"/>	<input type="checkbox"/>	<input type="checkbox"/>	<input type="checkbox"/>	<input type="checkbox"/>	1984	<input type="checkbox"/>	<input type="checkbox"/>	<input type="checkbox"/>	<input type="checkbox"/>	<input type="checkbox"/>	<input type="checkbox"/>	<input type="checkbox"/>	<input type="checkbox"/>	<input type="checkbox"/>	<input type="checkbox"/>	<input type="checkbox"/>
1985	<input type="checkbox"/>	<input type="checkbox"/>	<input type="checkbox"/>	<input type="checkbox"/>	<input type="checkbox"/>	<input type="checkbox"/>	<input type="checkbox"/>	<input type="checkbox"/>	<input type="checkbox"/>	<input type="checkbox"/>	<input type="checkbox"/>	<input type="checkbox"/>	1986	<input type="checkbox"/>	<input type="checkbox"/>	<input type="checkbox"/>	<input type="checkbox"/>	<input type="checkbox"/>	<input type="checkbox"/>	<input type="checkbox"/>	<input type="checkbox"/>	<input type="checkbox"/>	<input type="checkbox"/>	<input type="checkbox"/>
1987	<input type="checkbox"/>	<input type="checkbox"/>	<input type="checkbox"/>	<input type="checkbox"/>	<input type="checkbox"/>	<input type="checkbox"/>	<input type="checkbox"/>	<input type="checkbox"/>	<input type="checkbox"/>	<input type="checkbox"/>	<input type="checkbox"/>	<input type="checkbox"/>	1988	<input type="checkbox"/>	<input type="checkbox"/>	<input type="checkbox"/>	<input type="checkbox"/>	<input type="checkbox"/>	<input type="checkbox"/>	<input type="checkbox"/>	<input type="checkbox"/>	<input type="checkbox"/>	<input type="checkbox"/>	<input type="checkbox"/>
1989	<input type="checkbox"/>	<input type="checkbox"/>	<input type="checkbox"/>	<input type="checkbox"/>	<input type="checkbox"/>	<input type="checkbox"/>	<input type="checkbox"/>	<input type="checkbox"/>	<input type="checkbox"/>	<input type="checkbox"/>	<input type="checkbox"/>	<input type="checkbox"/>	1990	<input type="checkbox"/>	<input type="checkbox"/>	<input type="checkbox"/>	<input type="checkbox"/>	<input type="checkbox"/>	<input type="checkbox"/>	<input type="checkbox"/>	<input type="checkbox"/>	<input type="checkbox"/>	<input type="checkbox"/>	<input type="checkbox"/>
1991	<input type="checkbox"/>	<input type="checkbox"/>	<input type="checkbox"/>	<input type="checkbox"/>	<input type="checkbox"/>	<input type="checkbox"/>	<input type="checkbox"/>	<input type="checkbox"/>	<input type="checkbox"/>	<input type="checkbox"/>	<input type="checkbox"/>	<input type="checkbox"/>	1992	<input type="checkbox"/>	<input type="checkbox"/>	<input type="checkbox"/>	<input type="checkbox"/>	<input type="checkbox"/>	<input type="checkbox"/>	<input type="checkbox"/>	<input type="checkbox"/>	<input type="checkbox"/>	<input type="checkbox"/>	<input type="checkbox"/>
1993	<input type="checkbox"/>	<input type="checkbox"/>	<input type="checkbox"/>	<input type="checkbox"/>	<input type="checkbox"/>	<input type="checkbox"/>	<input type="checkbox"/>	<input type="checkbox"/>	<input type="checkbox"/>	<input type="checkbox"/>	<input type="checkbox"/>	<input type="checkbox"/>	1994	<input type="checkbox"/>	<input type="checkbox"/>	<input type="checkbox"/>	<input type="checkbox"/>	<input type="checkbox"/>	<input type="checkbox"/>	<input type="checkbox"/>	<input type="checkbox"/>	<input type="checkbox"/>	<input type="checkbox"/>	<input type="checkbox"/>
1995	<input type="checkbox"/>	<input type="checkbox"/>	<input type="checkbox"/>	<input type="checkbox"/>	<input type="checkbox"/>	<input type="checkbox"/>	<input type="checkbox"/>	<input type="checkbox"/>	<input type="checkbox"/>	<input type="checkbox"/>	<input type="checkbox"/>	<input type="checkbox"/>	1996	<input type="checkbox"/>	<input type="checkbox"/>	<input type="checkbox"/>	<input type="checkbox"/>	<input type="checkbox"/>	<input type="checkbox"/>	<input type="checkbox"/>	<input type="checkbox"/>	<input type="checkbox"/>	<input type="checkbox"/>	<input type="checkbox"/>
1997	<input type="checkbox"/>	<input type="checkbox"/>	<input type="checkbox"/>	<input type="checkbox"/>	<input type="checkbox"/>	<input type="checkbox"/>	<input type="checkbox"/>	<input type="checkbox"/>	<input type="checkbox"/>	<input type="checkbox"/>	<input type="checkbox"/>	<input type="checkbox"/>	1998	<input type="checkbox"/>	<input type="checkbox"/>	<input type="checkbox"/>	<input type="checkbox"/>	<input type="checkbox"/>	<input type="checkbox"/>	<input type="checkbox"/>	<input type="checkbox"/>	<input type="checkbox"/>	<input type="checkbox"/>	<input type="checkbox"/>
1999	<input type="checkbox"/>	<input type="checkbox"/>	<input type="checkbox"/>	<input type="checkbox"/>	<input type="checkbox"/>	<input type="checkbox"/>	<input type="checkbox"/>	<input type="checkbox"/>	<input type="checkbox"/>	<input type="checkbox"/>	<input type="checkbox"/>	<input type="checkbox"/>	2000	<input type="checkbox"/>	<input type="checkbox"/>	<input type="checkbox"/>	<input type="checkbox"/>	<input type="checkbox"/>	<input type="checkbox"/>	<input type="checkbox"/>	<input type="checkbox"/>	<input type="checkbox"/>	<input type="checkbox"/>	<input type="checkbox"/>
2001	<input type="checkbox"/>	<input type="checkbox"/>	<input type="checkbox"/>	<input type="checkbox"/>	<input type="checkbox"/>	<input type="checkbox"/>	<input type="checkbox"/>	<input type="checkbox"/>	<input type="checkbox"/>	<input type="checkbox"/>	<input type="checkbox"/>	<input type="checkbox"/>	2002	<input type="checkbox"/>	<input type="checkbox"/>	<input type="checkbox"/>	<input type="checkbox"/>	<input type="checkbox"/>	<input type="checkbox"/>	<input type="checkbox"/>	<input type="checkbox"/>	<input type="checkbox"/>	<input type="checkbox"/>	<input type="checkbox"/>
2003	<input type="checkbox"/>	<input type="checkbox"/>	<input type="checkbox"/>	<input type="checkbox"/>	<input type="checkbox"/>	<input type="checkbox"/>	<input type="checkbox"/>	<input type="checkbox"/>	<input type="checkbox"/>	<input type="checkbox"/>	<input type="checkbox"/>	<input type="checkbox"/>	2004	<input type="checkbox"/>	<input type="checkbox"/>	<input type="checkbox"/>	<input type="checkbox"/>	<input type="checkbox"/>	<input type="checkbox"/>	<input type="checkbox"/>	<input type="checkbox"/>	<input type="checkbox"/>	<input type="checkbox"/>	<input type="checkbox"/>
2005	<input type="checkbox"/>	<input type="checkbox"/>	<input type="checkbox"/>	<input type="checkbox"/>	<input type="checkbox"/>	<input type="checkbox"/>	<input type="checkbox"/>	<input type="checkbox"/>	<input type="checkbox"/>	<input type="checkbox"/>	<input type="checkbox"/>	<input type="checkbox"/>	2006	<input type="checkbox"/>	<input type="checkbox"/>	<input type="checkbox"/>	<input type="checkbox"/>	<input type="checkbox"/>	<input type="checkbox"/>	<input type="checkbox"/>	<input type="checkbox"/>	<input type="checkbox"/>	<input type="checkbox"/>	<input type="checkbox"/>
2007	<input type="checkbox"/>	<input type="checkbox"/>	<input type="checkbox"/>	<input type="checkbox"/>	<input type="checkbox"/>	<input type="checkbox"/>	<input type="checkbox"/>	<input type="checkbox"/>	<input type="checkbox"/>	<input type="checkbox"/>	<input type="checkbox"/>	<input type="checkbox"/>	2008	<input type="checkbox"/>	<input type="checkbox"/>	<input type="checkbox"/>	<input type="checkbox"/>	<input type="checkbox"/>	<input type="checkbox"/>	<input type="checkbox"/>	<input type="checkbox"/>	<input type="checkbox"/>	<input type="checkbox"/>	<input type="checkbox"/>
2009	<input type="checkbox"/>	<input type="checkbox"/>	<input type="checkbox"/>	<input type="checkbox"/>	<input type="checkbox"/>	<input type="checkbox"/>	<input type="checkbox"/>	<input type="checkbox"/>	<input type="checkbox"/>	<input type="checkbox"/>	<input type="checkbox"/>	<input type="checkbox"/>	2010	<input type="checkbox"/>	<input type="checkbox"/>	<input type="checkbox"/>	<input type="checkbox"/>	<input type="checkbox"/>	<input type="checkbox"/>	<input type="checkbox"/>	<input type="checkbox"/>	<input type="checkbox"/>	<input type="checkbox"/>	<input type="checkbox"/>
2011	<input type="checkbox"/>	<input type="checkbox"/>	<input type="checkbox"/>	<input type="checkbox"/>	<input type="checkbox"/>	<input type="checkbox"/>	<input type="checkbox"/>	<input type="checkbox"/>	<input type="checkbox"/>	<input type="checkbox"/>	<input type="checkbox"/>	<input type="checkbox"/>	2012	<input type="checkbox"/>	<input type="checkbox"/>	<input type="checkbox"/>	<input type="checkbox"/>	<input type="checkbox"/>	<input type="checkbox"/>	<input type="checkbox"/>	<input type="checkbox"/>	<input type="checkbox"/>	<input type="checkbox"/>	<input type="checkbox"/>
2013	<input type="checkbox"/>	<input type="checkbox"/>	<input type="checkbox"/>	<input type="checkbox"/>	<input type="checkbox"/>	<input type="checkbox"/>	<input type="checkbox"/>	<input type="checkbox"/>	<input type="checkbox"/>	<input type="checkbox"/>	<input type="checkbox"/>	<input type="checkbox"/>	2014	<input type="checkbox"/>	<input type="checkbox"/>	<input type="checkbox"/>	<input type="checkbox"/>	<input type="checkbox"/>	<input type="checkbox"/>	<input type="checkbox"/>	<input type="checkbox"/>	<input type="checkbox"/>	<input type="checkbox"/>	<input type="checkbox"/>
2015	<input type="checkbox"/>	<input type="checkbox"/>	<input type="checkbox"/>	<input type="checkbox"/>	<input type="checkbox"/>	<input type="checkbox"/>	<input type="checkbox"/>	<input type="checkbox"/>	<input type="checkbox"/>	<input type="checkbox"/>	<input type="checkbox"/>	<input type="checkbox"/>	2016	<input type="checkbox"/>	<input type="checkbox"/>	<input type="checkbox"/>	<input type="checkbox"/>	<input type="checkbox"/>	<input type="checkbox"/>	<input type="checkbox"/>	<input type="checkbox"/>	<input type="checkbox"/>	<input type="checkbox"/>	<input type="checkbox"/>

[Select All](#) or [Clear](#)

Figure 14: Date, Time and Step Selection Menu from ECMWF Website

Select parameter

- 2 metre dewpoint temperature
- 2 metre temperature
- 10 metre U wind component
- 10 metre V wind component
- 10 metre wind gust since previous post-processing
- Albedo
- Boundary layer dissipation
- Boundary layer height
- Charnock
- Clear sky surface photosynthetically active radiation
- Convective available potential energy
- Convective precipitation
- Convective snowfall
- Downward UV radiation at the surface
- Eastward gravity wave surface stress
- Eastward turbulent surface stress
- Evaporation
- Forecast albedo
- Forecast logarithm of surface roughness for heat
- Forecast surface roughness
- Gravity wave dissipation
- High cloud cover

Figure 15: Parameter Selection Menu from ECMWF Website

a. Wind Velocities Profile

Wind forcing is a crucial parameter in building a spectral wave model because most ocean waves are constructed by wind. We utilized wind velocities (u and v components) with variations in time and space. The u and v wind components can be extracted manually from wind speed and wind direction data, as shown in Figure 16. The data bank provides raw data on wind velocity for u and v components. Figures 17 to 20 show the profiles of wind velocity on June 1, 2014 at 12:00 AM and 03:00 AM for u and v components, respectively.

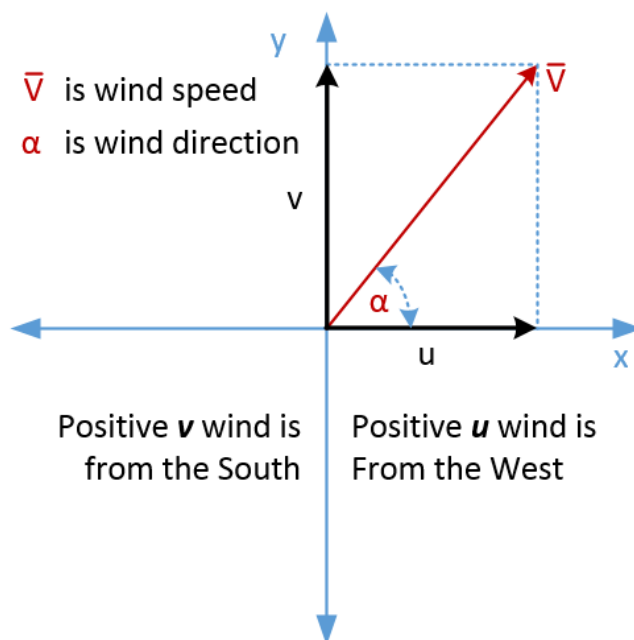


Figure 16: Wind Speed, Wind Direction and Wind Velocity u and v Components

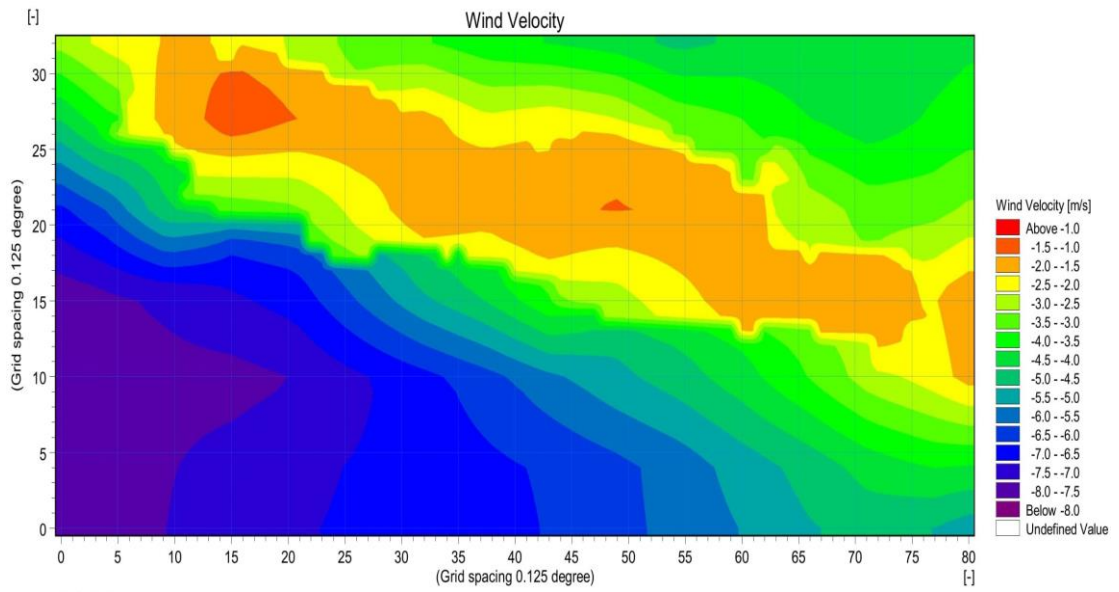


Figure 17: Wind Velocity u Profile in June 1st 2014 at 12:00 AM

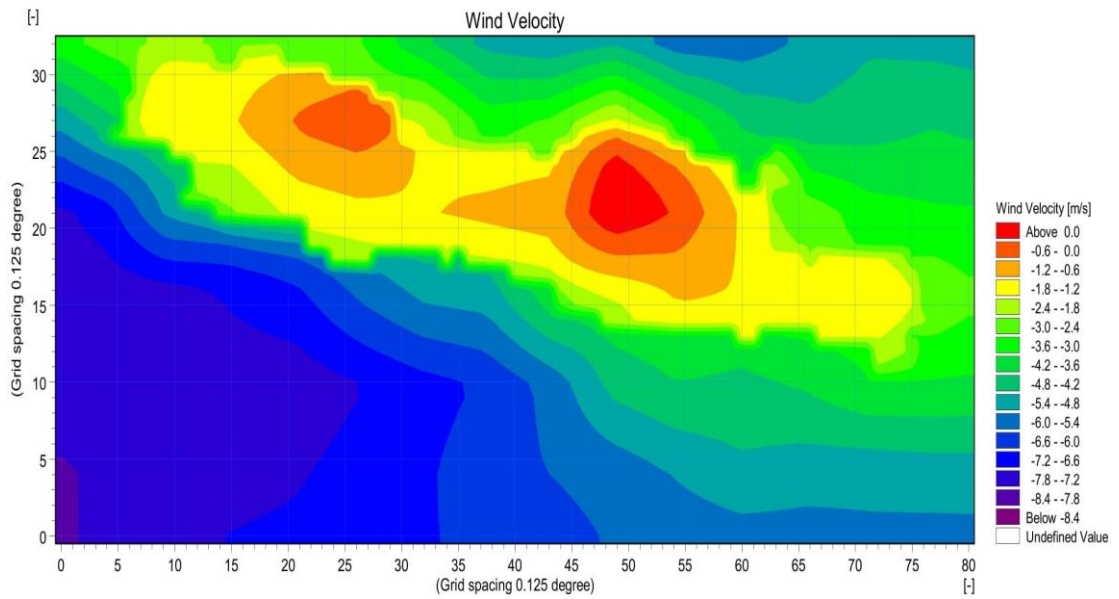


Figure 18: Wind Velocity u Profile in June 1st 2014 at 03:00 AM

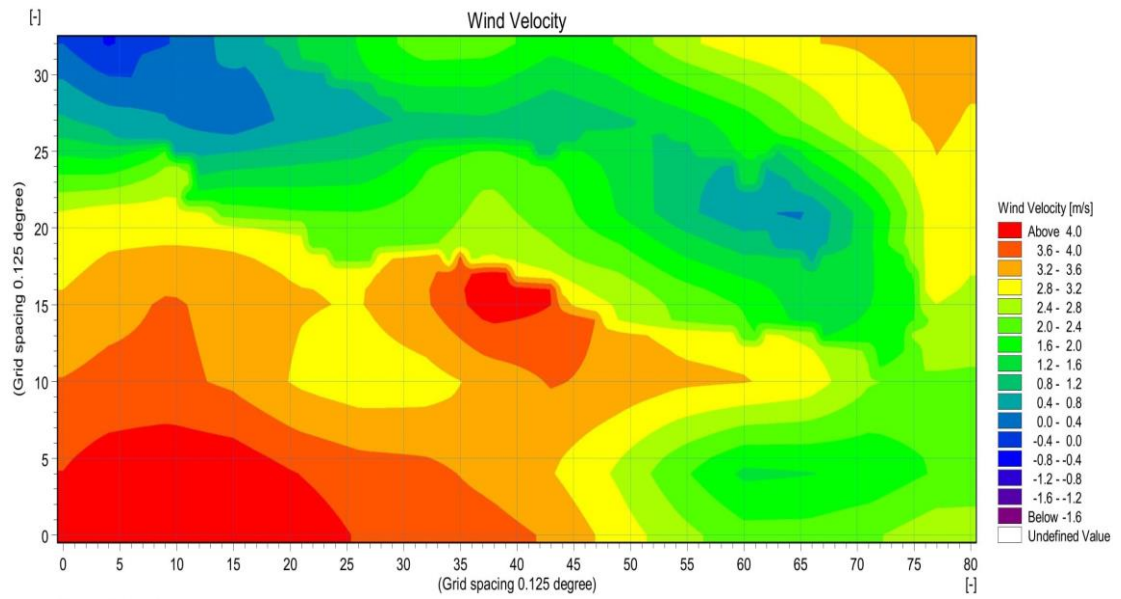


Figure 19: Wind Velocity v Profile in June 1st 2014 at 12:00 AM

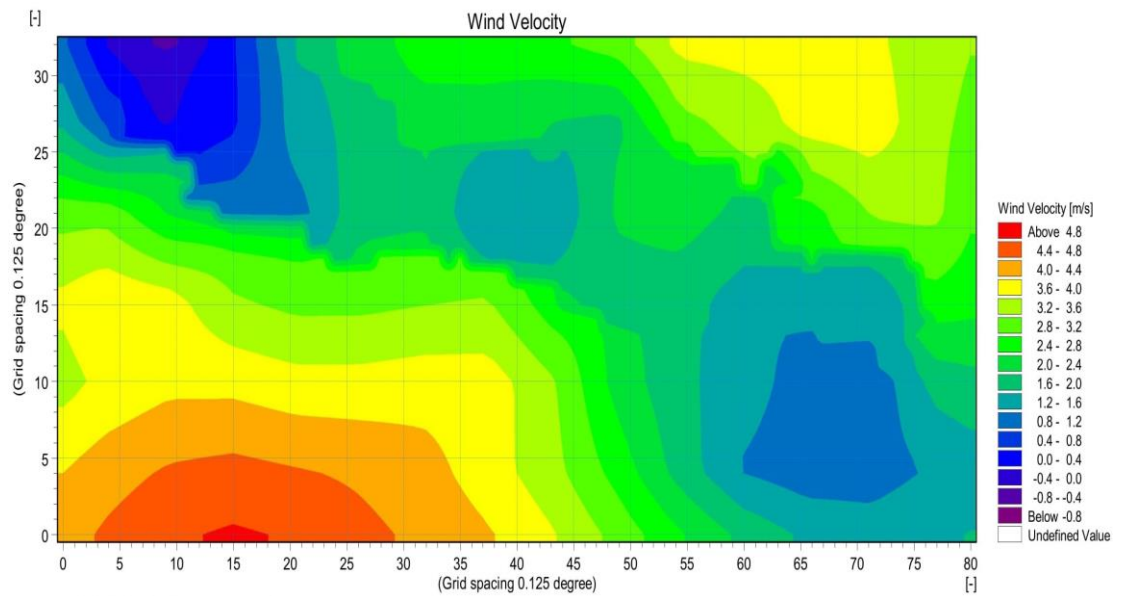


Figure 20: Wind Velocity v Profile in June 1st 2014 at 03:00 AM

b. Significant Wave Height Profile

Significant wave height was formulated using Equation (1). As mentioned in Section 1.2, H_s is the significant wave height, and m_0 is the initial moment of the spectral function. H_s is also defined as the average height of the highest one-third waves in a wave spectrum. Notably, the control simulation in this thesis was linked with the assessment result using the significant wave height. The profiles of H_s on June 1, 2014 at 12:00 AM and 03:00 AM is shown in Figures 21 and 22, respectively.

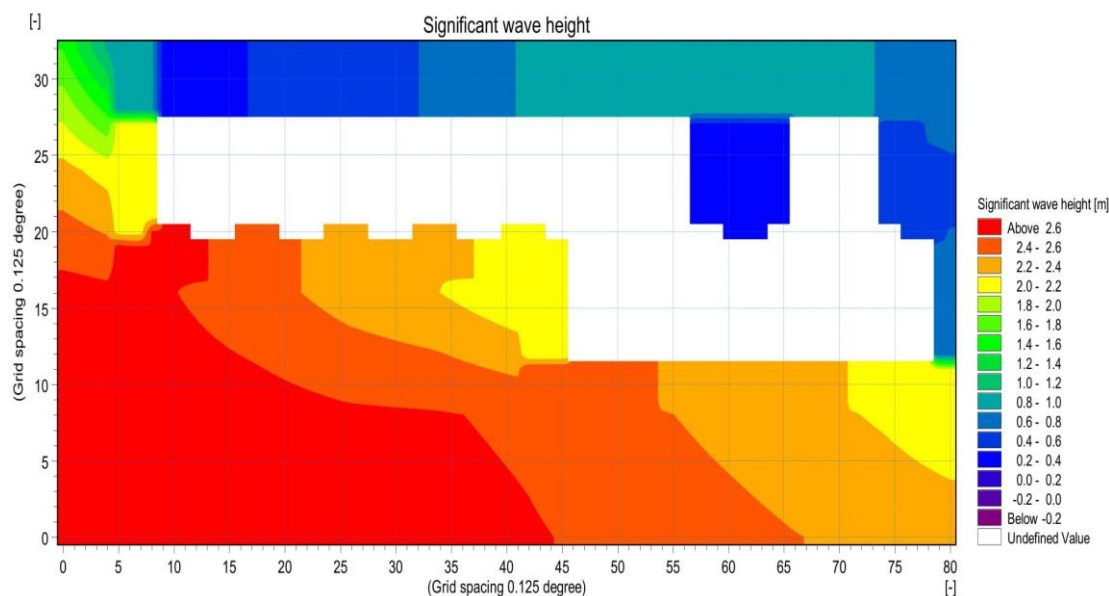


Figure 21: Significant Wave Height Profile in June 1st 2014 at 12:00 AM

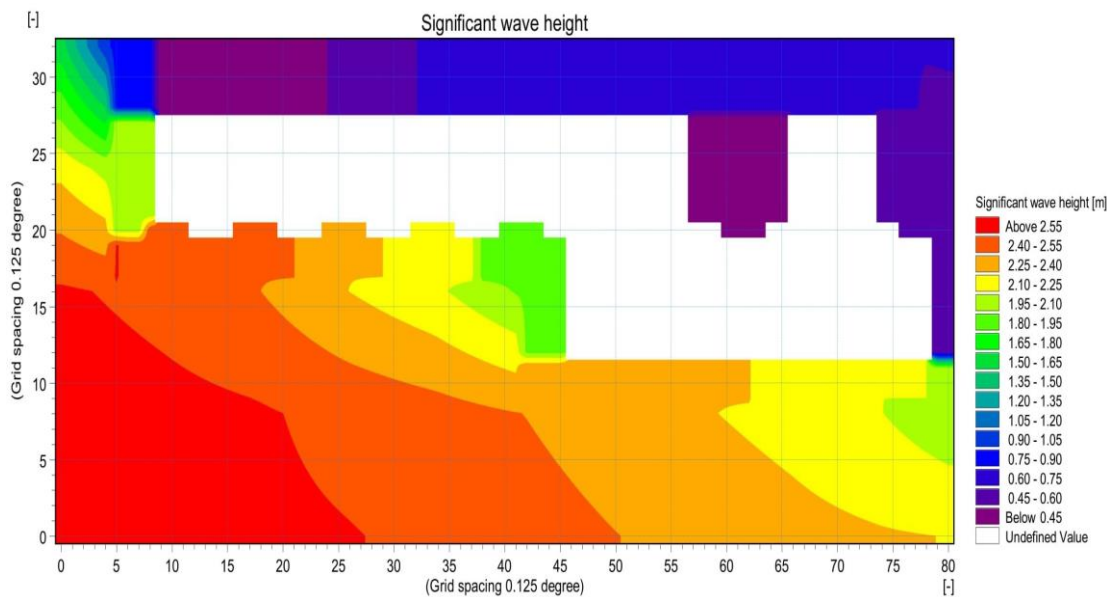


Figure 22: Significant Wave Height Profile in June 1st 2014 at 03:00 AM

c. Mean Wave Direction Profile

Wave direction shows the path of ocean waves. The direction does not need to be similar to the wind direction because of other parameters that affect the waves. The degree is measured with true north as the starting point and increases clockwise, as shown in Figure 23.

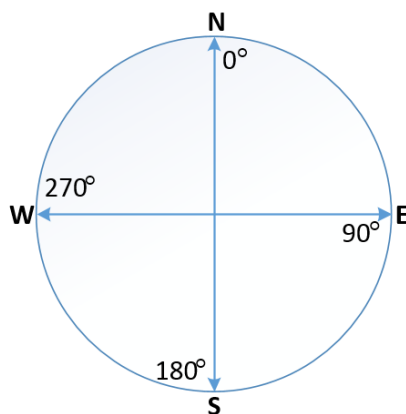


Figure 23: Wave Direction Regulation

The mean value was used in this work because it is required in the spectral wave model. Figures 24 and 25 show the profiles of mean wave direction on June 1, 2014 at 12:00 AM and 03:00 AM, respectively.

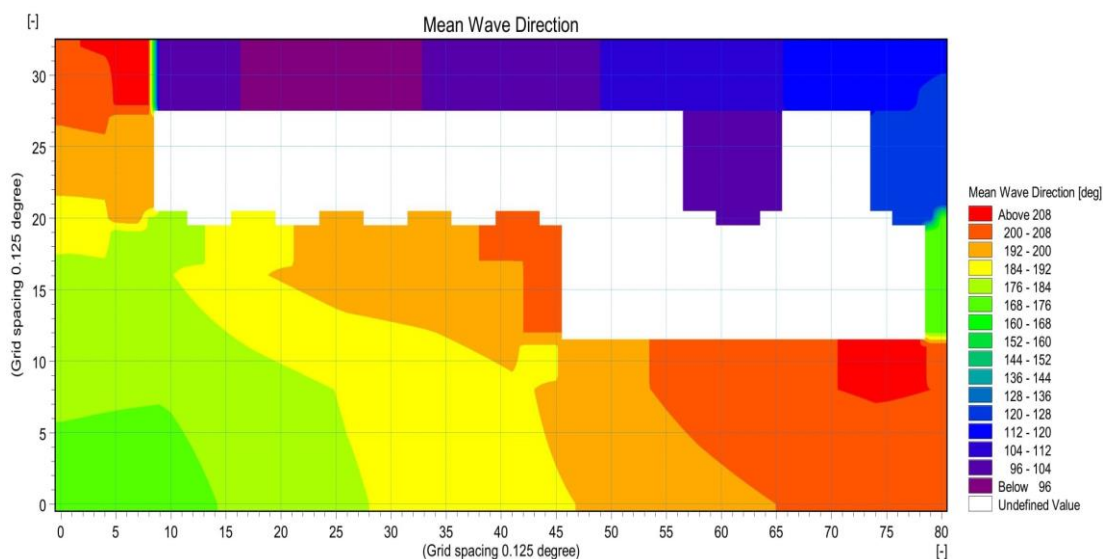


Figure 24: Mean Wave Direction Profile in June 1st 2014 at 12:00 AM

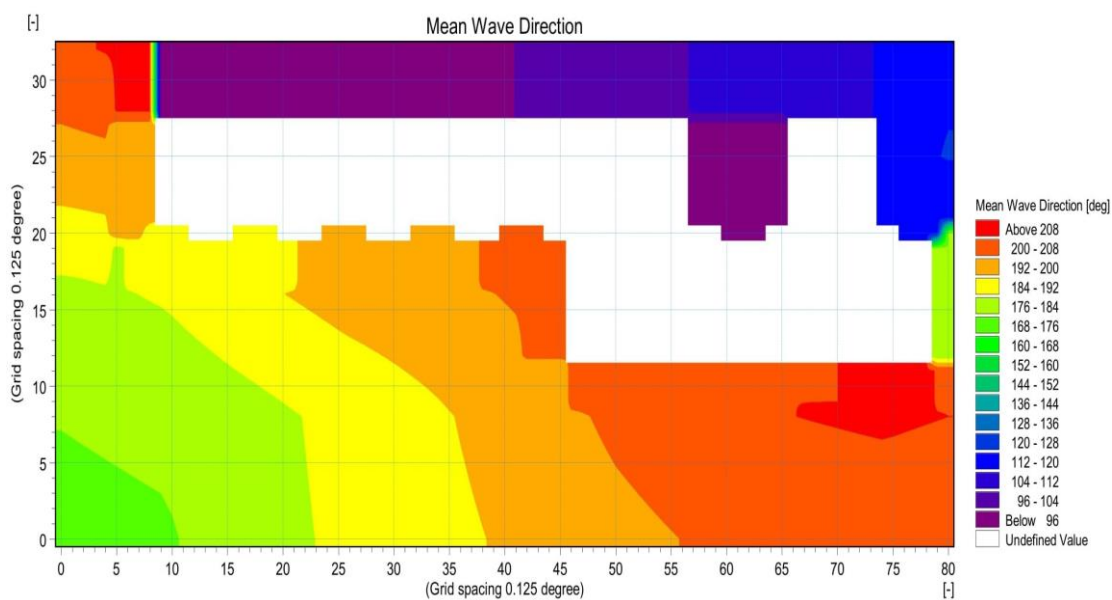


Figure 25: Mean Wave Direction Profile in June 1st 2014 at 03:00 AM

d. Wave Period Profile

Wave period is the time interval between the arrivals of consecutive peaks at a stationary point. Various types of waves according to wave period are shown in Figure 26.

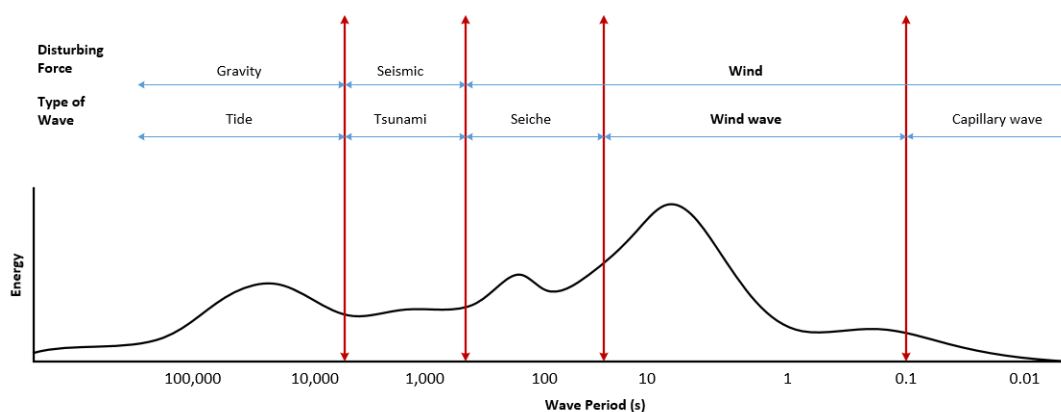


Figure 26: Wave Types Based on Wave Period

The profiles of the wave period on June 1, 2014 at 12:00 AM and 03:00 AM are shown in Figures 27 and 28.

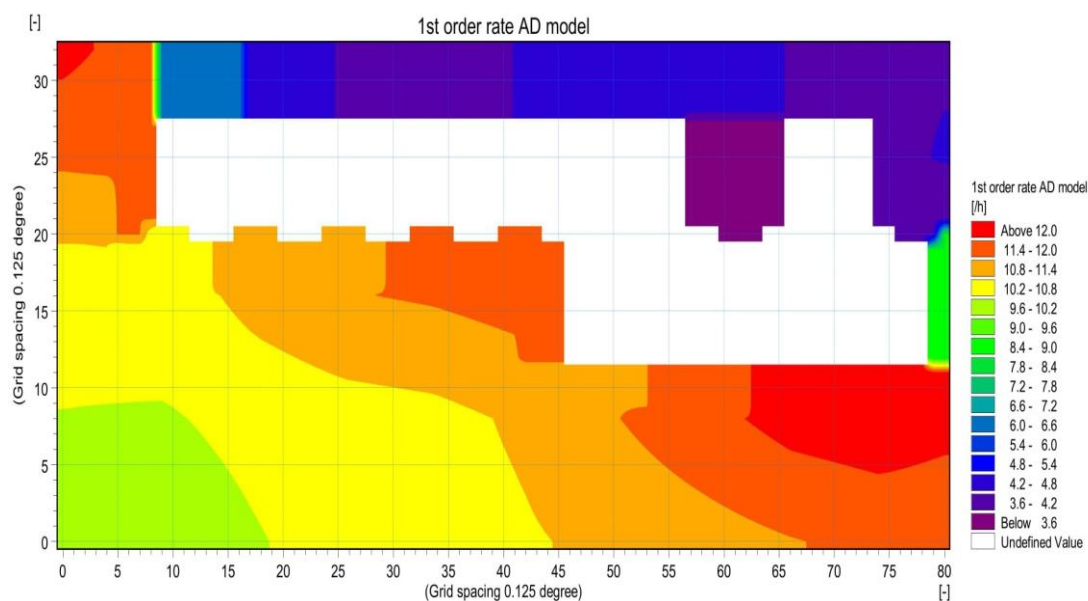
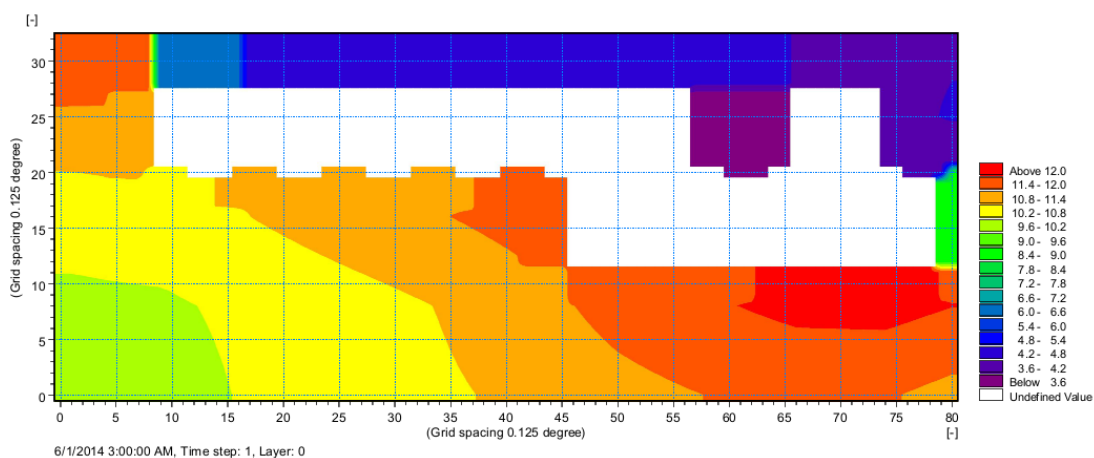


Figure 27: Wave Period Profile in June 1st 2014 at 12:00 AMFigure 28: Wave Period Profile in June 1st 2014 (a) at 03:00 AM

e. Bathymetry Profile

Bathymetry was originally the study of the floors of water bodies (oceans, lakes, streams, or rivers). The term bathymetry is interpreted as the ocean topography, depth, or shape of the ocean terrain. One of the trusted sources of bathymetry data is the General Bathymetric Chart of the Oceans (GEBCO). The data are available on GEBCO's official website, namely, http://www.gebco.net/data_and_products/gridded_bathymetry_data/. The data have a spatial interval of 30 arcseconds or approximately equal to 0.008333 degrees or 1 km. Figure 29 shows the scattered bathymetry data around Java Island.

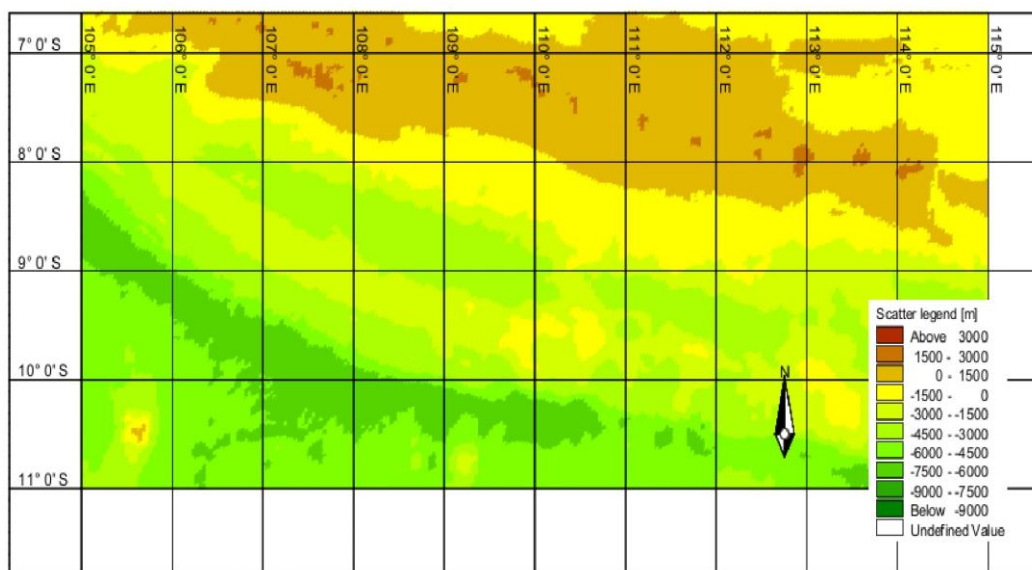


Figure 29: Scattered Bathymetry Data

2.3.2 Boundary Conditions

For computation, boundary conditions need to be determined appropriately and well posed. Boundary conditions should be set on the boundary of the simulation domain. In this work, three out of nine types of boundary conditions were used as shown below.

a. Closed Boundary

The closed boundary is used for the boundary where no water flows, such as the coastline. In Figure 30, the closed boundary is denoted by code 1 (dark green color).

b. Lateral Boundary

The lateral boundary is used for the side boundary that is parallel to the direction of wave propagation. In Figure 30, the lateral boundary is denoted by codes 2 and 8 (maroon and light green colors).

c. Wave Parameters 2

This type of boundary condition requires four data items, which are significant wave height, wave period, mean wave direction, and directional standard deviation. These data were downloaded in the previous section, except for directional standard deviation, which was set to a constant value.

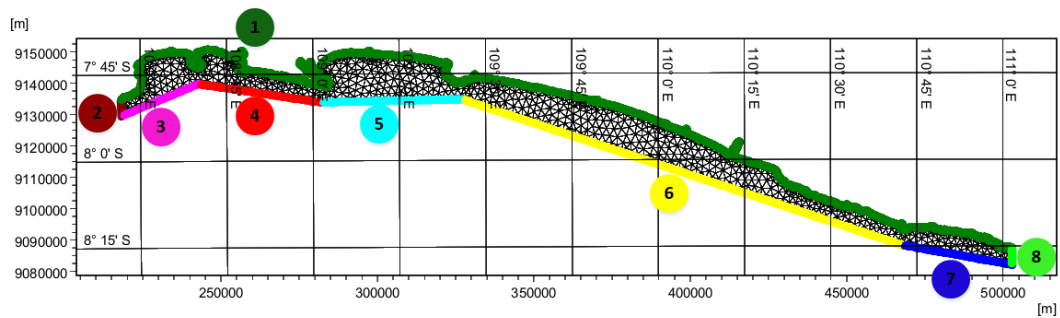


Figure 30: Boundary Condition Codes

2.3.3 Mesh Generation

The purpose of mesh generation is to discretize a computation domain with particular polygonal elements (triangular, rectangular, or another shape), in which each element is inter-connected at discrete nodes, as shown in Figure 31.

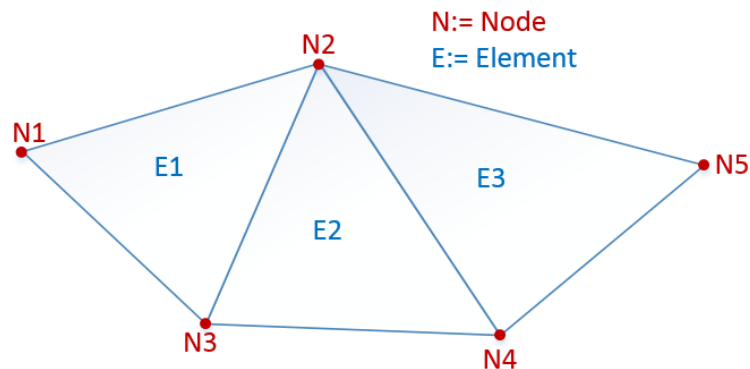


Figure 31: Triangular Meshes with Nodes and Elements

In this work, Mesh Generator MIKE Zero using the finite element method (FEM) with a triangular mesh was used to generate a mesh. The generated mesh contained 4,982 nodes and 7,539 elements. Figure 32 depicts the mesh generated by MIKE Zero.

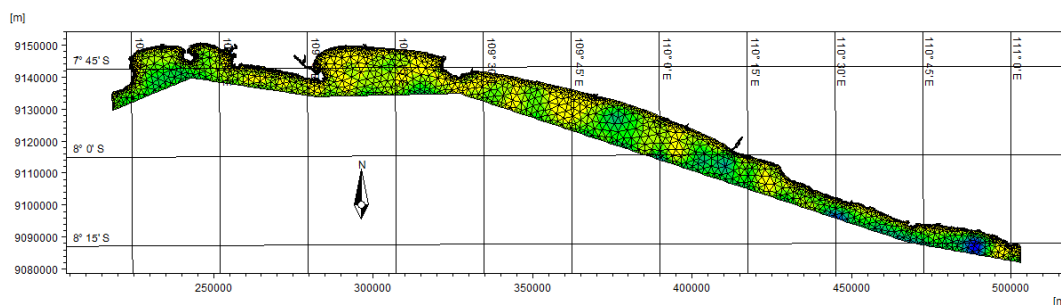


Figure 32: Generated Mesh

2.3.4 Bathymetry Interpolation

Bathymetry data collected from GEBCO have an interval of around 1 km, which is too large. Additionally, the elements of the mesh do not fit with the coordinate point of scattered bathymetry data. However, MIKE Zero has an interpolation function to provide the best estimation value for each of element in the mesh. Figure 33 shows the bathymetry profile after the interpolation process.

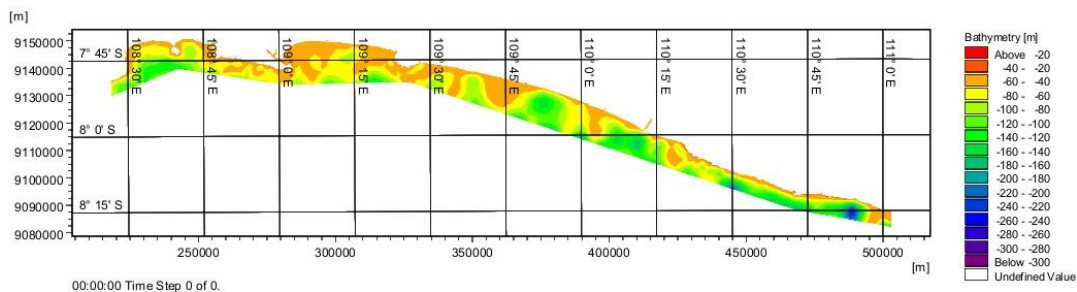


Figure 33: Interpolated Bathymetry Profile

2.4 Model Validation

Model validation or verification has to be conducted by comparing the simulation data with the measured data to achieve good system representation. The data observed from the buoy station in Baron Beach, Indonesia, are time series data on significant wave height and wave period in June 2014 with an hourly interval. Various variables affect the model to a certain degree. These parameters were examined to obtain a simulation result that fit the measured data as much as possible. After several calibration processes, the final parameters were as follows.

a. Basic Equation

Spectral formulation has two options, which are fully spectral (FS) and directionally decoupled parametric (DDP) formulations. In this work, FS formulation was selected due to its completeness. The wind–wave model in MIKE 21 SW was formulated in the form of wave action density spectrum N . Equation (2) shows the wave action equation in Cartesian coordinates.

$$\frac{\partial N}{\partial t} + \nabla \cdot (\bar{v}N) = \frac{S}{\sigma}, \quad (5)$$

where $N(\bar{x}, \sigma, \theta, t)$ is the action density with \bar{x} containing two Cartesian coordinate axes (x, y) , σ is the relative angular frequency, θ is the wave propagation direction, t is a time parameter, and \bar{v} is the propagation velocity of a wave group in 4D space (\bar{x} , σ , and θ). Instationary formulation was selected over quasi-stationary as the time formulation.

b. Spectral Discretization

Two types of discretization are used in MIKE 21 SW; these two are frequency and directional. For frequency discretization, the logarithmic discretization technique is used over equidistant technique for effectiveness. The parameters are

as follows: the frequency is 25 (minimum of 0.05 Hz) and the frequency factor is 1.1. For directional discretization, circular with 360° rose discretization was selected, and the number of directions was 16.

c. Solution Technique

A low-order and fast algorithm technique was selected for geographical space discretization to reduce the simulation time. The maximum number of levels in transport calculation was set to 32, and the number of steps in source calculation was 1 (minimum and maximum time steps of 0.01 and 30 s, respectively).

d. Wind Forcing

As a forcing parameter, the u and v components of wind velocity with time-domain varying data were imported to the model. The data were selected from the previous data collection. Air and sea were coupled, and the background Charnock constant was set to 0.01.

e. Wave Breaking

The wave breaking dissipation parameter must be set to accommodate wave-breaking phenomena that occur in shallow water. Wave breaking dissipation occurs due to the wave amplitude reaching the extreme value at which the wave peak actually overturns. The gamma parameter was set to 0.8.

f. Bottom Friction

Bottom friction is an important dissipation parameter that depends on wave and sediment properties. The model is formulated by using the Johnson and Kofoed–Hansen approach. The parameter was set to 0.04.

g. White Capping

White capping is a wave-breaking phenomenon that occurs in deep oceans when the wavelength is far less than the wave height. The model of this dissipation is formulated based on theory of Hasselman (1974) and Jansenn (1989). Two dissipation coefficients, C_{ds} and δ_{ds} , must be selected. These parameters were set to 4.5 and 0.5, respectively.

Based on these parameter settings, the validation process was statistically successful. Figure 34 shows the comparison of simulation and observation data on significant wave height. These data are close to each other with only a minor error (Figure 35). The maximum error was only 0.15%, and the average was 0.042%. This result indicates that the model is suitable and ready to use in assessment simulation.

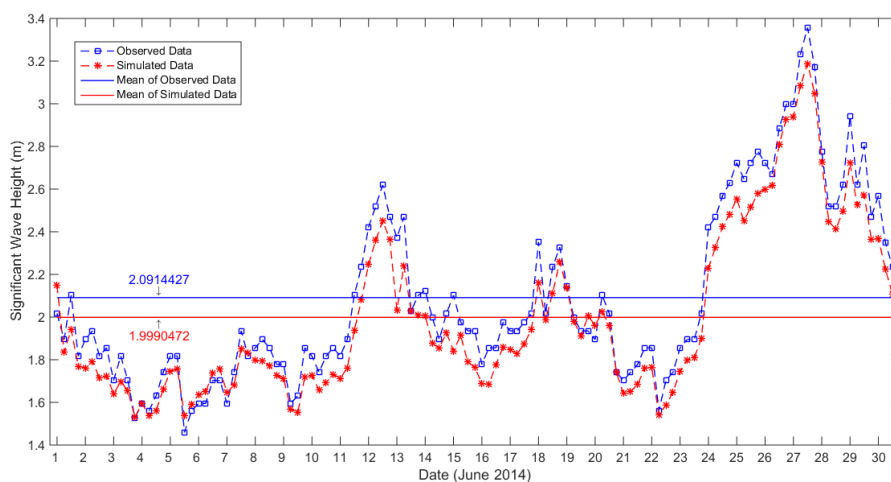


Figure 34: Observed and Simulated Significant Wave Height for Baron Observation Station

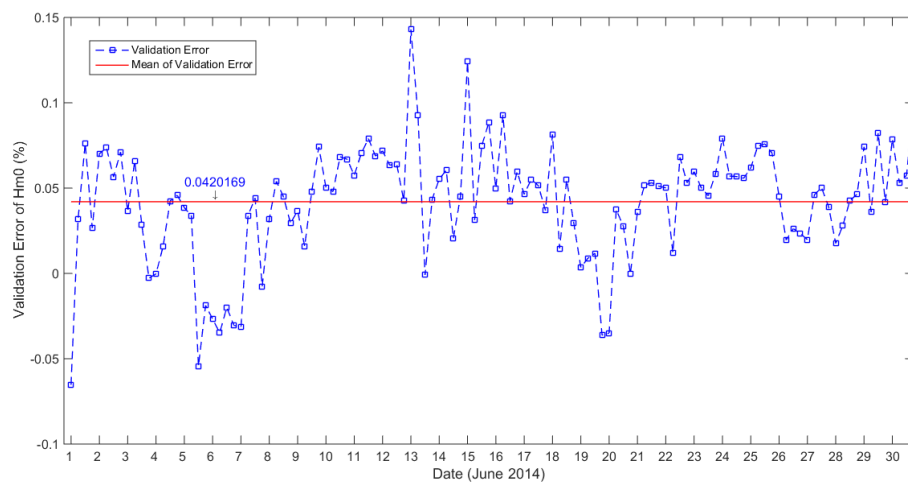


Figure 35: Error Percentage Significant Wave Height for Baron Observation Station

Chapter 3: Mechanical and Electrical Modeling

In this study, the sea-based WEC proposed by Uppsala University (Figure 36) was adopted. The WEC consists of a buoy, connecting rod, and permanent magnet linear generator (PMLG). The mechanical and electrical models of the WES were considered.

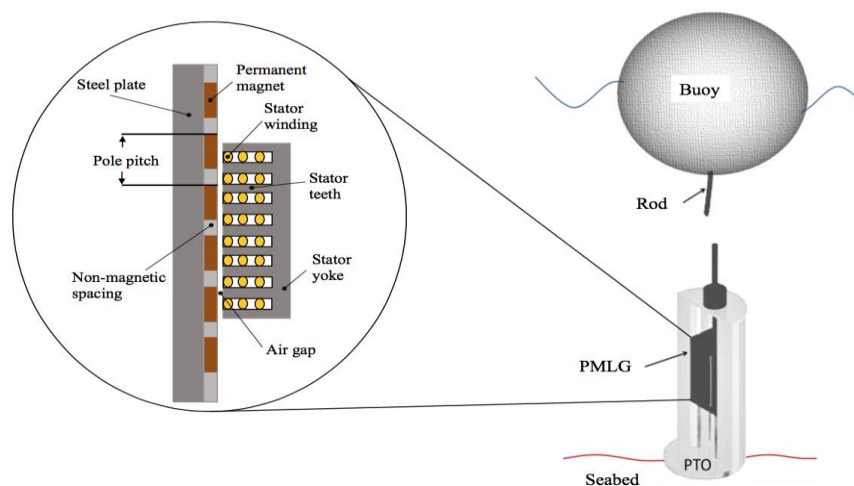


Figure 36: Configuration of the proposed control system for WEC systems [41]

The mechanical model describes the forces acting on the buoy. Control force, which is one of the forces acting on the buoy, was calculated with the proposed control strategy by using the mechanical model. Control force was implemented by controlling the current in the stator of the PMLG. The power converter module generates the current by controlling the switches.

The electrical model of the PMLG calculates the controlling current and other electrical quantities. In this research, the mathematical model of the power converter

was not considered because this study does not consider implementing the control system using power electronics in the converter.

3.1 The Mechanical Model

The mechanical model describes the mechanical forces acting on the buoy. Within its linear region, the buoy's elevation, $z(t)$, is described using the following equation.

$$f_e(t) - f_r(t) - f_b(t) - f_l(t) - f_s(t) + f_u(t) = m\ddot{z}(t), \quad (6)$$

where $\ddot{z}(t)$ is the heaving acceleration of the buoy and $f_e(t)$, $f_r(t)$, $f_b(t)$, $f_l(t)$, $f_s(t)$, and $f_u(t)$ are the excitation force, radiation force, buoyancy force, losses force, spring force, and control force, respectively [11]. Constant m is the total mass of power take-off (PTO), which comprises the buoy, the rod, and the translator of the PMLG. The connector is considered rigid.

Excitation force $f_e(t)$ is the force applied by incident waves on the floating body when it is held motionless. The force consists of diffraction and Froude–Krylov terms. The diffraction term can be lost because the size of the buoy is significantly smaller than the wavelength [42]. In the frequency domain, excitation force is formulated as

$$F_e(s) = \Phi(s)H(s), \quad (7)$$

where $F_e(s)$ and $H(s)$ are the Laplace transform of $F_e(t)$ and wave elevation $\eta(t)$. The transfer function of $\Phi(s)$ can be determined by implementing an identification technique for the simulated data. The data are generated with a hydrodynamic

program (such as WAMIT [43]) according to the buoy geometry and sea parameters. Radiation force $f_r(t)$ is modeled as

$$f_r(t) = m_\infty \ddot{z}(t) + \int_0^t k_r(t-\tau) \dot{z}(\tau) d\tau, \quad (8)$$

where m_∞ and k_r are the body-added mass in infinite frequency and the radiation convolution kernel, respectively. By using the procedure in [42], the radiation convolution kernel was modeled with the following fourth-order state-space equation

$$\int_0^t k_r(t-\tau) \dot{z}(\tau) d\tau \approx C_r q_r(t),$$

$$\dot{q}_r(t) = A_r q_r(t) + B_r \dot{z}(t),$$

where $q_r(t)$ is the fictitious radiation state vector and A_r , B_r , and C_r are the state, input, and output of the radiation force matrix, respectively.

Buoyancy force $f_b(t)$ is an opposite upward force as the buoy is immersed in the seawater. For a spherical buoy, the force is formulated as

$$f_b(t) = \rho g A_w(t) z(t), \quad (9)$$

where ρ , g , $A_w(t)$, and $z(t)$ are seawater density, gravitational acceleration, water plane area, and heaving position of the body, respectively. The water plane area is

$$A_w = \pi r^2 \left(1 - \frac{|z(t)|^2}{3r^2}\right).$$

In this research, the conservative movement of the buoy was considered. Therefore, the seawater plane can be approximated as

$$A_w = \pi r^2.$$

Spring force $f_s(t)$ is obtained from the restoring and end-stop springs. Spring force is modeled as

$$f_s(t) = S_s z(t), \quad (10)$$

where S_s is the spring coefficient. Losses force $f_l(t)$ includes viscous losses introduced to test the controlled systems against unknown or poorly known forces, which can decrease the captured power. For this purpose, the losses force is added to the mathematical model, but the control force is designed without involving this force. The force is modeled as

$$f_l(t) = R_{loss} \dot{z}(t), \quad (11)$$

where R_{loss} is the losses resistance. By using Equations (7)–(11), Equation (6) can be written as the following state-space equation.

$$\begin{aligned} \dot{X}(t) &= Ax(t) + B(f_u(t) + f_e(t)), \\ \dot{z}(t) &= Cx(t), \end{aligned} \quad (12)$$

where $x(t) = [z(t) \dot{z}(t) q_r(t)^T]^T \in R^{6 \times 1}$ is the overall system state vector. The state-space matrices, $A \in R^{6 \times 6}$, $B \in R^{6 \times 1}$, and $C \in R^{1 \times 6}$, are

$$A = \begin{bmatrix} 0 & 1 & 0 \\ \frac{-(\rho g A_w + S_s)}{m + m_\infty} & \frac{-R_{loss}}{m + m_\infty} & \frac{-C_r}{m + m_\infty} \\ 0_{4 \times 1} & B_r & A_r \end{bmatrix},$$

$$B = \begin{bmatrix} 0 & 0 \\ 1 & 1 \\ \frac{m + m_\infty}{m + m_\infty} & \frac{m + m_\infty}{m + m_\infty} \\ 0_{4 \times 1} & 0_{4 \times 1} \end{bmatrix},$$

$$C = [0 \quad 1 \quad 0_{4 \times 1}].$$

3.2 The Electrical Model

The calculated $f_u(t)$ was implemented by controlling the current in the PMLG. To calculate the controlling current, PMLG was modeled using its d–q equivalent circuit, which represents the synchronous-frame direct and quadrature components, as shown in Figure 37. Park transformation was used to transform the three phase voltages and currents into synchronous-frame components [32]. The d–q components of stator voltage $v_s(t)$ at the terminal were formulated with the following equations.

$$v_{sd}(t) = R_s i_{sd}(t) - \omega_e(t) \lambda_{sq}(t) + \frac{d}{dt} (L_{sd} i_{sd}(t) + \lambda_{PM}),$$

$$v_{sq}(t) = R_s i_{sq}(t) - \omega_e(t) \lambda_{sd}(t) + \frac{d}{dt} (L_{sq} i_{sq}(t)),$$

$$\lambda_{sd}(t) = L_{sd} i_{sd}(t) + \lambda_{PM},$$

$$\lambda_{sq}(t) = L_{sq} i_{sq}(t),$$

where $i_s(t)$, λ_{PM} , λ_s , R_s , and L_s are the stator current, permanent magnet flux, stator flux linkage, machine synchronous resistance, and inductor, respectively. The variable $\omega_e(t)$ is the electrical angular frequency, which is provided by the following equation.

$$\omega_e(t) = \frac{2\pi \dot{z}(t)}{p_\omega},$$

where p_ω is the pole width of the PMLG. In this study, a surface-mounted PMLG was used; the stator inductance quantities on the d-axis and q-axis were almost identical or $L_{sd} \approx L_{sq}$ [44].

The converted (electrical) power, $P_e(t)$, is provided by

$$P_e(t) = \frac{3}{2} p \lambda_{PM} \omega_e(t) i_{sq}(t), \quad (13)$$

where p is the number of magnetic pole pairs. The mechanical power, $P_m(t)$, is expressed by

$$P_m(t) = f_u(t) \dot{z}(t). \quad (14)$$

By using Equations (8) and (9) and under the assumption that no loss exists in the conversion between $P_m(t)$ and $P_e(t)$, the following is obtained.

$$f_u(t) \dot{z}(t) = \frac{3p \lambda_{PM} \omega_e(t) i_{sq}(t)}{2}$$

Therefore, controlling current $i_{sq}(t)$ is obtained as

$$i_{sq}(t) = \frac{2f_u(t) \dot{z}(t)}{3p \lambda_{PM} \omega_e(t)}. \quad (15)$$

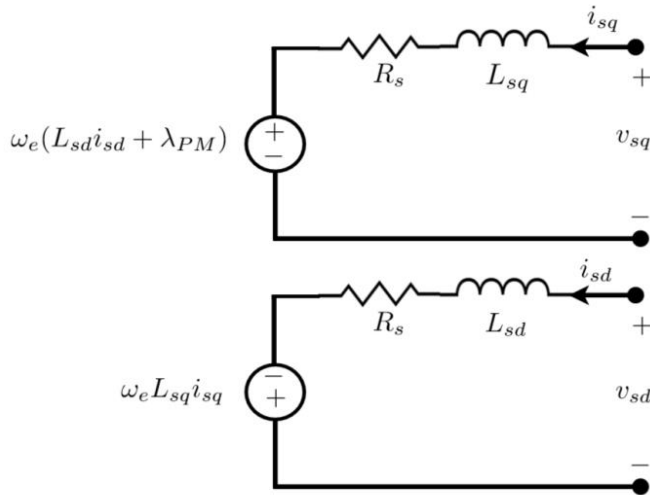


Figure 37: Corresponding circuit of the PMLG

Chapter 4: Proposed Control Strategy

This thesis presents a novel reference-based HPA control method. The novelty lies in the generation of the velocity reference and in the design of the controller for the servo feedback control system. Common control strategies utilize radiation resistance as a damping factor in excitation force to produce the reference velocity, such as in [29]. Nevertheless, this strategy presents a main disadvantage: the reference velocity is tuned based on a single frequency of radiation resistance. This approach is inadequate due to the nature of unpredictable sea waves. Additionally, the reference velocity generation does not consider the limits of control force and allows the required control force to exceed its acceptable value. In active sea states, this condition can create reversed power absorption, in which the PTO consumes power instead of producing it. With a specific end goal to address these issues, a new technique was proposed to produce the reference velocity; the goal was to expand the power transformation from mechanical to electrical power. Unlike in [30, 10, 31, 33], the velocity reference was generated by utilizing the forces acting on the oscillating body and the electrical model of the PTO. In addition, the technique combines limitations for control force and use index. The use index is the ratio between the peak and mean values of electrical power. With the goal to utilize this index as a part of irregular (polychromatic) sea states, the reference velocity was differed based on the value of the peak angular frequency and significant height of the waves. Moreover, a straightforward proportional–integral–derivative (PID) controller was utilized in the servo feedback control system. The PID controller is expected to demonstrate tracking capability and robustness despite the modelling uncertainties.

4.1 Servo Feedback Control System

The servo feedback control system involves two transfer functions, namely, the mechanical models of the WEC and PID controller, which are denoted as $\mathcal{P}(s)$ and $K(s)$, respectively. In this study, $\mathcal{P}(s)$ comprises a nominal plant model $P(s)$ with input multiplicative uncertainty and receives three input forces. Force $f_u(t)$ is a manipulable force, whereas $f_e(t)$ and disturbance force $f_d(t)$ are non-manipulable forces. $f_d(t)$ is an example of unmodeled force. Without $f_u(t)$ and $f_d(t)$ (freely oscillating system), the transfer function $P(s) = V(s)/F_e(s) = N_P(s)/D_P(s)$ is formulated using Equation (12), where $V(s)$ is the Laplace transform of $\dot{z}(t)$ and $N_P(s)$ and $D_P(s)$ are the numerator and denominator of $P(s)$, respectively. Furthermore, $\Delta(s)$ is a stable and proper transfer function with $\|\Delta\|_\infty \leq 1$. The transfer functions $W_T(s) = N_T(s)/D_T(s)$ and $W_S(s) = N_S(s)/D_S(s)$ are weighting functions that represent the model uncertainty and nominal performance specification, respectively. The transfer function of the PID controller is formulated as

$$K(s) = k_p + \frac{1}{k_i s} + k_d s = \frac{k_i + k_p s + k_d s^2}{s}. \quad (16)$$

The objectives of the PID controller in the servo feedback control system are as follows:

- To stabilize the nominal feedback control system
- To follow the reference velocity despite the existence of uncertainties in the model

The first objective can be satisfied by placing the closed-loop poles of the nominal feedback control system in the left-half plane of the complex plane, or equivalently,

$$\alpha(s, k_p, k_i, k_d) \triangleq sD_p(s) + (k_d s^2 + k_p s + k_i)N_p(s) \quad (17)$$

is Hurwitz. The second objective is solved by using the \mathcal{H}_∞ design technique framework [45]. We defined the complementary sensitivity function as

$$T(s) = \frac{K(s)P(s)}{1+K(s)P(s)}.$$

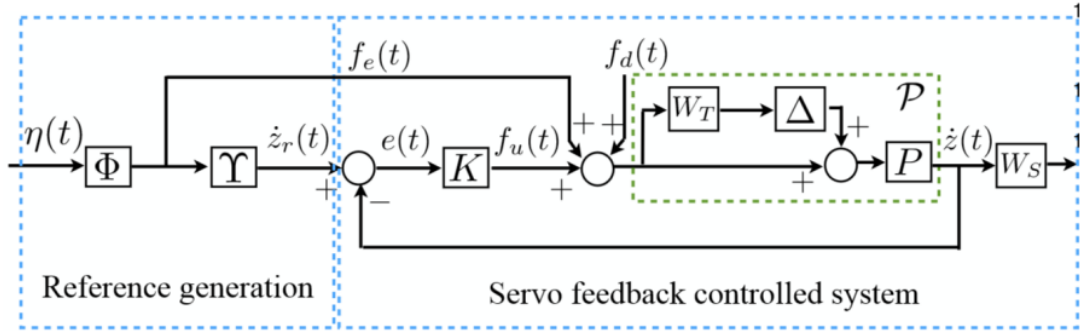


Figure 38: Proposed control system configuration for WEC Systems [41]

The system demonstrates robustness stability if the following equation is satisfied.

$$\|W_T(s)T(s)\|_\infty < 1 \quad (18)$$

Tracking performance can be measured by defining the sensitivity function as the following transfer function, which relates the reference with the error.

$$S(s) = \frac{1}{1 + K(s)P(s)}$$

By using \mathcal{H}_∞ theory, the nominal tracking performance for minimizing the tracking error can be formulated as

$$\|W_S(s)S(s)\|_\infty < 1. \quad (19)$$

The robust performance for solving the second objective is obtained by combining Equations (18) and (19) as follows:

$$\| |W_S(s)S(s)| + |W_T(s)T(s)| \|_\infty < 1. \quad (20)$$

The complex polynomial stabilization method was used to determine the parameters of the PID controller that satisfy Equations (17) and (20) [46]. We selected this method because the transfer function of the obtained controller has the same structure/transfer function as in Equation (16), and the method provides all (not just one) admissible PID controller gains for a selected k_p gain. The method requires the control problems to be written as a polynomial stabilization. Although Equation (17) is evidently a polynomial stabilization problem, Equation (20) needs the following lemma to be converted into a polynomial stabilization problem.

Lemma 1 [46]. Let

$$\frac{L(s)}{M(s)} = \frac{l_0 + l_1s + \dots + l_x s^x}{m_0 + m_1s + \dots + m_x s^x}$$

and

$$\frac{Y(s)}{Z(s)} = \frac{y_0 + y_1s + \dots + y_y s^y}{z_0 + z_1s + \dots + z_y s^y}$$

be stable and proper rational functions with $m_x \neq 0$ and $z_y \neq 0$. Then,

$$\left\| \left| \frac{L(s)}{M(s)} \right| + \left| \frac{Y(s)}{Z(s)} \right| \right\|_\infty < 1$$

if and only if

- a) $M(s)Z(s) + e^{j\theta}L(s)Z(s) + e^{j\phi}Y(s)M(s)$ Is Hurwitz for all θ and $\phi \in [0, 2\pi)$,
- b) $|l_x/m_x| + |y_y/z_y| < 1$.

By using Lemma 1, the robust performance condition in Equation (20) can be converted into the following polynomial stabilization.

$$\begin{aligned}
\beta(s, \theta, \phi, k_p, k_i, k_d) & \\
& \triangleq sD_S(s)D_T(s)D_P(s) + e^{j\theta}sN_S(s)D_T(s)D_P(s) \\
& + (k_p + k_i s + k_d s^2)[D_S(s)D_T(s)N_P(s) \\
& + e^{j\phi}D_S(s)N_T(s)N_P(s)]
\end{aligned} \tag{21}$$

This equation is Hurwitz, and

$$|W_S(\infty)S(\infty)| + |W_T(\infty)T(\infty)| < 1. \tag{22}$$

Therefore, the PID controller needs to satisfy the objectives of the servo feedback control system for WECs to be obtained by solving the following equations simultaneously [41].

(C1) $\alpha(s, k_p, k_i, k_d)$ is Hurwitz.

(C2) $\beta(s, \theta, \phi, k_p, k_i, k_d)$ is Hurwitz for all θ and $\phi \in [0, 2\pi)$.

(C3) $|W_S(\infty)S(\infty)| + |W_T(\infty)T(\infty)| < 1$.

Solving Equation (C3) is easy when an admissible PID controller that satisfies Equations (C1) and (C2) exists. Equations (C1) and (C2) can be solved by using the complex polynomial algorithm shown in Figure 39 [46]. This algorithm converts the

stabilization problem into a set of linear equations. Equations (C1), (C2), and (C3) are denoted as R_{C1} , R_{C2} , and R_{C3} , respectively. Therefore, the admissible gains of the PID controller satisfying Equation (17) are $R_{C1} \cap R_{C2} \cap R_{C3}$ [41].

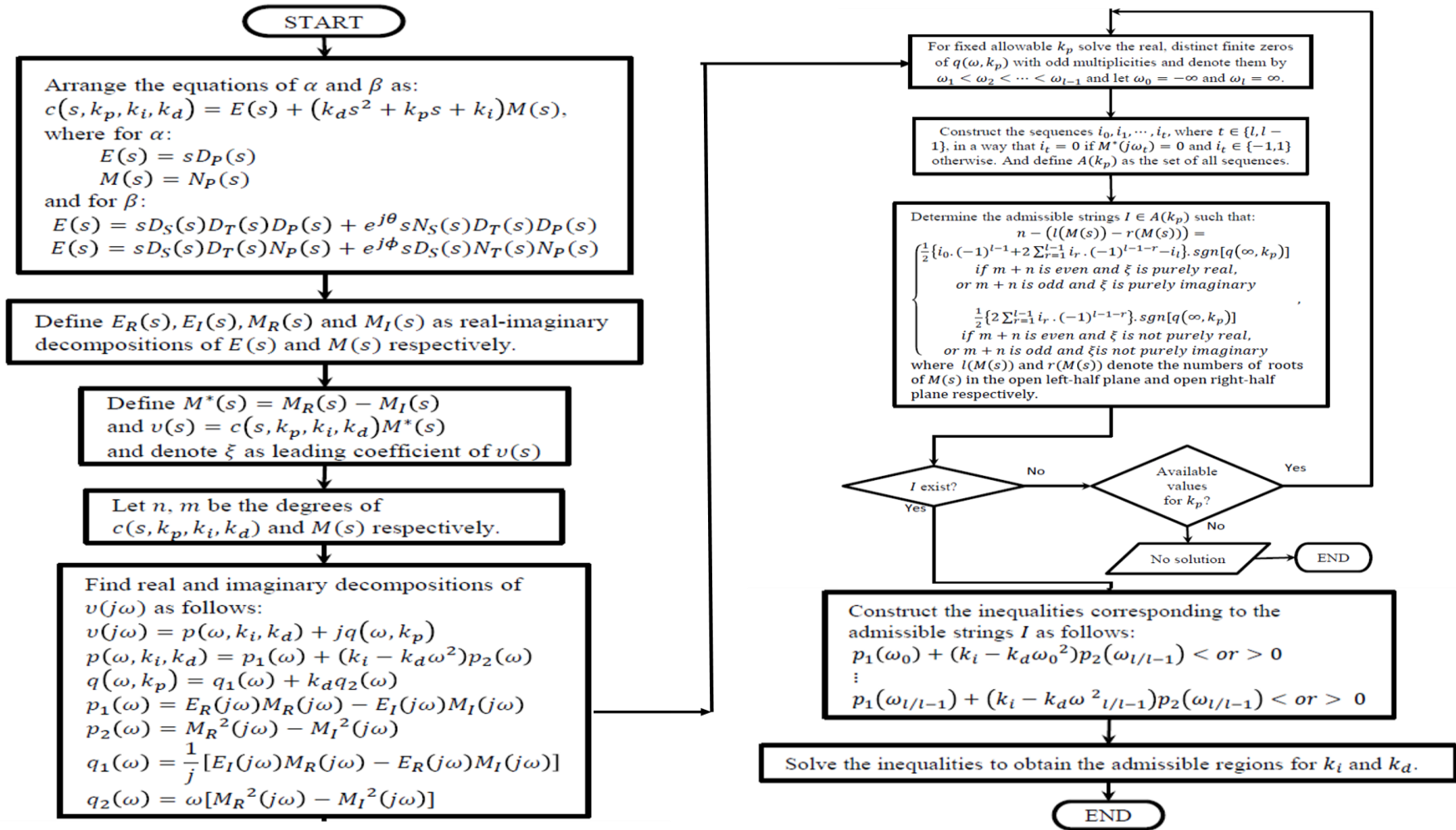


Figure 39: Flow Chart for Complex Polynomial Stabilization [41]

4.2 Reference Generation

The objective of reference generation is to provide reference velocity $\dot{z}_r(t)$, which maximizes the conversion from mechanical to electrical power. Velocity reference tracking is commonly used as a control strategy to achieve resonance, as mentioned in [9]. Reference generation includes two transfer functions: $\Phi(s)$ and $Y(s)$. $\Phi(s)$ is the transfer function between the excitation force and elevation of waves, as shown in Equation (7). Transfer function $Y(s)$ relates reference velocity $\dot{z}_r(t)$ to the excitation force and is formulated as

$$Y(s) = \frac{F_e(s)}{V_r(s)} = \frac{1}{\bar{R}}, \quad (23)$$

where $V_r(s)$ is the Laplace transform of $\dot{z}_r(t)$ and \bar{R} is a constant that represents intrinsic resistance. The objective of reference generation can be achieved by designing the value of \bar{R} using the following procedure. The energy conversion between mechanical power $P_m(t)$ and electrical power $P_e(t)$ is formulated as

$$P_e(t) = P_m(t) - P_{loss}(t) = f_u(t)\dot{z}(t) - \frac{3R_s i_{sq}^2(t)}{2}, \quad (24)$$

where $P_{loss}(t)$ denotes the power losses in the PMLG. The mechanical model of the PMLG is related to its mechanical model using the following equation

$$f_u(t) = \frac{3\pi\lambda_{PM}i_{sq}(t)}{2p_w}. \quad (25)$$

Substituting Equation (25) into Equation (24) results in

$$P_e(t) = \frac{3\pi\lambda_{PM}i_{sq}(t)\dot{z}(t)}{2p_w} - \frac{3R_s i_{sq}^2(t)}{2}. \quad (26)$$

In the resonance condition, $\dot{z}(t)$ becomes equal to $\dot{z}_r(t)$ by deploying the servo feedback control system. Maximizing $P_e(t)$ by taking partial derivative $P_e(t)$ over $i_{sq}(t)$ equal to zero in Equation (26) and evaluating it in the resonance condition, the following is obtained [41].

$$\frac{\partial P_e}{\partial i_{sq}} = \frac{3\pi\lambda_{PM}i_{sq}(t)\dot{z}_r(t)}{2p_w} - 3R_S i_{sq}(t) = 0 \quad (27)$$

Variable $i_{sq}(t)$ can be fixed by fixing $f_u(t)$ to be equal to its maximum designed value f_u^m in Equation (25) as follows:

$$f_u^m = \frac{3\pi\lambda_{PM}i_{sq}^m}{2p_w}, \quad (28)$$

where i_{sq}^m is the maximum rated value of $i_{sq}(t)$. By substituting Equations (7), (23), and (28) into (27), the following equation can be derived.

$$\bar{R}(s) = \frac{3\pi\lambda_{PM}H(s)\Phi(s)}{6p_w R_S i_{sq}^m} \quad (29)$$

For regular (monochromatic) sea states, $\eta(t)$ is a sinusoidal waveform with specific significant height H_s and peak frequency ω_p . Therefore, for regular sea states, \bar{R} can be obtained using the Bode magnitude of the following equation.

$$\bar{R}(\omega_p) = \left| \frac{3\pi\lambda_{PM}\eta_p\Phi(s)}{6p_w R_S i_{sq}^m} \right|, \quad (30)$$

where η_p is equal to half of H_s , e.g., $\eta_p = 0.5$ for $H_s = 1$ m. A look-up table can be constructed using the resulting Bode magnitude plot.

Constant \bar{R} in Equation (30) gives the maximum power conversion efficiency for various ω_p without exceeding the values of f_u^m . However, this does not mean that we

obtain the maximum $P_e(t)$. The maximum power conversion tends to result in a large value of \bar{R} and hence reduces the value of $P_m(t)$. To improve the captured power, Equation (30) can be modified by adding weighting constant γ to $P_{loss}(t)$ in Equation (24). The value of $P_{loss}(t)$ will be large if the value of γ is greater than 1. Although a large value of $P_{loss}(t)$ decreases the power conversion efficiency, the value of \bar{R} is reduced and the value of $P_m(t)$ and $P_e(t)$ can be improved. Therefore, Equation (30) can be written as

$$\bar{R}(\omega_p) = \left| \frac{3\pi\lambda_P M \eta_P \Phi(s)}{\gamma 6 p_w R_s i_{sq}^m} \right|. \quad (31)$$

Apart from reducing the power conversion between $P_m(t)$ and $P_e(t)$, a large value of γ can increase the peak value of $f_u(t)$ and the utilization index in the electrical power, which is formulated as $P_e^m(t)/\bar{P}_e$, where $P_e^m(t)$ and \bar{P}_e are the peak and mean values of electrical power, respectively. A low utilization index value indicates efficient usage of the PTO, whereas a high number indicates a high content of reactive power in the PTO. Excessively large values of the utilization index can lead to power reversion. The following shows the procedure to tune γ in Equation (31) and satisfy other constraints in f_u^m and the utilization index.

1. Select the value of H_s and operating region of ω_p . Set $\gamma = 1$. As mentioned earlier, this represents the maximum power conversion between $P_m(t)$ and $P_e(t)$.
2. Find the value of \bar{R} using Equation (31).
3. For a specific value of H_s , simulate the system using the monochromatic sea state for two values of ω_p , i.e., the highest and lowest values, which represent the most and least energetic sea states, respectively.

4. Check the values of $f_u^m(t)$ in the most energetic sea state and the utilization index in the least energetic sea state.
5. If the values of $f_u^m(t)$ and the utilization index are below their designed values, increase the value of γ and return to step 2. Otherwise, stop the procedure.

This algorithm is a fast procedure for finding the value of \bar{R} that satisfies the design constraints. A look-up table can be generated using the Bode magnitude plot. This table gives the value of \bar{R} based on the information on H_s and ω_p . In irregular or polychromatic sea states, this information can be obtained by performing a fast Fourier transform over future sea states. This involves a prediction method, which is beyond the scope of this study. Changing the value of \bar{R} over a rapid sampling instant is unnecessary because the sea state will not change its profile (i.e., H_s and ω_p) for a duration of 20–30 min [47].

The proposed control technique was compared with the existing resistive loading (RL) method. The control force for the RL method is formulated as

$$f_u(t) = -\sqrt{(R_r(\omega))^2 + (\omega^2 m + \omega^2 M_r(\omega) - S_b - S_{rs})^2}.$$

The RL method is well known for its high conversion efficiency between mechanical and electrical powers.

Chapter 5: WEC Assessment Simulation Results and Discussion

Simulations were conducted on a computation machine with 2.60 GHz CPU and 8 GB of RAM. The simulation lasted for 95 hours for one-year duration and around 40 days for 10-year duration. For easy data analysis, the simulations were divided into 10 steps based on the year. The simulation results and analysis are separated into two parts, which are time domain analysis and spatial analysis.

5.1 Time Domain Analysis

Analysis in the time domain is necessary because it provides the evolution of wave parameters over time and the ability to determine the time range of optimum wave power. Considering a comprehensive mean value analysis as well as partial analysis is important. Thus, time domain analysis was divided into two portions.

5.1.1 10-Year Mean Analysis

This comprehensive analysis was performed by taking the average value of the entire duration (10 years) for three parameters, namely, H_s , P , and T . Figure 40 shows the 10-year mean wave period with a maximum value of 10.1240 seconds. Figure 41 shows the histogram of the mean wave period, in which most of the elements (places) have a mean wave period of around 7.5–9.5 seconds.

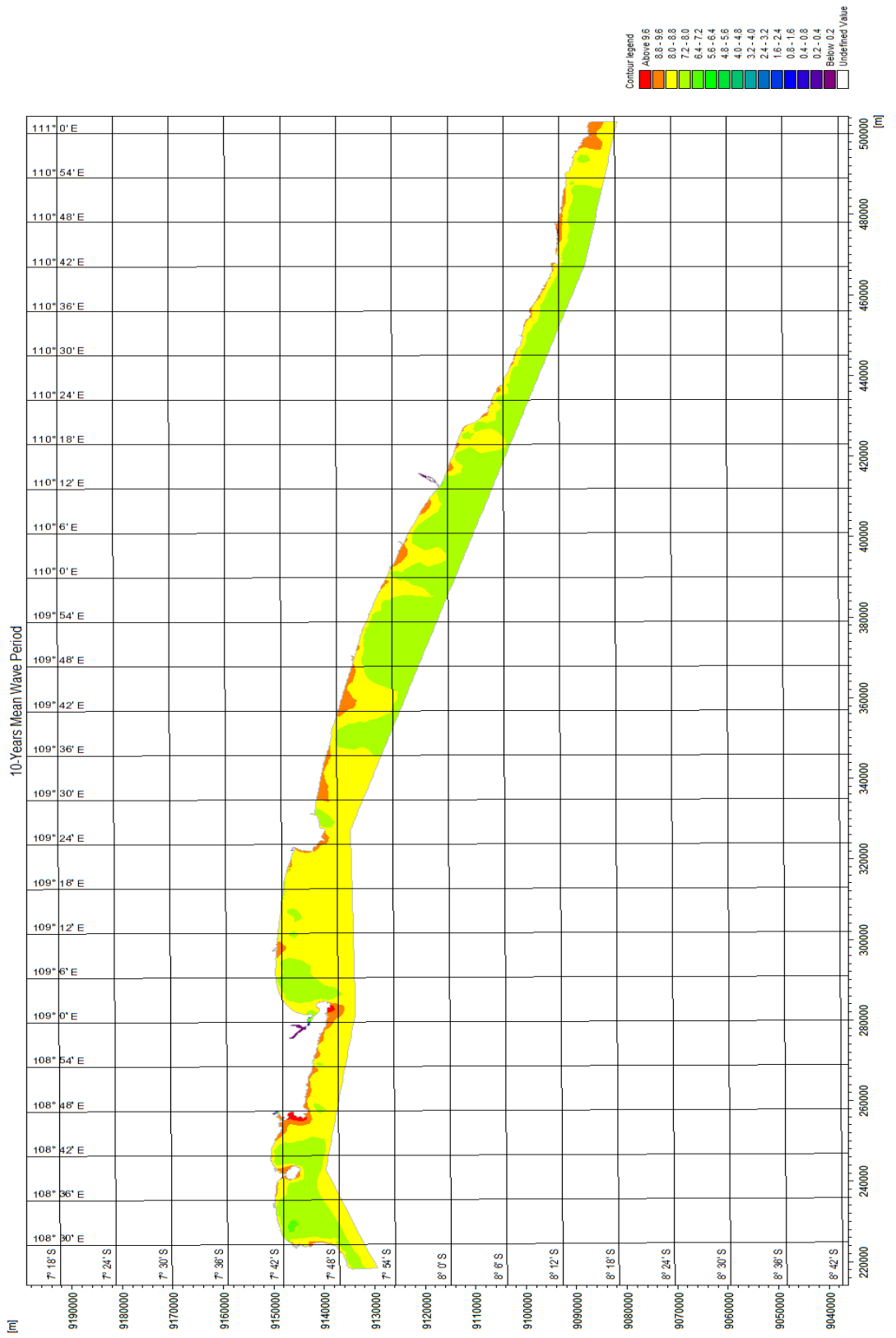


Figure 40: Distribution of 10-year Mean Wave Period

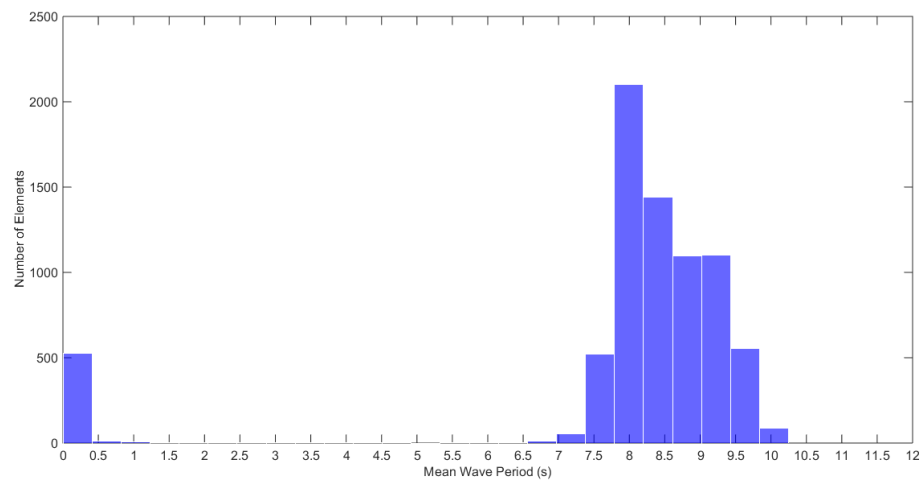


Figure 41: Histogram of 10-year mean Wave Period

Figure 42 shows the contour of the mean significant wave height for the 10-year duration. The maximum value is 2.2679 m. The distribution is prevalent, as shown in Figure 43. The histogram shows that most of the elements have a mean significant wave height of around 1.75 m, which shows a potential for wave energy conversion.

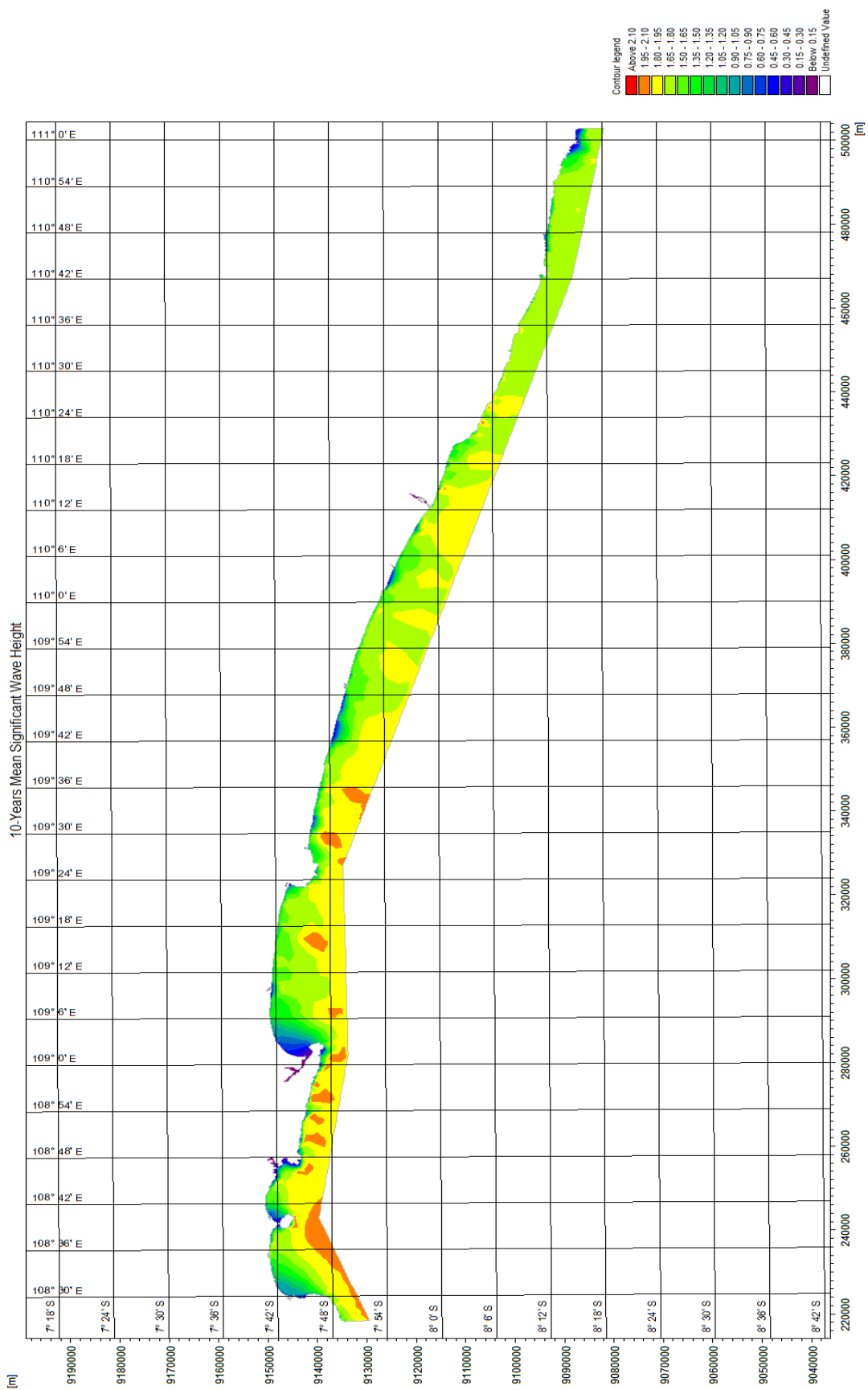


Figure 42: Distribution of 10-year Mean Significant Wave Height

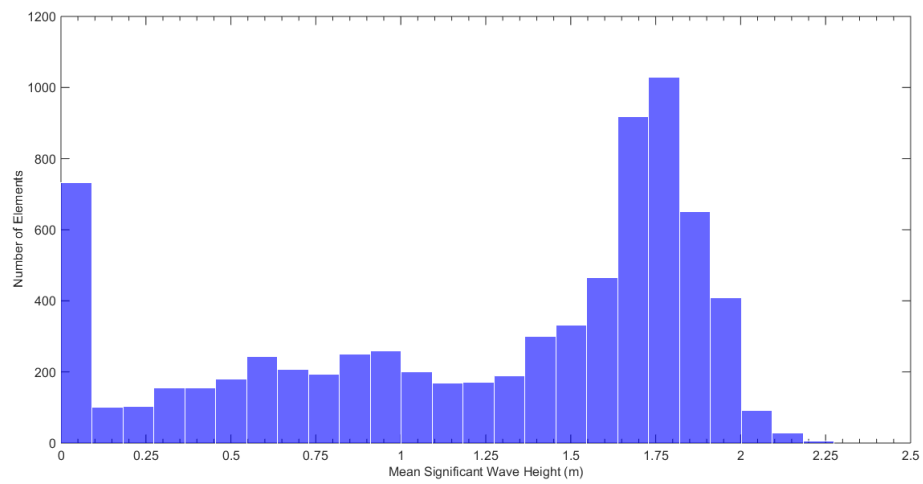


Figure 43: Histogram of 10-year Mean Significant Wave Height

The main parameter to examine is mean wave power. Figure 44 shows the contour of 10-year mean wave power. Most of the elements have a mean wave power of around 12.5 kW/m, which is high as shown in Figure 45.

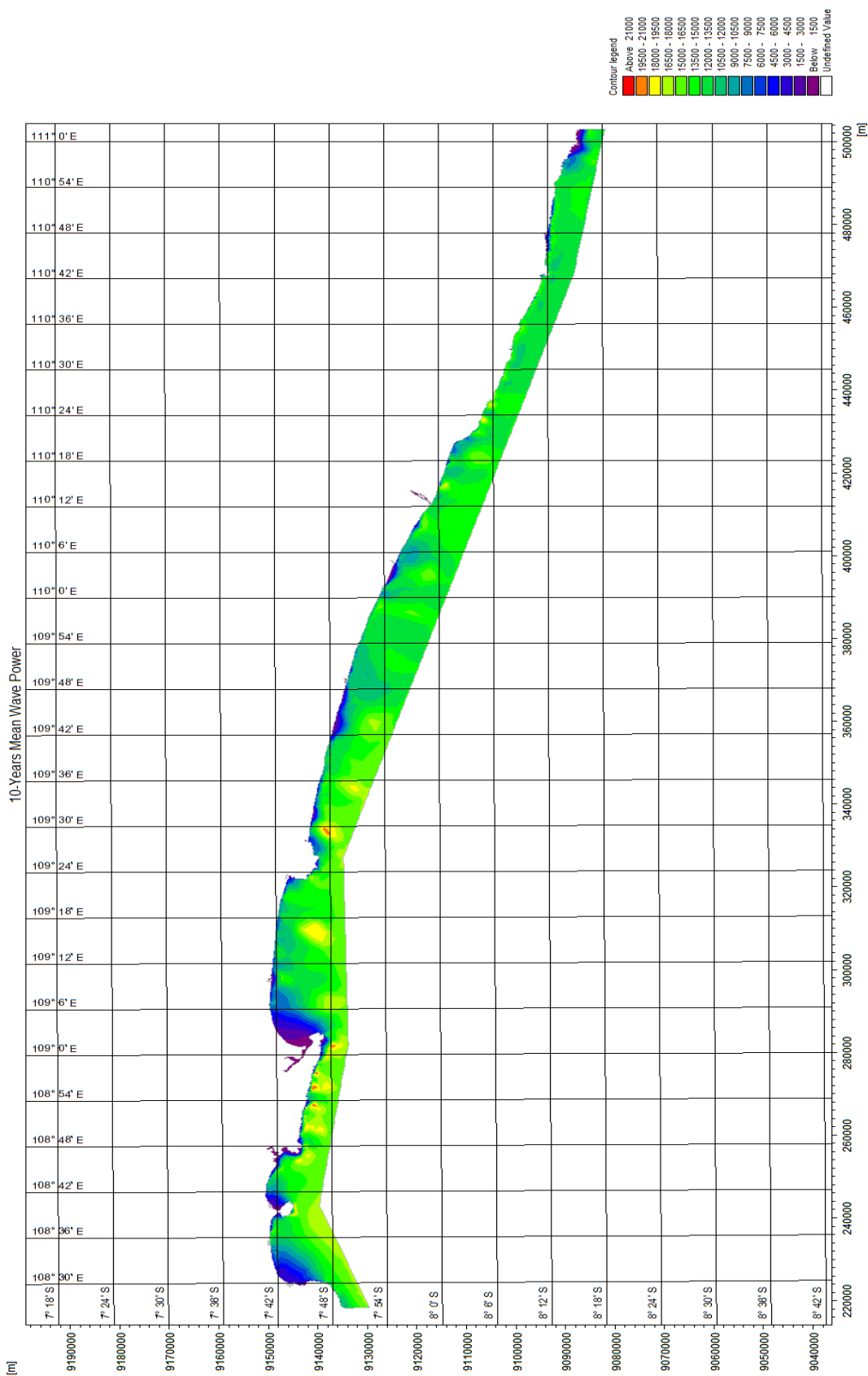


Figure 44: Distribution of 10-year Mean Wave Power

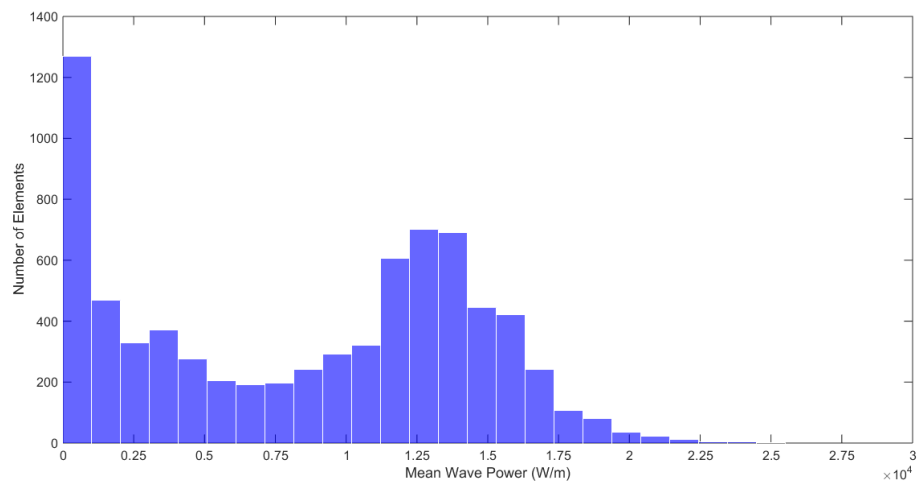


Figure 45: Histogram of 10-year Mean Wave Power

5.1.2 Monthly Analysis

This part is also significant to the time domain analysis. Figures 46–57 show the distribution of mean wave power for each month for the 10-year duration. The colors change from green to red and back to green again, thus revealing the quality of the mean wave power. Figure 58 shows the total mean wave power for each month. The maximum mean wave power appears in July, August, and September.

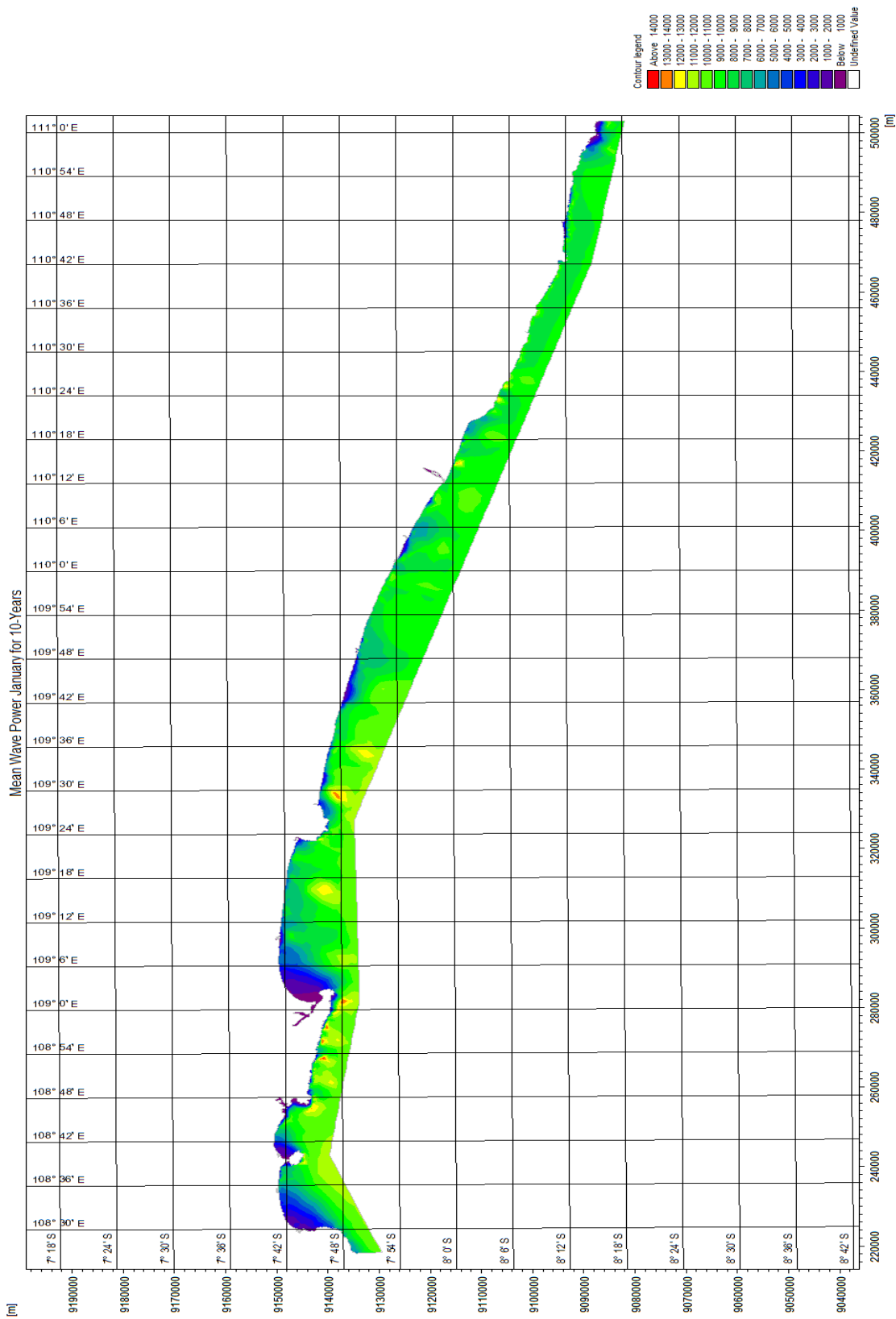


Figure 46: Distribution of 10-year Mean Wave Power of January

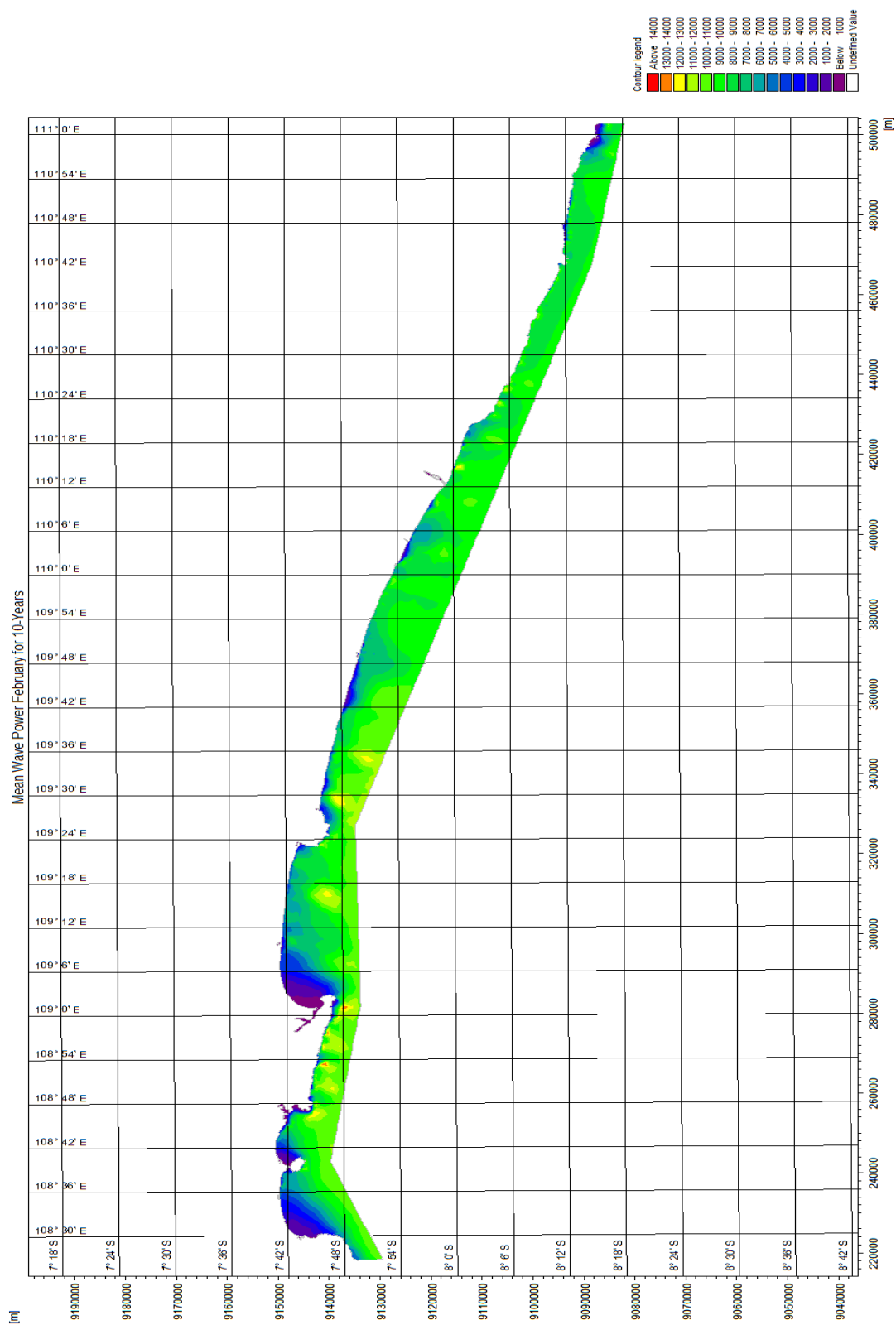


Figure 47: Distribution of 10-year Mean Wave Power of February

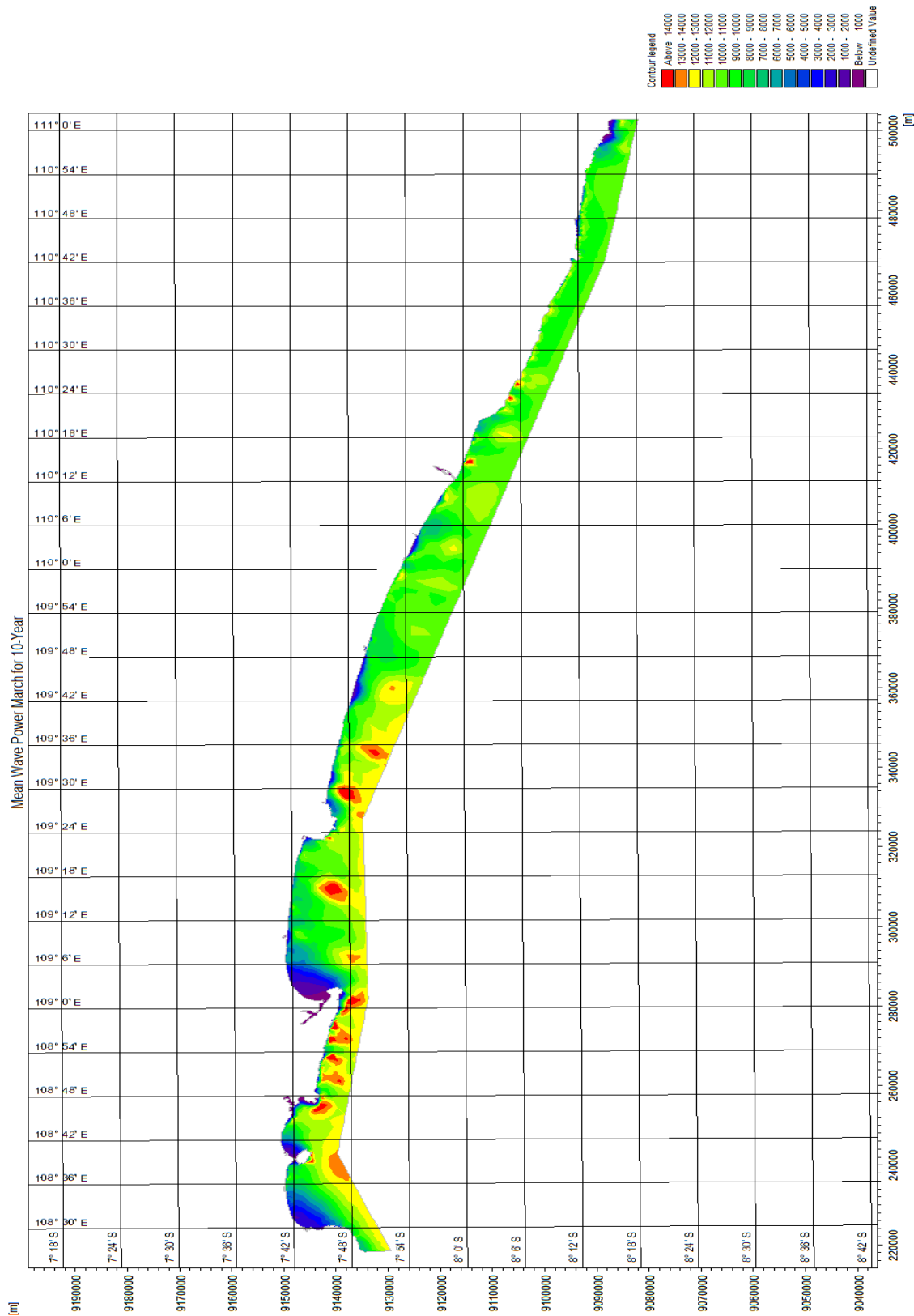


Figure 48: Distribution of 10-year Mean Wave Power of March

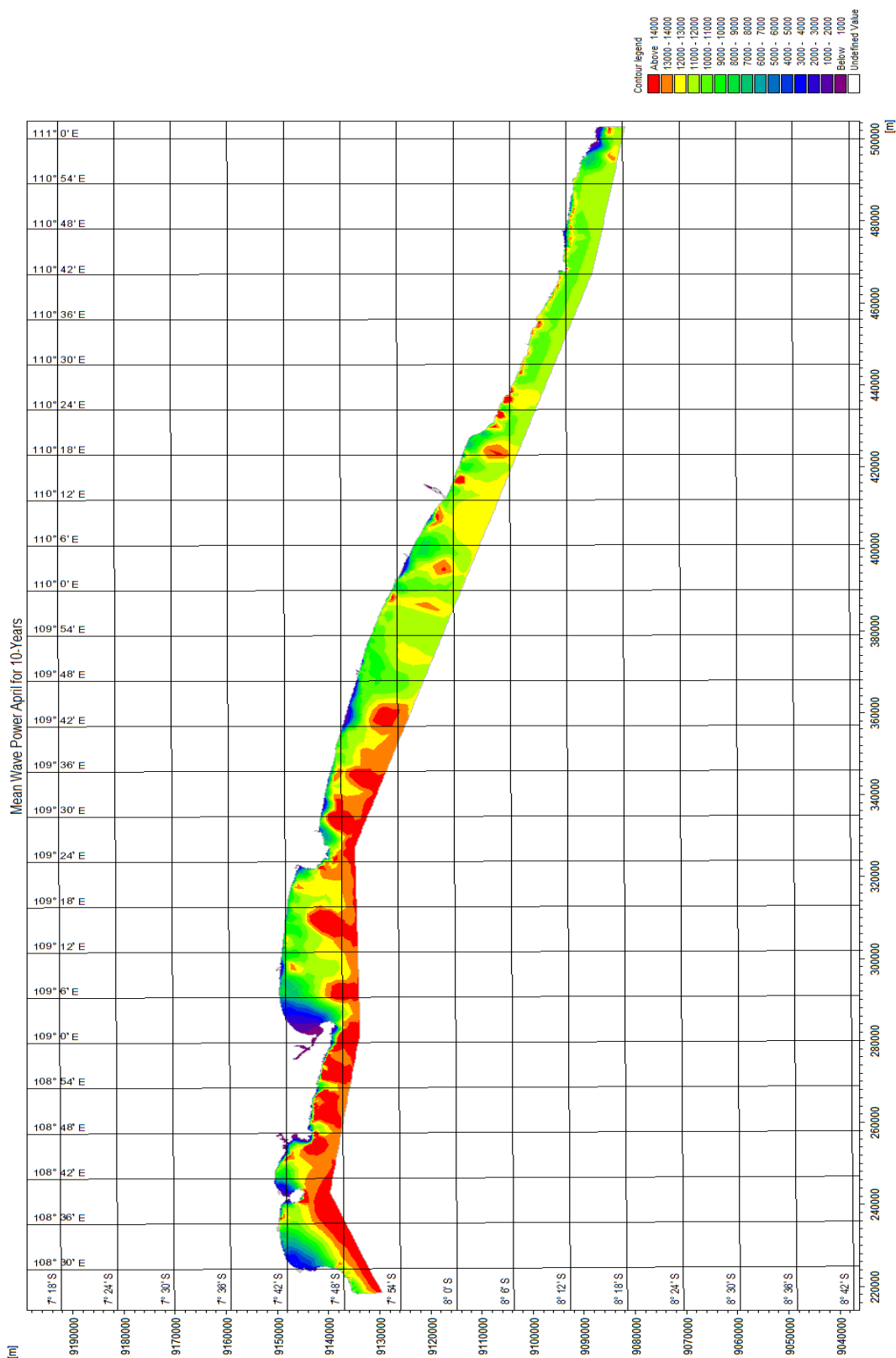


Figure 49: Distribution of 10-year Mean Wave Power of April

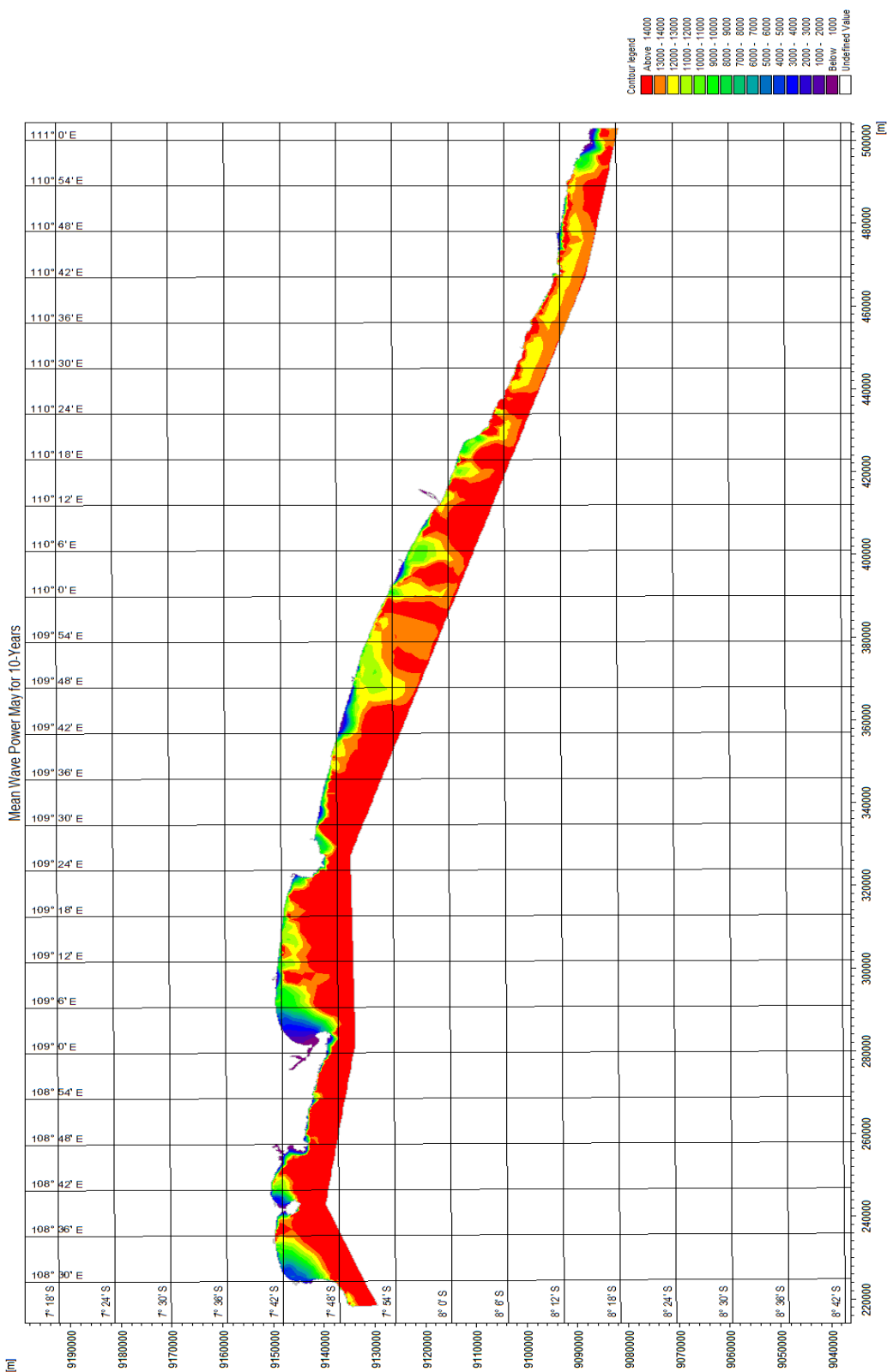


Figure 50: Distribution of 10-year Mean Wave Power of May

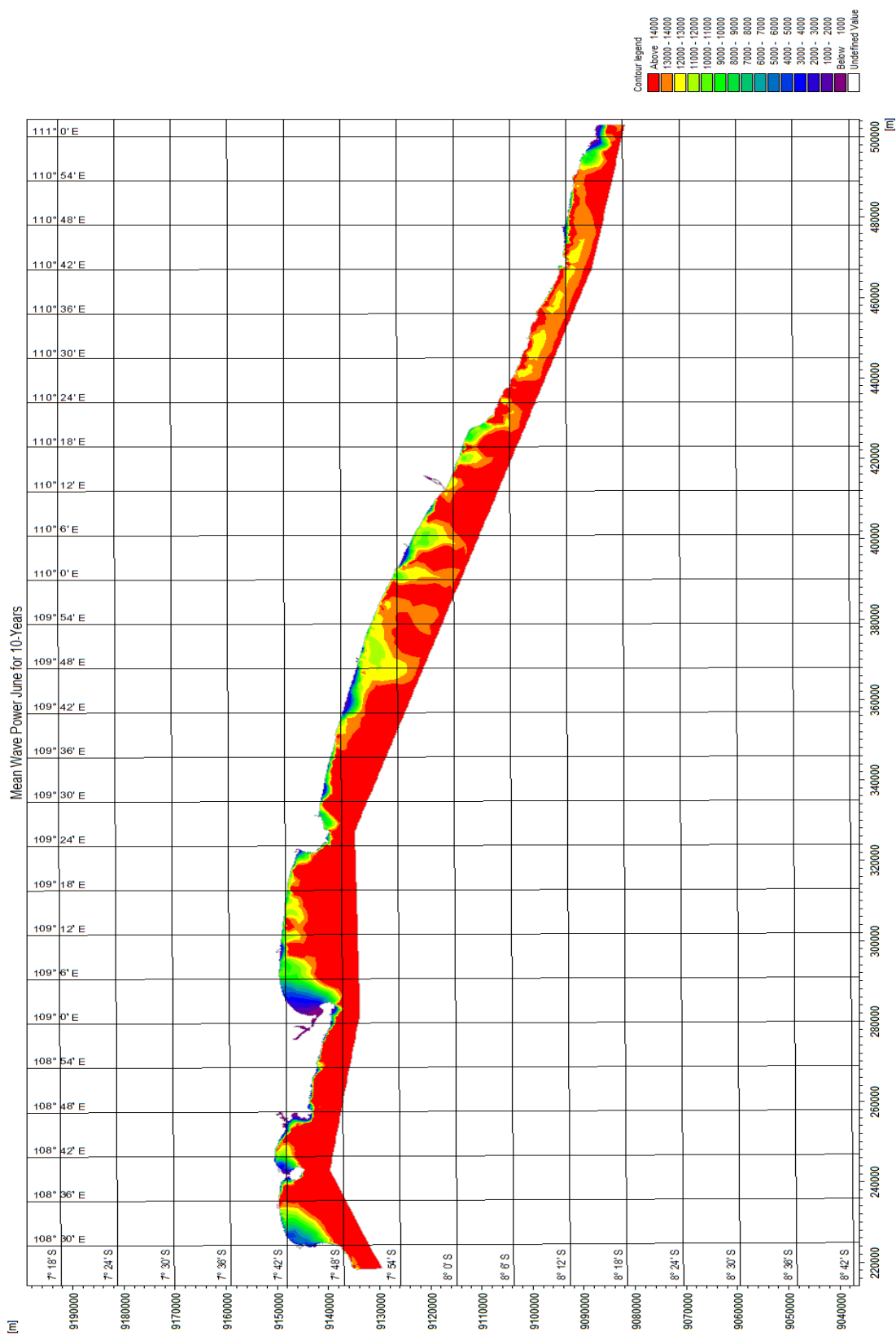


Figure 51: Distribution of 10-year Mean Wave Power of June

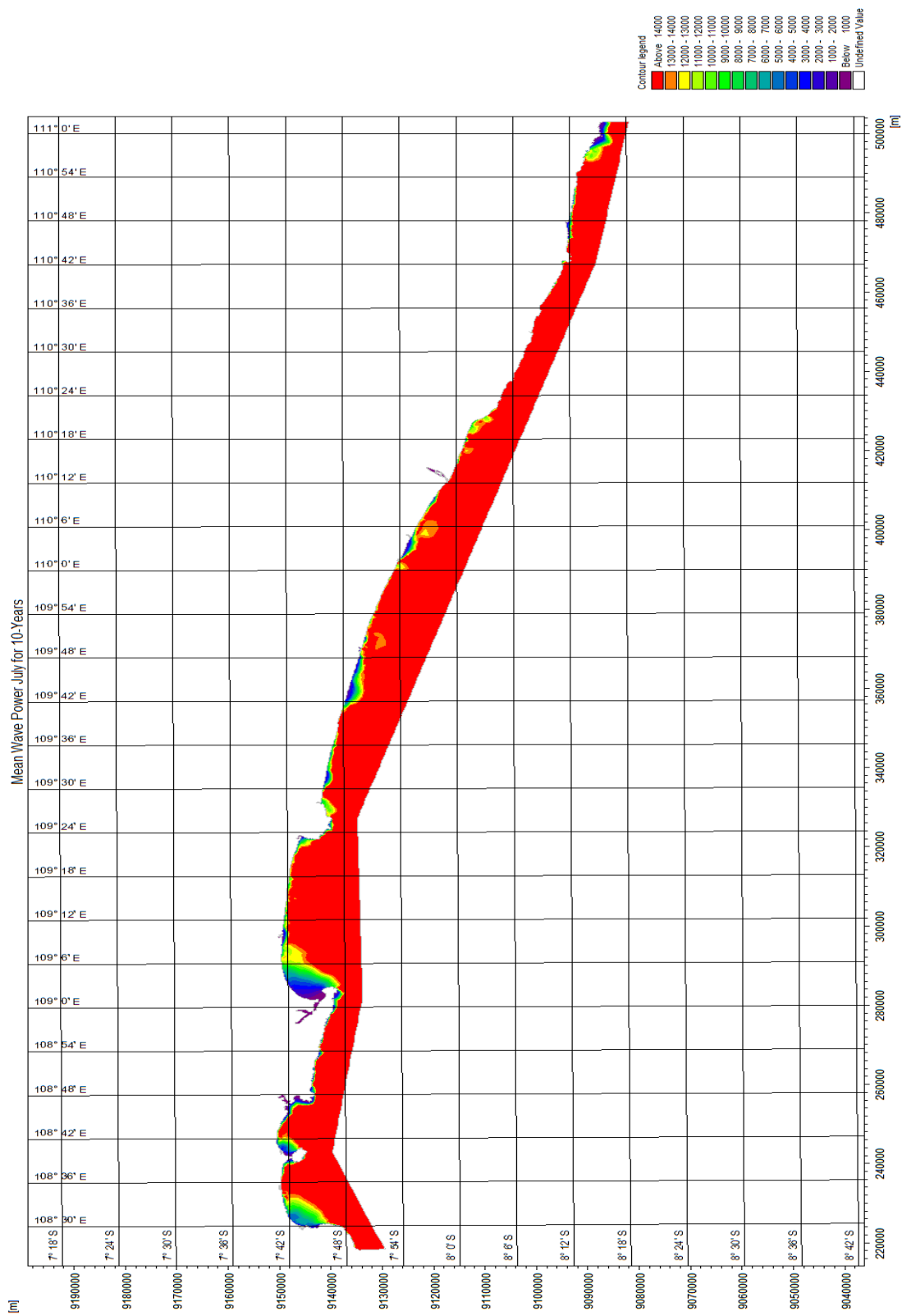


Figure 52: Distribution of 10-year Mean Wave Power of July

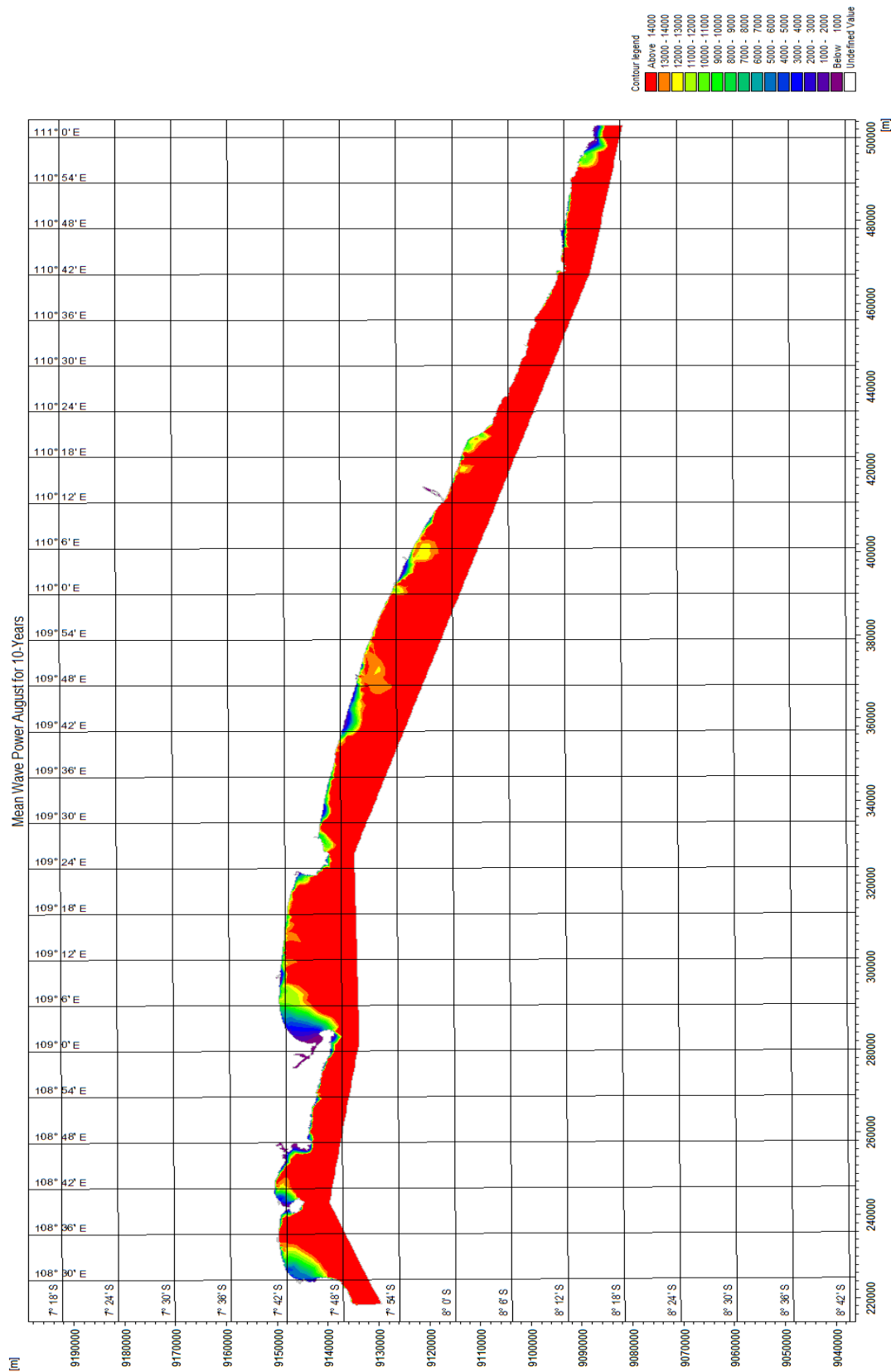


Figure 53: Distribution of 10-year Mean Wave Power of August

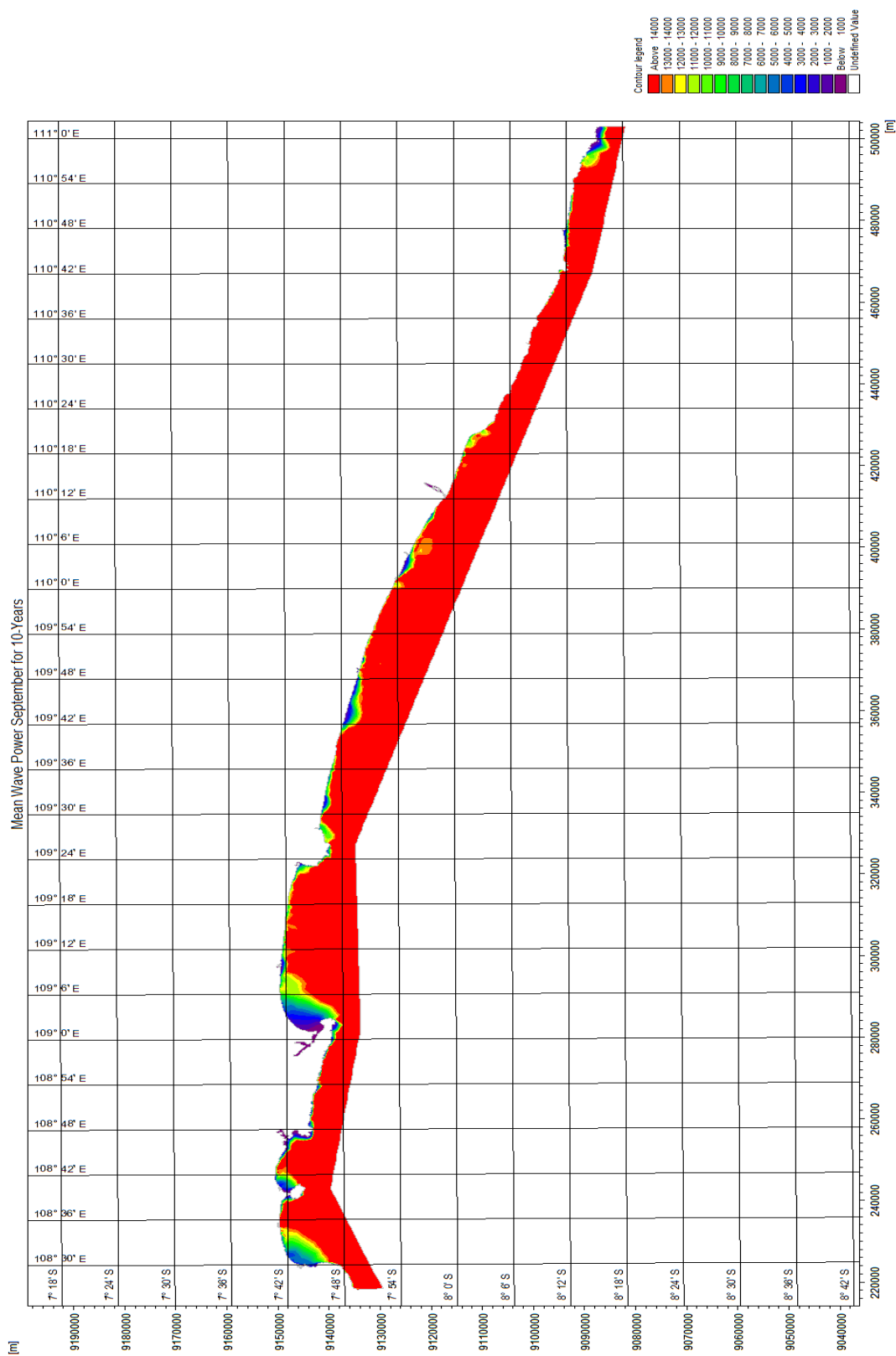


Figure 54: Distribution of 10-year Mean Wave Power of September

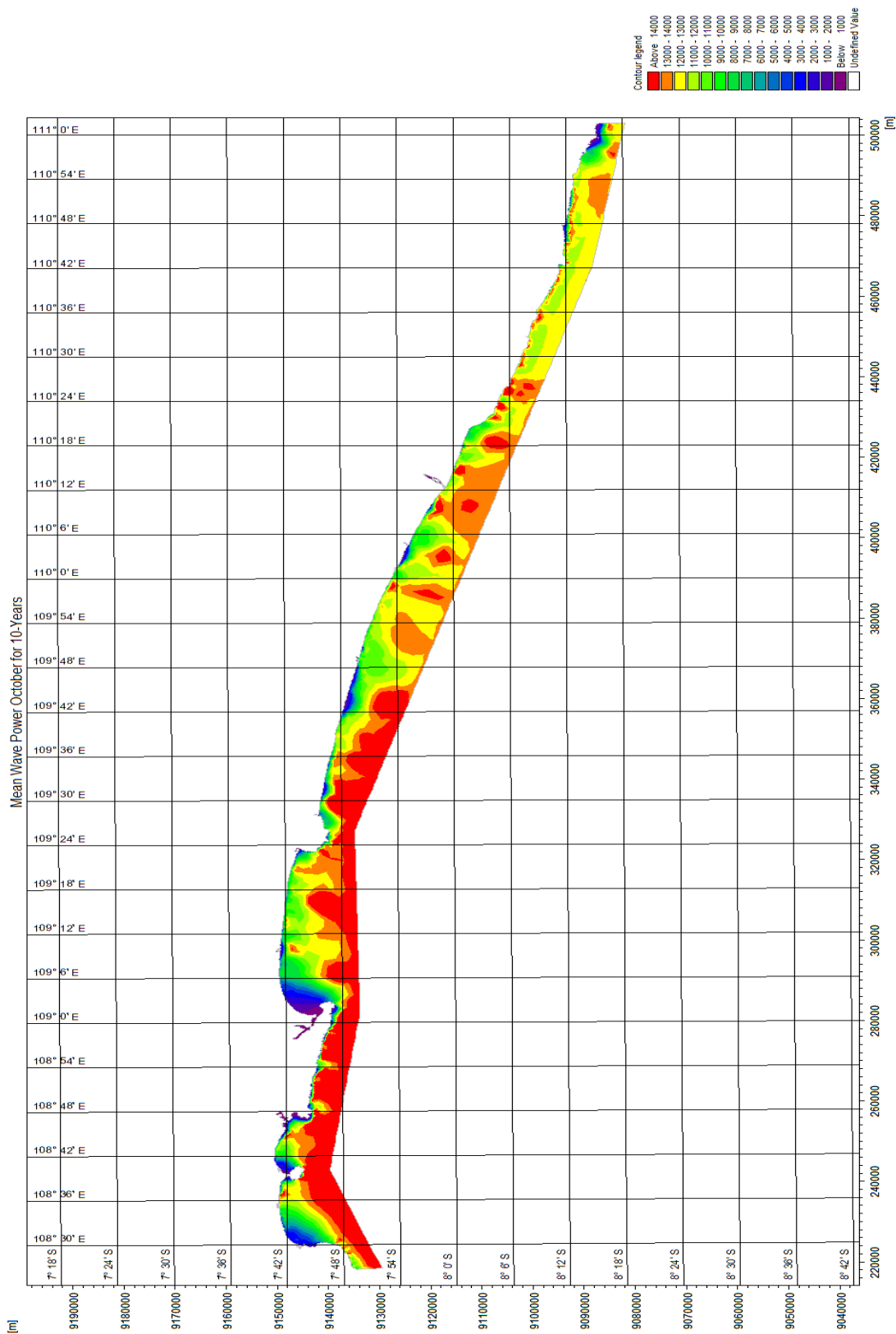


Figure 55: Distribution of 10-year Mean Wave Power of October

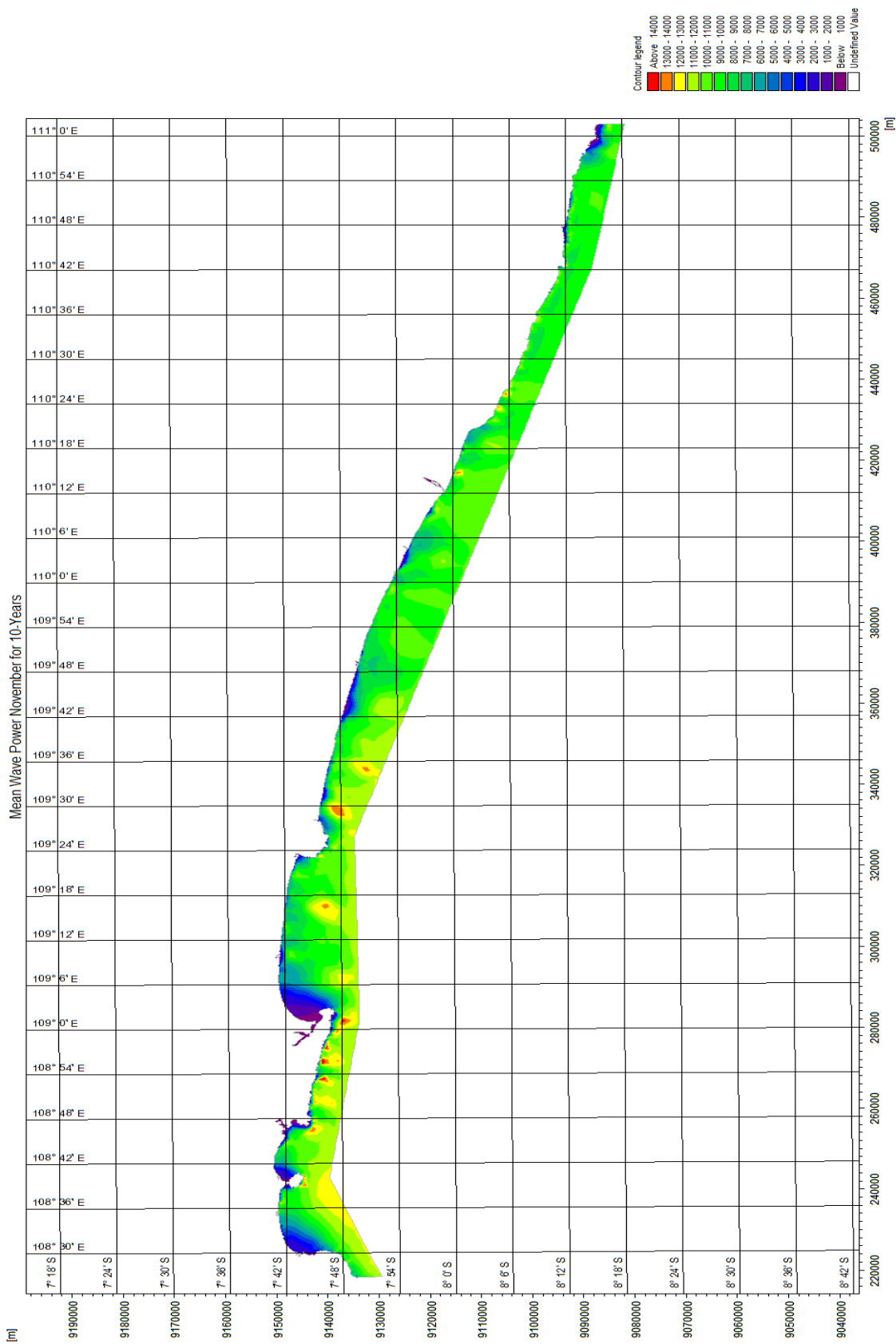


Figure 56: Distribution of 10-year Mean Wave Power of November

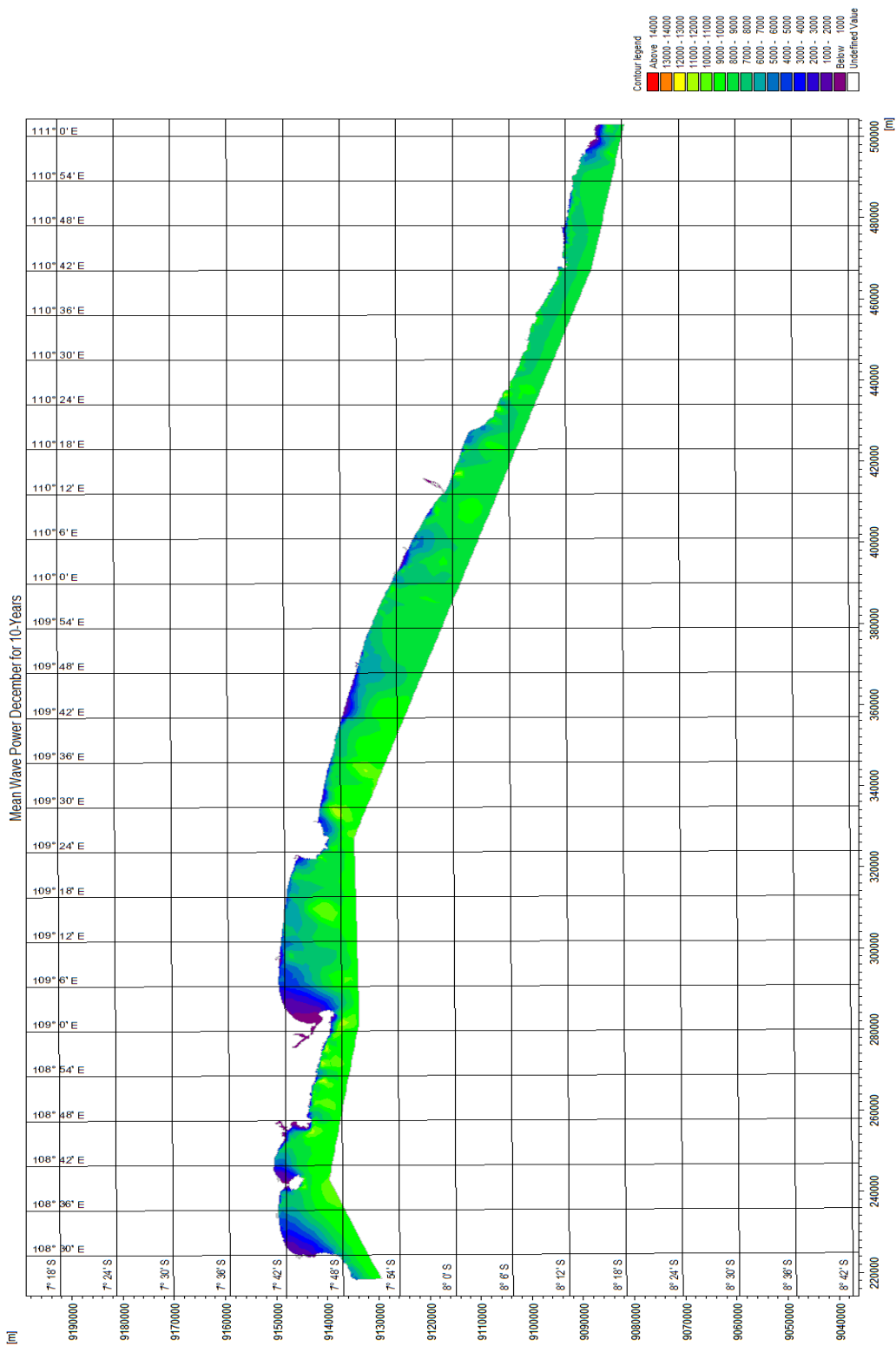


Figure 57: Distribution of 10-year Mean Wave Power of December

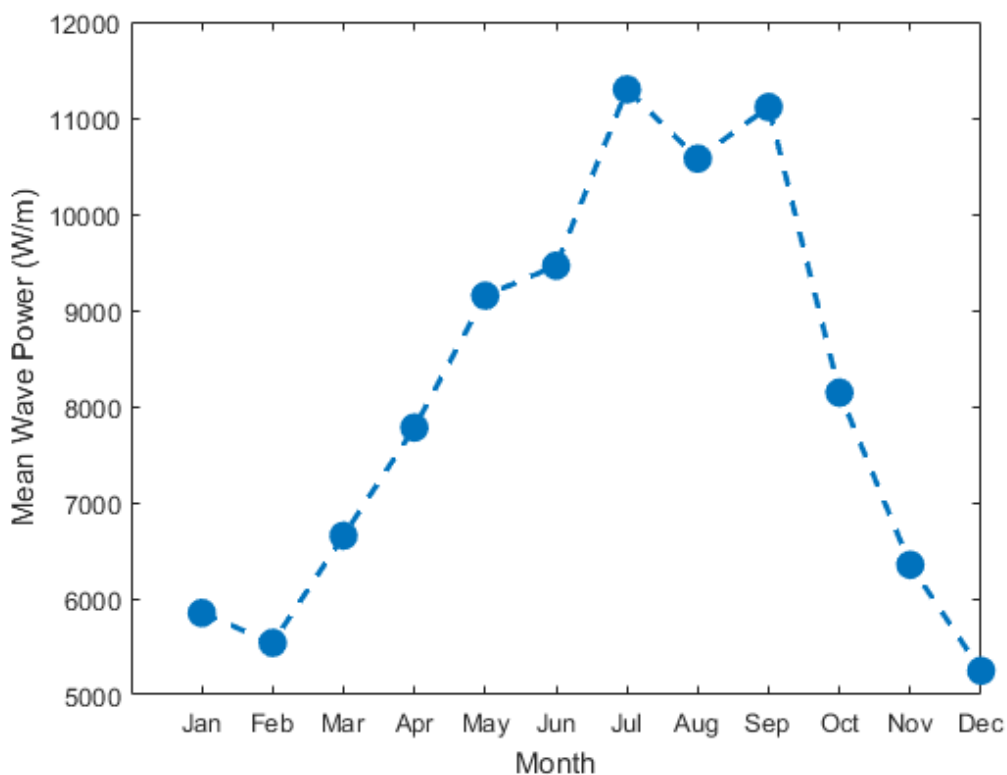


Figure 58: Monthly Mean Wave Power Potential Based on 10-year Assessment Data

5.2 Spatial Analysis

Analysis in the space domain is also important to determine a specific area to be a candidate for WEC location. Several parameters can determine the suitable candidate. For example, the area should be close to populated regions and/or industrial areas with high mean wave power and close to land. In this work, two large areas were selected and analyzed. These two areas are Penyu Bay and beaches along *Daerah Istimewa Yogyakarta* (DIY) or Special Region of Yogyakarta Coastline.

5.2.1 Penyu Bay

Penyu Bay is located next to Cilacap Regency, Central Java Province. According to the Population Density Report of the Indonesia Statistic Center Department, Cilacap was the most populated regency in Central Java Province in 2014 and has the largest area in the province. The total population is about 1,685,573

with a population density of about $788 \text{ people}/\text{km}^2$. Additionally, Cilacap is home to various industries, such as PT. Pertamina UP IV Cilacap (oil company), PT. Holcim Tbk (cement), PT. Panganmas Inti Persada (flour), PT. Juifa International Foods (fish canning), PT. Sinar Mas (cooking oil distributor), PT. Aspal Mitra Utama (asphalt distributor), PT. Lautan Murti (fish freezing), and many others. These indicate that the demand for electricity is relatively high in the area.

Figure 59 shows the discrete study area, which includes Penyu Bay with 2.5 km distance from the farthest coastal point and a 40 km span. The distribution of mean wave power for the 10-year duration is depicted in Figure 60. The histogram in Figure 61 shows that the distribution is prevalent for mean wave power in the range of $2.5\text{--}15 \text{ kW}/\text{m}$.



Figure 59: Penyu Bay Area

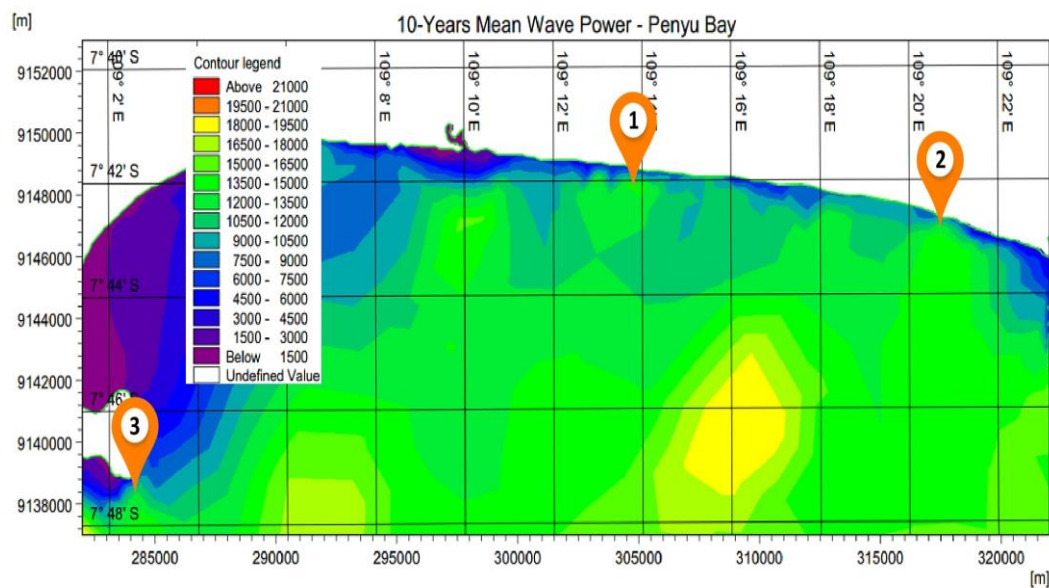


Figure 60: Distribution of 10-year Mean Wave Power in Penyu Bay Area and Pin Points of WEC Location Candidates

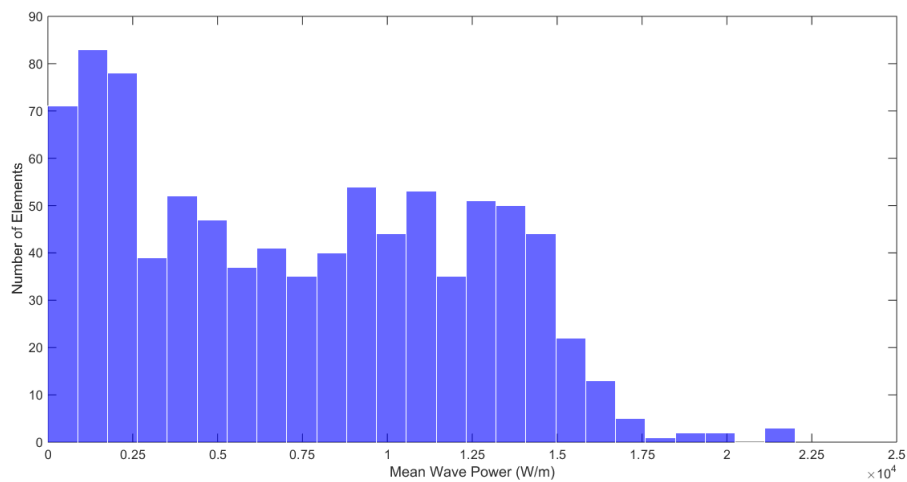


Figure 61: Histogram of 10-year Mean Wave Power in Penyu Bay

Based on observation and consideration of mean wave power and distance from the coastline, three points were considered suitable candidates for WEC location (pinned points in Figure 60). These three points are tabulated in Table 3, including the mean wave power, mean significant wave height, mean wave period, and distance from the coastline.

Table 3: Point Candidates for WEC Location in Penyu Bay

Point	Latitude	Longitude	Distance	\bar{P} (kW/m)	\bar{H}_s (m)	\bar{T} (s)
1	-7.699648	109.229929	< 325 m	~15	1.8114	8.8790
2	-7.714494	109.344889	< 300 m	~14	1.7056	8.8046
3	-7.788433	109.043550	< 350 m	~13	1.5237	8.7978

5.2.1 DIY Coastline

Another potential area is along the beaches on the DIY coastline. According to the Indonesia Statistic Center Department, the total population of DIY in 2015 was around 3.7 million with a population density of more than 1000 people/km²; the value increases annually. In terms of industry, in 2012, DIY had 391 industries in various sectors, such as manufacturers of computers and electronic products, foods and beverages, textiles, leather products, wood products, chemicals, pharmacies, and refined oil products. DIY is known as a progressive region with high economic growth. In 2015, DIY achieved around 5% economic growth. This shows that the demand for electricity in this region is high.



Figure 62: Beaches along DIY Coastline

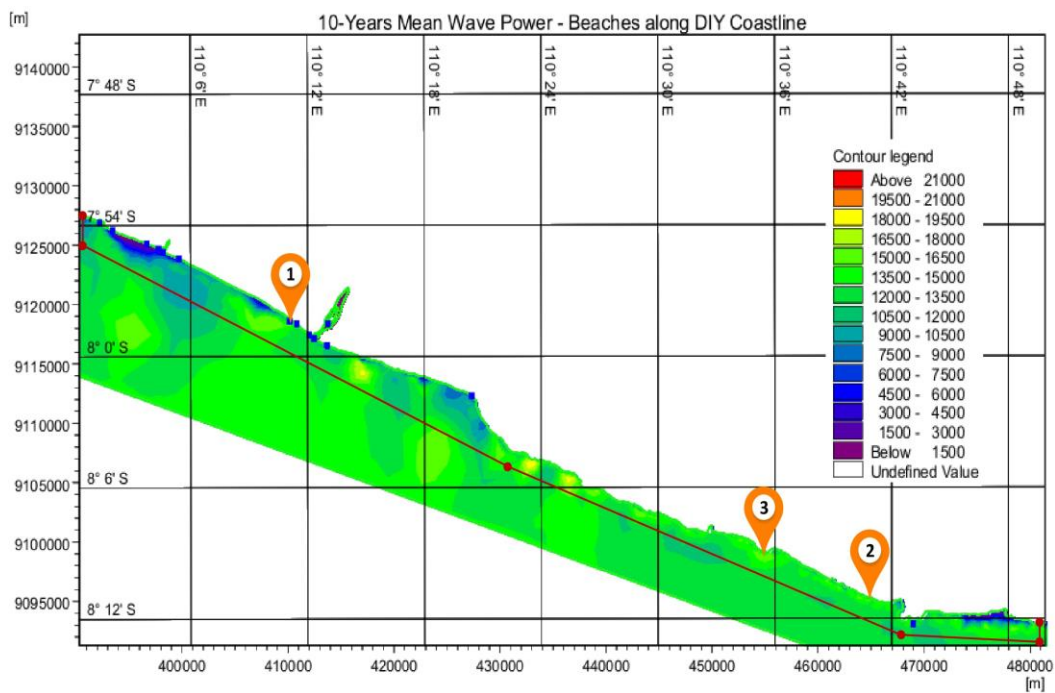


Figure 63: Distribution of 10-year Mean Wave Power along DIY Coastline and Pin Points of WEC Location Candidates

Table 4: Point Candidates for WEC Location in DIY Coastline

Point	Latitude	Longitude	Distance	\bar{P} (kW/m)	\bar{H}_s (m)	\bar{T} (s)
1	-7.974645	110.186874	< 250 m	~16	1.8421	8.5709
2	-8.189942	110.693915	< 200 m	~13	1.8534	8.8502
3	-8.139225	110.569732	< 225 m	~13	1.8963	8.150

Figure 62 shows the beach along >96 km DIY coastline with a width of around 2.5 km. The distribution of mean wave power for the 10-year duration is shown in Figure 63. Table 4 shows the point candidates for WEC location along the DIY coastline.

Chapter 6: Control Simulation Results and Discussion

This chapter presents the simulation results and analysis of the control part. The simulation setup and controller design are presented in Section 6.1. The strategies used for the control simulation are in Section 6.2. Section 6.3 shows the results and analysis for each controller to determine the performance in nominal conditions and at various sea states. An analysis of the system under perturbations and external disturbances is also presented. The simulation was performed using MATLAB Simulink.

6.1 Simulation Setup and Controller Design

Table 5: Electrical and Mechanical Parameters of the WEC

Parameter (symbol)	Value unit
Buoy's Radius (r)	5 m
Buoy and translator mass (m_b)	2.68×10^5 kg
Infinite added mass (m_∞)	1.34×10^5 kg
Water plane area (A_w)	78.54 m ²
Submerged Volume (V_s)	261.80 m ³
Sea water density (ρ)	1025 kg/m ³
Gravitational acceleration (g)	9.81 m/s ²
Seabed depth (d)	80 m
Resonance angular frequency (ω_0)	1.56 rad/s
Buoyancy stiffness coefficient (S_b)	7.89×10^5 N/m
Nominal restoring stiffness coefficient (S_{rs0})	2×10^5 N/m
Nominal losses resistance (R_{loss0})	0.4×10^5 N.s/m
PMLG synchronous resistance (R_s)	0.29 Ohm
Permanent magnet flux (λ_{PM})	23 Wb
PMLG pole width (p_ω)	0.05 m

Table 5 presents a list of the mechanical and electrical model parameters. A spherical buoy was used in this study. The transfer function in Equation (7) was obtained using the parameters in Table 5. WAMIT and a system identification technique were adopted as follows:

$$F_e(s) = \Phi(s)H(s),$$

$$\Phi(s) = \frac{(4.3 \times 10^5)s^8 + (4 \times 10^5)s^7 + (1.1 \times 10^6)s^6 + (7.3 \times 10^5)s^5 + (8.8 \times 10^5)s^4 + (3.6 \times 10^5)s^3 + (2.1 \times 10^5)s^2 + (4 \times 10^4)s - (6.1 \times 10^{-9})}{s^8 + 0.8s^7 + 2.4s^6 + 1.3s^5 + 1.8s^4 + 0.5s^3 + 0.4s^2 + 0.04s + 0.01}.$$

By using the same technique used to find $\Phi(s)$, the radiation force in Equation (12) was obtained as follows:

$$A_r = \begin{bmatrix} -3.4376 & -6.3533 & -4.9714 & -1.7168 \\ 1 & 0 & 0 & 0 \\ 0 & 1 & 0 & 0 \\ 0 & 0 & 1 & 0 \end{bmatrix}$$

$$B_r = [1 \ 0 \ 0 \ 0]^T$$

$$C_r = [0.96 \times 10^5 \ 3.6 \times 10^5 \ 1.57 \times 10^5 \ 0].$$

To fit the simulated data generated by WAMIT, by using the smallest order satisfying the numerical solution and estimation for radiation force, the fourth-order equation is sufficient. In this study, the effective peak frequency of a wave lies between 0.5 and 1 *rad/s*, and its significant height lies between 1 and 2 *m*. A sea state with a significant height greater than 2 *m* and peak frequency lower than 0.5 *rad/s* is too energetic, whereas a sea state with a significant height lower than 1 *m* and frequency greater than 1 *rad/s* possesses an immaterial energy content.

The highest values for control force $f_u^m(t)$ and the usage index are equivalent to 3 MN and 10, respectively. The tuned estimation values of γ for $H_s = 1$ *m* and $H_s = 2$ *m* are $\gamma =$

2 and $\gamma = 3$, respectively. By using the Bode plot, a look-up table was created and is presented in Table 6.

Table 6: Look-up Table for $\bar{R} \times 10^6$ [Ns/m] for Various Values of H_s [m], ω_p [rad/s] and γ

ω_p	$H_s = 1$		$H_s = 2$	
	$\gamma = 1$	$\gamma = 2$	$\gamma = 1$	$\gamma = 3$
0.50	0.60	0.30	1.20	0.40
0.55	0.58	0.29	1.16	0.39
0.60	0.56	0.28	1.12	0.37
0.65	0.54	0.27	1.07	0.36
0.70	0.51	0.25	1.02	0.34
0.75	0.49	0.24	0.98	0.33
0.80	0.47	0.23	0.94	0.31
0.85	0.44	0.22	0.89	0.30
0.90	0.42	0.21	0.83	0.28
0.95	0.40	0.20	0.81	0.27
1.00	0.37	0.19	0.75	0.25

Complex polynomial adjustment was employed to decide the acceptable PID gains fulfilling the design requirements of the servo feedback control system. By using the following procedure [48], which is the robust control toolbox in MATLAB, weighting function W_S was determined. The main parameter perturbations in the spring and losses coefficients were considered. The nominal values of S_s and R_{loss} were 2×10^5 N/m and 0 Ns/m, respectively. This implies that no loss forces existed in the nominal system. The perturbed system was simulated with the following equations.

$$S_s = S_{s0} + \Delta_s S_{s0},$$

$$R_{loss} = R_{loss0} + \Delta_l R_{loss0},$$

where S_{s0} is the nominal value of S_s and R_{loss0} is the initial value of R_{loss} . The highest perturbation is assumed to be equivalent to 50% of S_{s0} and R_{loss0} . In this manner, the estimations of Δ_s and Δ_l were shifted inside the scope of $[0 - 0.5]$. Transfer function $W_S(s)$, which is shown below, was obtained by using the system identification technique.

$$W_S(s) = \frac{0.0016s^5 + 0.2s^4 + 1.8s^3 + 7.6s^2 + 10.8s + 18.7}{s^5 + 4.5s^4 + 10.6s^3 + 33.4s^2 + 25.5s + 59.2}$$

Transfer function $W_T(s)$ was selected to be a low-pass filter that includes all the operating wave frequencies. Weighting function $W_T(s)$ was composed as the following equation.

$$W_T(s) = \frac{100}{s + 100}$$

The region examined to obtain the k_p gain was dependent on the magnitude of $f_e(t)$ because the magnitude of $f_u(t)$ depends on the value of k_p gain. The magnitude of $f_u(t)$ must be higher than $f_e(t)$ to produce a sufficient damping force for the PTO. The value of k_p gain was set to 10^6 . Multi-Parametric Toolbox was utilized to solve the linear programming because locating the acceptable gains of k_i and k_d is difficult [49]. All acceptable gains of k_i and k_d that fulfill the robust performance requirement for $k_p = 10^6$ are specified in the next inequality.

$$-k_i \leq 1$$

$$1.57 \times 10^{-23}k_i - k_d \leq 32360.7$$

$$-1.658 \times 10^{-24}k_i + k_d \leq 10514.6$$

Within an acceptable region, a set of k_i and k_d gains was selected. Transfer function $K(s)$ in Equation (16) is expressed by the following equation.

$$K(s) = \frac{100s^2 + 10^6s + 6.6 \times 10^7}{s} \quad (32)$$

Keeping in mind the end goal to evaluate mathematically whether the obtained PID controller fulfills the robust performance specification, transfer functions $W_S(s)$, $W_T(s)$, and $K(s)$ were substituted into Equation (20).

The proposed strategy was compared with diverse controllers. P1-RB and PT-RB demonstrate the proposed strategy with γ equal to one and γ equal to its tuned value, respectively. SPT-RB is a simplified version of PT-RB, in which estimation of γ is settled for all sea state conditions. The maximum value in Table 4 was selected to guarantee that the requirements in $f_u^m(t)$ and the use index were fulfilled. SPT-RB is less costly than P1-RB and PT-RB.

The proposed result was verified by utilizing regular (monochromatic) and irregular (polychromatic) sea states as well as in nominal and perturbation scenarios. Irregular sea states were generated with the JONSWAP spectrum [50], which is described by its H_s and ω_p . Simulink was utilized to run the simulation with a time sampling of 1 ms.

6.2 Simulation Strategy

The main simulation steps were as follows:

1. The values listed below were plotted against the specified peak frequency range (0.5–1 *rad/s*) of a nominal system in a regular (monochromatic) sea state with specific wave heights $H_s = 1\text{ m}$ and $H_s = 2\text{ m}$.
 - Average mechanical power \bar{P}_m
 - Average electrical power \bar{P}_e
 - Maximum control force f_u^m
 - Maximum electrical power P_e^m
 - Maximum electrical power to the average electrical power P_e^m / \bar{P}_e
 - Percentage of conversion efficiency between \bar{P}_m and \bar{P}_e
2. The response in the time domain of the nominal system in an irregular (polychromatic) sea state with wave height $H_s = 2\text{ m}$ and peak frequency $\omega_p = 0.7\text{ rad/s}$ was determined. The following measurements were performed in the time interval 20–140 *s*.

Mechanical quantities

- Reference \dot{z}_r and out velocities \dot{z} of excitation force and heaving buoy
- Output of heaving buoy η and excitation force position z
- Excitation force f_e and control force f_u
- Mechanical power p_m and its average \bar{P}_m

Electrical quantities

- d–q components of the stator voltage, v_{sq} and v_{sd}
- q-axis current component that implements control force

- EMF voltage of the linear generator
 - Electrical converted power p_e and its average \bar{P}_e
3. The performance of an irregular (polychromatic) sea state with $H_s = 2 \text{ m}$ and peak frequency $\omega_p = 0.7 \text{ rad/s}$ was examined under the presence of a disturbance force. The results are shown in tables, and these tables are arranged to contain nine cases of perturbations and a tenth one (the worst case) where external disturbance force $f_d(t)$ is added. The measurements for each case were as follows:
- Energy drop percentage based on the energy calculated for the nominal case,
 - Mean square error (MSE).

6.3 Results and Analysis

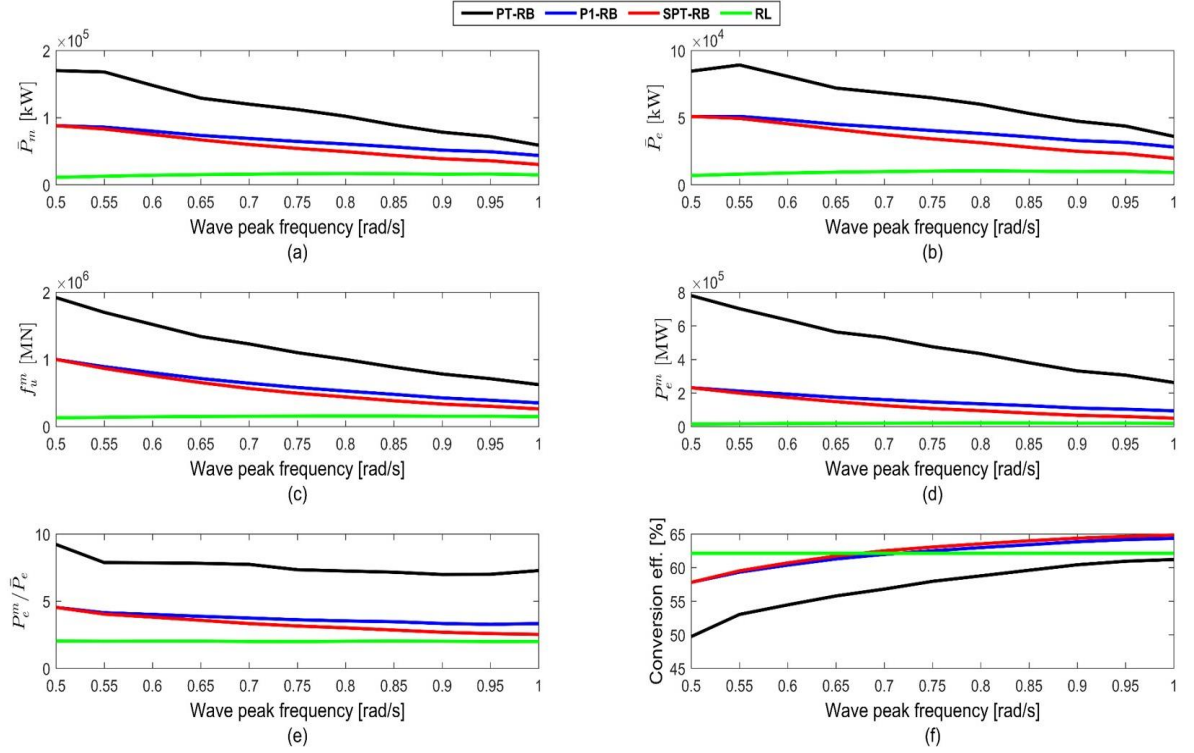


Figure 64: Simulation Results Obtained by the RL, P1-RB, PT-RB, and SPT-RB Methods for Regular (Monochromatic) Waves with $H_s = 1m$

The simulation results obtained by P1-RB, PT-RB, SPT-RB, and RL methods for regular (monochromatic) waves with $H_s = 1m$ are presented in Figure 64. The PT-RB method demonstrated a performance that is superior to that of the other methods in terms of \bar{P}_m and \bar{P}_e , as shown in Figures 64a–64b.

Figure 64c shows that the tuning value of γ was decided by the utilization index constraint rather than the maximum value of f_u^m . Figure 64e shows that PT-RB had the highest value of P_e^m / \bar{P}_e among all the methods. A high value of \bar{P}_e can be achieved if the design constraints in f_u^m and the maximum value of the utilization index are relaxed.

The RL method obtained the best conversion efficiency in the low-frequency range, i.e., 0.50–0.65 rad/s , among all the methods. P1-RB and SPT-RB had efficiencies in the frequency range of above 0.65–1 rad/s , as shown in Figure 64f. However, this does not mean that the RL method had the highest \bar{P}_e . The P1-RB method had better conversion efficiency than the PT-RB method because of the tuning value of γ .

The simulation results obtained by PT-RB, P1-RB, SPT-RB, and RL methods for regular (monochromatic) waves with $H_s = 2$ m are shown in Figure 65. PT-RB, P1-RB, and SPT-RB methods showed the well-designed values of \bar{R} in Equation (23). The tuning value of γ for PT-RB increased \bar{P}_e to more than twice the time within the majority of operating frequencies. For $H_s = 2$ m, the tuning value of γ was decided by the constraint in the maximum value of f_u^m rather than the utilization index. The performance of SPT-RB was improved for $H_s = 2$ m because the selected single value of its \bar{R} was designed for $H_s = 2$ m. The RL method had the highest conversion efficiency, and the conversion efficiency of the SPT-RB and P1-RB methods was slightly better than that of the PT-RB method.

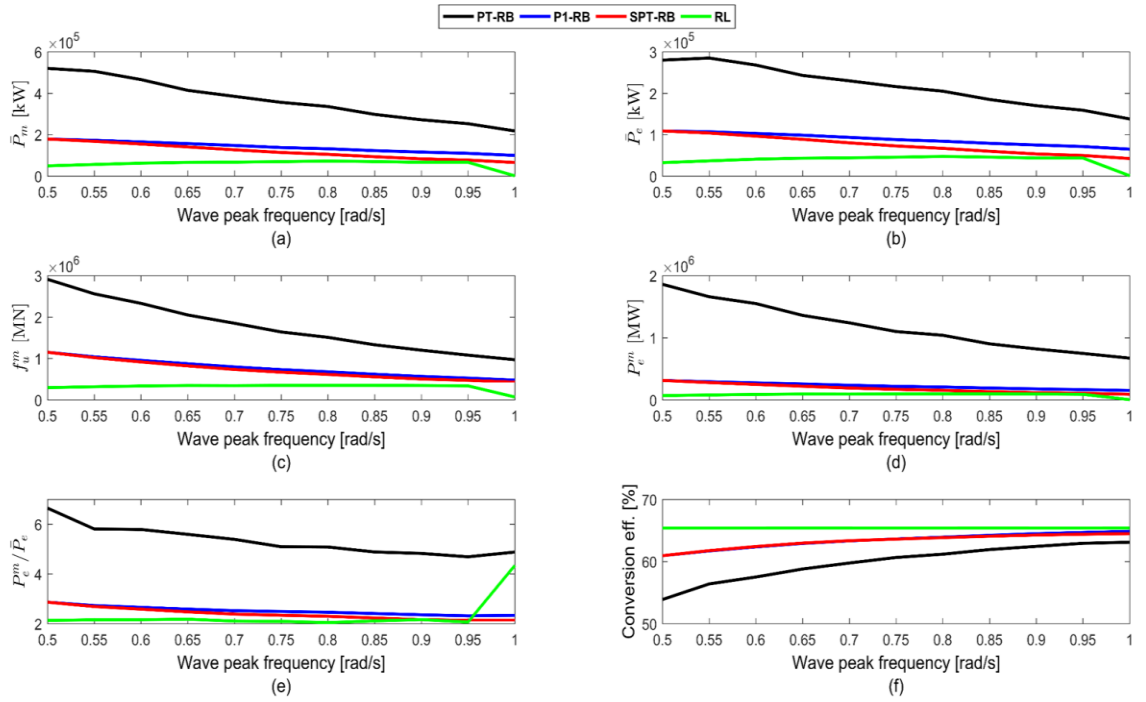


Figure 65: Simulation Results Obtained by the RL, P1-RB, PT-RB, and SPT-RB Methods for Regular (Monochromatic) Waves with $H_s = 2\text{ m}$

The selected value of \bar{R} is the largest value in Table 6, which is designed for $H_s = 2\text{ m}$ to ensure that the design constraints are not violated in all operating sea states. The simulation was conducted using $H_s = 1\text{ m}$. The value of \bar{P}_e can be increased for the SPT-RB method if a low value of \bar{R} is selected (e.g., the value of \bar{R} in the middle of Table 6 or the value of \bar{R} for dominant sea states).

The simulation results in terms of mechanical quantities obtained using the PT-RB method for irregular (polychromatic) waves with $H_s = 2\text{ m}$ and $\omega_p = 0.7\text{ rad/s}$ are shown in Figure 66. This figure shows the tracking capability of the obtained PID controller. The PTO almost perfectly tracked the reference velocity. A very small minimum square error (MSE) of 3.90×10^{-4} resulted from the simulation. The control action did not cause extreme excursions for the buoy (such as the buoy jumping out of the ocean surface or becoming totally submerged), as shown in Figure 66b. In this example, the maximum level of $f_u(t)$ was below its design value, as depicted in Figure 66c. The magnitude of $f_u(t)$ is reasonable because it

should be slightly higher than $f_e(t)$. The instantaneous mechanical power, $P_m(t)$, is shown in Figure 66d. An average mechanical power of 158 kW was obtained by the simulation.

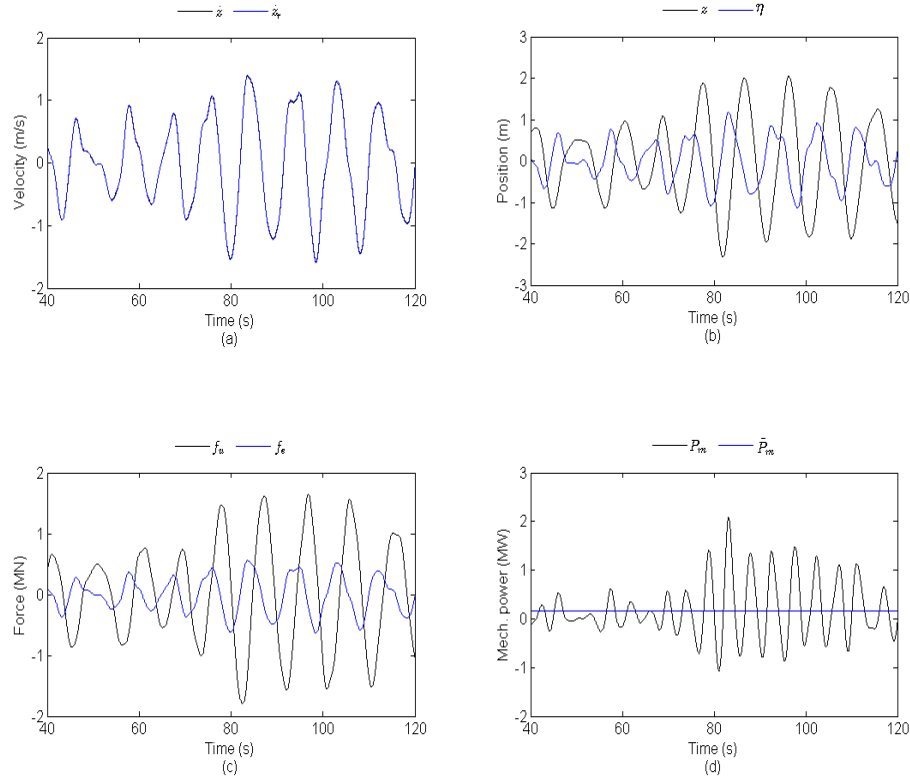


Figure 66: Simulation Results in Terms of Mechanical Quantities Obtained using the PT-RB Methods for Irregular (Polychromatic) Waves with $H_s = 2m$ and $\omega_p = 0.7 rad/s$

The simulation results in terms of electrical quantities obtained using the PT-RB method for irregular (polychromatic) waves with $H_s = 2 m$ and $\omega_p = 0.7 rad/s$ are shown in Figure 67. Figures 67a–67b show the voltages and currents for the direct and quadrature components, respectively. The EMF voltage is shown in Figure 67c, and instantaneous electrical power $P_e(t)$ is shown in Figure 67d. An average electrical power of 96 kW was obtained by the simulation. By comparing \bar{P}_m with \bar{P}_e , a conversion efficiency of 60.6% was obtained.

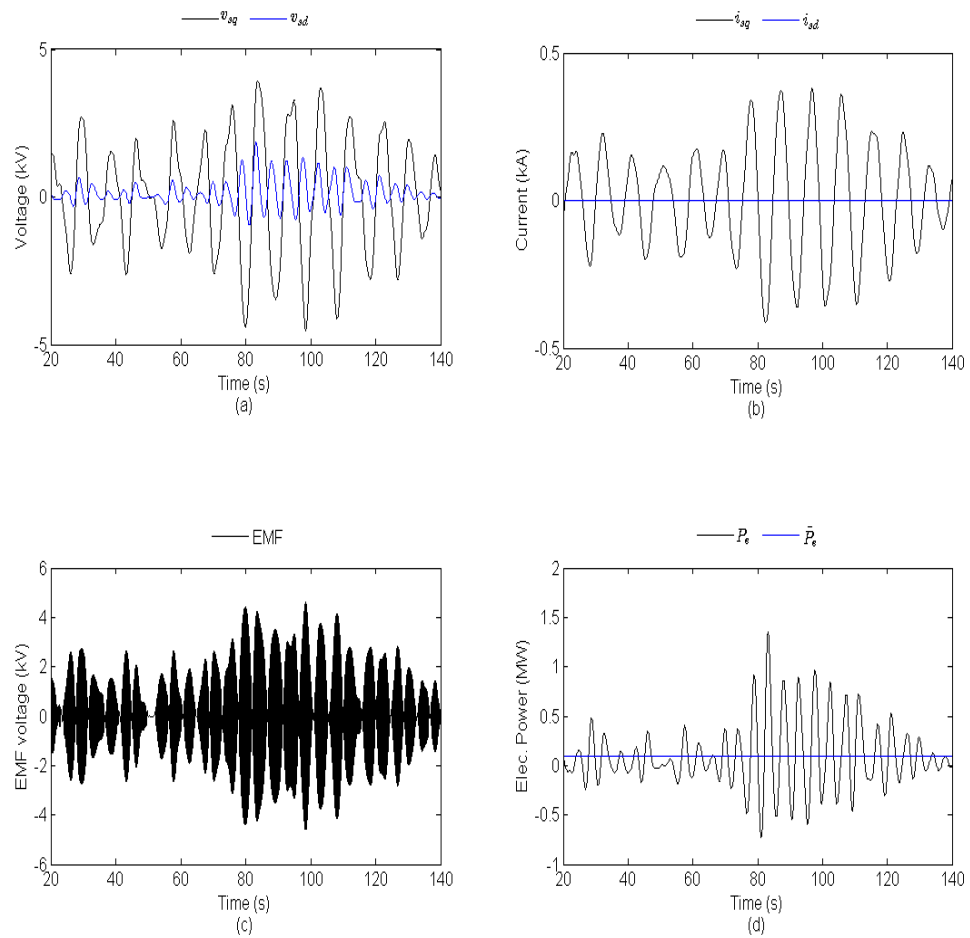


Figure 67: Simulation Results in Terms of Electrical Quantities Obtained using the PT-RB Methods for Irregular (Polychromatic) Waves with $H_s = 2m$ and $\omega_p = 0.7rad/s$

Table 7: Different Perturbation Scenarios in f_s and f_l using PT-RB Method

Cases	Δ_l [%]	Δ_s [%]	Energy [kWh]	Energy drop [%]	MSE
	-	-	6.6324	-	3.90E-04
Case 1	0	0	5.7035	14.0059	3.77E-04
Case 2	0	25	5.6994	14.0679	3.86E-04
Case 3	0	50	5.6953	14.1297	3.97E-04
Case 4	25	0	5.4712	17.5074	3.73E-04
Case 5	25	25	5.4675	17.5641	3.83E-04
Case 6	25	50	5.4637	17.6208	3.94E-04
Case 7	50	0	5.239	21.0089	3.70E-04
Case 8	50	25	5.2356	21.0604	3.80E-04
Case 9	50	50	5.2322	21.1118	3.90E-04
Worst	50	50	5.2247	21.224	4.27E-04

Table 8: Different Perturbation Scenarios in f_s and f_l using RL Method

Cases	Δ_l [%]	Δ_s [%]	Energy [kWh]	Energy drop [%]
	-	-	1.1831	-
Case 1	0	0	1.1366	3.9299
Case 2	0	25	1.0605	10.3608
Case 3	0	50	0.9906	16.2696
Case 4	25	0	1.1253	4.8847
Case 5	25	25	1.0506	11.2036
Case 6	25	50	0.9818	17.0159
Case 7	50	0	1.1141	5.8284
Case 8	50	25	1.0407	12.0373
Case 9	50	50	0.973	17.7546
Worst	50	50	0.7662	35.2394

Further simulations using the PT-RB method were conducted on the parameter perturbations to test the robustness of the control system. The parameter perturbations in S_s and R_{loss} that occur in the scenario described in Section 6.1 were considered.

The simulations were conducted by using the irregular sea state used in Figure 67 for the first 140 s only. The generated electrical energy and MSE between $z(t)$ and $z_r(t)$ were measured. The PT-RB method was compared with the RL method. The result is depicted in Tables 7 and 8. The PT-RB method maintained a low MSE value for all the perturbation cases. No MSE value was obtained for the RL method because RL is not a reference-based control method. PT-RB suffered an energy drop of 21.1% in case 9, where S_s and R_{loss} deviated by 50% from their nominal and initial values, respectively. A similar relative drop in energy was experienced by the RL method. However, PT-RB generated a larger amount of electrical energy than the RL method. In the PT-RB method, the perturbation in R_{loss} had a larger impact on the energy drop than the perturbation in S_s because the losses force is assumed to be unknown by the mathematical model.

Finally, the PT-RB method was tested by using the worst-case scenario. The worst-case scenario is defined as the parameter perturbations of case 9 in Tables 7 and 8 with the existence of unmodelled external force $f_d(t)$. The external force was formulated using the following equation.

$$f_d(t) = -S_{s0} - R_{loss0} - \alpha_d z(t) |z(t)| \sin(\omega_d t),$$

where $\alpha_d = 0.5 \times 10^4$ and $\omega_d = 0.5 \text{ rad/s}$. Similar to that in the previous test, the energy drop and MSE were measured. The results were compared with those of the RL method. The result of the test is shown in the last row of Tables 7 and 8 for each

method. PT-RB maintained the same energy drop compared with case 9, but the value of MSE slightly increased. The opposite condition occurred with the RL method. The method suffered almost twice the energy drop of case 9. and a drop of 35.24% with respect to its nominal case. This result indicates that the PT-RB method can better cope with the existence of unmodeled $f_d(t)$ compared with the RL method.

Chapter 7: Conclusion

In this study, hindcast data of 10 years were used to implement wave energy assessment for the Java Island coastline. MIKE 21 SW was used for the simulation. The model was developed by combining wind data from ECMWF. Then, the model was validated with observation buoy data provided by *Badan Pengkajian dan Penerapan Teknologi* (BPPT) or Agency for Assessment and Application of Technology, Indonesia. The validation result showed that the model results matched the observation data, and the average error was around 0.042%.

In addition, a modeling and control strategy for WECs was discussed. The main control objective of the proposed method was to maximize the captured mechanical power with the limitation of the maximum control force. This study used two levels of controllers: high-level and low-level controllers. The high-level controller provided the optimum reference velocity to fulfill the control objective. The low-level controller tracked the reference and provided robustness against model uncertainties. Simulation analyses were conducted. The results revealed the nominal and perturbation cases as well as monochromatic and polychromatic sea states.

7.1 Main Research Outcomes

This section presents a summary of the results of the assessment and control. In the energy assessment part, the simulation results and analysis were divided into two parts, which are time domain and spatial analyses.

1. Time domain analysis

Time domain analysis was split into two portions: 10-year mean analysis and monthly analysis.

a) For the 10-year mean analysis, the results are as follows:

- Maximum mean wave period = 10.1240 s,
- Maximum mean wave height = 2.2679 m,
- Most of the elements have mean wave power = 12.5 kW/m.

b) For the monthly analysis, the results are as follows:

- The maximum mean wave power appears in July, August, and September with a value of more than 10 kW/m;
- The minimum mean wave power appears in December, January, and February.

2. Spatial analysis

- a. In the spatial analysis, two large areas were selected and analyzed. These two areas are Penyu Bay and the beaches along the DIY coastline. Penyu Bay has a mean wave power between 2.5 and 15 kW/m, and the beaches along the DIY coastline have a mean wave power of around 12 kW/m.
- b. For each area (Penyu Bay and beaches along the DIY coastline), three different locations were selected. These locations have the most powerful sea parameters in terms of mean wave power, mean significant wave height, mean wave period, and distance from the coastline.

In terms of the control result, three scenarios, namely, regular conditions (monochromatic), irregular conditions (polychromatic), and perturbation situation, were adopted.

1. Regular conditions (monochromatic) for various sea states and for $H_s = 1\text{ m}$ and

$$H_s = 2\text{ m}.$$

- The PT-RB method had the highest value of P_e^m/\bar{P}_e among all the compared methods.
- The RL method achieved the best conversion efficiency among all the

methods (but this does not mean that the RL method had the highest \bar{P}_e).

2. Irregular conditions (polychromatic) for $H_s = 2 \text{ m}$ and $\omega_p = 0.7 \text{ rad/s}$ using the PT-RB method.
 - a. Mechanical quantities:
 - PTO almost perfectly tracked the reference velocity with a small MSE
 - Average mechanical power = 158 kW
 - b. Electrical quantities:
 - Average electrical power = 96 kW
 - The conversion efficiency between \bar{P}_m and $\bar{P}_e = 60.6\%$
3. Perturbation scenario in f_s and f_l using PT-RB and RL methods.
 - The PT-RB method can better handle the existence of unmodelled $f_d(t)$ compared with the RL method.

7.2 Future Work

Although this work analyzed the wave energy in Central Java and DIY regions with potency and control techniques for PMLG WECs, many opportunities for extending the scope of this study remain. Several directions can be pursued as follows:

1. Simulation domain enlargement

The simulation domain in this work is limited to Central Java and DIY regions. Knowing that the program is resourceful and powerful, a study on a similar topic in other areas is possible. Simulation domain enlargement will increase the simulation time. In this case, the simulation machine should be upgraded.

2. Time duration extension

The 10-year duration used in this study can be extended. ECMWF provides data from 1979. The result will be more valid with a longer hindcast duration for wave energy assessment. Considering that this will increase the simulation time, CPU improvement is necessary.

3. Experimental test for the Central Java SW model

The SW model for the Central Java region generated in this work can be used to perform an initial analysis for experimental study. The model can be applied in the Laboratory Test Linear Generator in the UAEU Laboratory to study related phenomena, determine the real wave energy potency, and design effective and optimum control techniques.

4. Implement this model in different regions around the world

The results and experiences obtained from this research will help in implementing wave energy assessment in different places around the world. The results can be applied to the United Arab Emirates due to the similarity in wave characteristics between the two regions.

5. Expansion of renewable energy and sustainable

New research on renewable energy and sustainable developments should be supported. Researchers should be encouraged to develop and conduct research on wave energy projects to generate clean energy, desalinated seawater, and cooling devices by passing the seawater (heat exchanger).

References

- [1] A. Omri and D. Nguyen. On the determinants of renewable energy consumption: International evidence. *Energy*, 72:554–560, 2014.
- [2] P. Moriarty and D. Honnery. What is the global potential for renewable energy? *Renewable and Sustainable Energy Reviews*, 16:244252, 2012.
- [3] T. Corsatea. Increasing synergies between institutions and technology developers: Lessons from marine energy. *Energy Policy*, 74:682696, 2014.
- [4] International Energy Agency (IEA). Implementing agreement on ocean energy systems (iea-oes), annual report, 2012. Technical report.
- [5] J. Cruz. *Ocean Wave Energy, Current Status and Future Perspectives*. Springer, Berlin, Germany, 2010.
- [6] J. Falnes. A review of wave-energy extraction. *Marine Structures*, 20: 185–201, 2007.
- [7] M. McCormick. *Ocean Engineering Mechanics with Applications*. Cambridge University Press, Cambridge, UK, 2010.
- [8] R. Dean and R. Dalrymple. *Ocean Engineering Mechanics with Applications*. World Scientific, Singapore, 1991.
- [9] J. Falnes. *Ocean Waves and Oscillating Systems*. Cambridge University Press, 2002.
- [10] F. Fusco and J. Ringwood. A simple and effective real-time controller for wave energy converters. *IEEE Transactions on Sustainable Energy*, 4:21–30, 2014.
- [11] O. Falcao. Wave energy utilization: a review of the technologies. *Journal of Renewable and Sustainable Energy Reviews*, 14:899, 2010.
- [12] R. Henderson. Design, simulation, and testing of a novel hydraulic power take-off system for the pelamis wave energy converter. *Renewable Energy*, 31:271283, 2006.
- [13] R. Ekstrom and M. Leijon. Control of offshore marine substation for grid-connection of a wave power farm. *International Journal of Marine Energy*, 5:24–37, 2014.

- [14] Seabased AB. Projects, 2013. URL <http://www.seabased.com/en/>.
- [15] A. Price. New Perspectives on Wave Energy Converter Control. Ph.D. thesis, University of Edinburgh, 2009.
- [16] C. Bostrom, B. Ekergard, and M. Leijon. Electric resonance-rectifier circuit for renewable energy conversion. *Appl Phys Lett*, page 100(043511), 2013.
- [17] C. Bostrom, B. Ekergard, and M. Leijon. Electrical damping of linear generators for wave energy converters a review. *Renewable and Sustainable Energy Reviews*, 42:116128, 2015.
- [18] J.P. Sierra, C. Mösso, D. González-Marco, Wave energy resource assessment in Menorca (Spain), *Renewable Energy*, Volume 71, November 2014, Pages 51-60, ISSN 0960-1481
- [19] P. Mota, J.P. Pinto, Wave energy potential along the western Portuguese coast, *Renewable Energy*, Volume 71, November 2014, Pages 8-17, ISSN 0960-1481,
- [20] Michael G. Hughes, Andrew D. Heap, National-scale wave energy resource assessment for Australia, *Renewable Energy*, Volume 35, Issue 8, August 2010, Pages 1783-1791, ISSN 0960-1481,
- [21] Gunwoo Kim, Weon Mu Jeong, Kwang Soo Lee, Kicheon Jun, Myung Eun Lee, Offshore and nearshore wave energy assessment around the Korean Peninsula, *Energy*, Volume 36, Issue 3, March 2011, Pages 1460-1469, ISSN 0360-5442,
- [22] Luca Liberti, Adriana Carillo, Gianmaria Sannino, Wave energy resource assessment in the Mediterranean, the Italian perspective, *Renewable Energy*, Volume 50, February 2013, Pages 938-949, ISSN 0960-1481, <http://dx.doi.org/10.1016/j.renene.2012.08.023>.
- [23] JB Settelmaier, A Gibbs, P Santos, T Freeman, D Gaer , simulating waves nearshore (swan) modeling efforts at the national weather service (nws) southern region (sr) coastal weather forecast offices (wfos) ,P roc. 91 st AMS Annual Meeting, 2011
- [24] SWAN, User manual, Delft University of Technology, Environmental Fluid Mechanics Section, Version 41.10, June 2016.
- [25] SWAN, Technical documentation, Delft University of Technology, Environmental Fluid Mechanics Section, Version 40.51, June 2016.
- [26] TOMAWAC Program, OPERATING MANUAL, TELEMAC MODELLING SYSTEM, Release 7.1, 2016.

- [27] TOMAWAC, Wave propagation in coastal areas, retrieved from <http://www.opentelemac.org/index.php/presentation?id=20>
- [28] MIKE 21 Wave Modelling, DHI, Agern Allé 5 DK-2970 Hørsholm Denmark, 2015.
- [29] T. Brekken, T. "On model predictive control for point absorber wave energy converters", Proc. of IEEE Trondheim Power Tech., 2011.
- [30] F. Fusco, J. Ringwood, J. "Hierarchical robust control of oscillating wave energy converters with uncertain dynamic", IEEE Transactions on Sustainable Energy, 5, pp. 598-966, 2014.
- [31] A. Wahyudie, M. Jama, Saeed, O. et al. "Robust and low computational cost controller for improving captured power in heaving wave energy converters", Elsevier Journal of Renewable Energy, 82, pp. 114-124, 2015.
- [32] A. Wahyudie, M. Jama, Saeed, O. "Robust Hierarchical Control Strategy for Heaving Wave Energy Converters", In Proc. of IEEE Oceans Conference, 2015.
- [33] M. Jama, H. Noura, A. Wahyudie, et al. "Enhancing the performance of heaving wave energy converters using model-free control approach", Elsevier Journal of Renewable Energy", 83, pp. 931-941, 2015.
- [34] A. Jaen, D. Andrade, A. Santana. "Increasing the efficiency of the passive loading strategy for wave energy conversion", Journal of Renewable and Sustainable Energy, 5, 053132, 2013.
- [35] M. Schoen, J. Hals, T. Moan. "Wave prediction and robust control of heaving wave energy devices for irregular waves", IEEE Transactions on Sustainable Energy, 26, pp. 627-638, 2011.
- [36] M. Jama, A. Wahyudie, A. Assi, et al. "An intelligent fuzzy logic controller for maximum power capture of point absorbers", Energies, 7, pp. 4033-4053, 2014.
- [37] E. Amon, T. Brekken, A. Schacher. "Maximum power point tracking for ocean wave energy conversion", IEEE Transactions on Industry Applications, 48, pp. 1079-1086, 2012.
- [38] D. Andrade, A. Jaen, A. Santana. "Considering linear generator copper losses on model predictive control of a point absorber wave energy converter", Elsevier Journal of Energy conversion and management, 78, pp. 173-183, 2014.

- [39] M. Richter, M. Magana, O. Sawodny, T. Brekken. “Nonlinear model predictive control of a point absorber wave energy converter”, *IEEE Transactions on Sustainable Energy*, 4, pp. 118-126, 2013.
- [40] U. Rachmawati, H. Suhartanto. “Analysis of Indonesia e-Government grid services simulation based on population”. *International Journal of Software Engineering and Its Applications*. 8: 89-100, 2014.
- [41] A. Wahyudie, O. Saeed, M. Jama, H. Noura and K. Harib, “Maximising power conversion for heaving point absorbers using a reference-based control technique”, *IET Renewable Power Generation*, 2016.
- [42] R. Taghipoura, T. Perez and T. Moan, “Hybrid frequency-time domain for dynamic response analysis of marine structures”, *Elsevier Journal of Ocean Engineering*, Vol 4, pp. 685–705, 2008.
- [43] WAMIT, User Manual, Wamit Inc, retrieved from <http://www.wamit.com>.
- [44] S. K. Sul, “Control of electric machine drive systems”, Wiley, 2011.
- [45] J. Doyle, B. Francis, and A. Tannenbaum, “Feedback control theory”, Macmillan Publishing Co., 1990.
- [46] M. Ho and C. Lin, “PID controller design for robust performance”, *IEEE trans. on Automatic Control*, Vol. 48, No. 8, pp. 1404–1409, 2003.
- [47] M. Tucker, “Waves in ocean engineering: measurement, analysis, and interpretation”, Ellis Horwood LTD, 1991.
- [48] S. Skogestad and I. Postlethwaite, “Multivariable feedback control: analysis and design”, Wiley, 2005.
- [49] “Multi-parametric toolbox 3”, ETH Zurich, available online: <http://people.ee.ethz.ch/~mpt/3/>
- [50] V. Kumar and K. Kumar, “Spectral characteristic of high shallow water waves”, *Elsevier Journal of Ocean Engineering*, Vol. 35, pp. 900–911, 2008.